NOTICE

The quality of this microform is heavily dependent upon the quality of the original thesis submitted for microfilming. Every effort has been made to ensure the highest quality of reproduction possible.

If pages are missing, contact the university which granted the degree.

Some pages may have indistinct print especially if the original pages were typed with a poor typewriter ribbon or if the university sent us an inferior photocopy.

Reproduction in full or in part of this microform is governed by the Canadian Copyright Act, R.S.C. 1970, c. C-30, and subsequent amendments.

AVIS

La qualité de cette microforme dépend grandement de la qualité de la thèse soumise au microfilmage. Nous avons tout fait pour assurer une qualité supérieure de reproduction.

S'il manque des pages, veuillez communiquer avec l'université qui a conféré le grade.

La qualité d'impression de certaines pages peut laisser à désirer, surtout si les pages originales ont été dactylographiées à l'aide d'un ruban usé ou si l'université nous a fait parvenir une photocopie de qualité inférieure.

La reproduction, même partielle, de cette microforme est soumise à la Loi canadienne sur le droit d'auteur, SRC 1970, c. C-30, et ses amendements subséquents.

Canada

MATHEMATICAL MODELLING OF MONOTONIC AND CYCLIC BEHAVIOUR OF POLYCRYSTALLINE FRESH WATER ICE

AHMED DERRADJI-AOUAT, B.Sc., M.Sc.

A Thesis

submitted under the supervision of

Drs. Nirmal K. Sinha and Erman Evgin

in partial fulfillment of the requirements
for the degree of Doctor of Philosophy in Civil Engineering

The Doctoral Program is a joint program with
Carleton University, administered by the
Ottawa-Carleton Institute for Civil Engineering

National Library of Canada
Acquisitions and Bibliographic Services Branch
395 Wellington Street
Ottawa, Ontario
K1A 0N4

Bibliothèque nationale du Canada
Direction des acquisitions et des services bibliographiques
395, rue Wellington
Ottawa (Ontario)
K1A 0N4

Your file Votre référence

Our file Notre référence

ISBN 0-315-85762-5

Canada

UNIVERSITÉ D'OTTAWA
UNIVERSITY OF OTTAWA

Dedication

To J. Hineman

ACKNOWLEDGEMENTS

I wish to express my gratitude to the many individuals who made this work possible.

My deepest thanks go to my supervisors: Dr. Nirmal K. Sinha and Dr. Erman Evgin who were a constant source of inspiration and helpful guidance during my enrollment at the University of Ottawa. Their intellectual support, expressed in numerous exchanges and discussions, played a significant rapid progress of this work.

The author expresses his sincere appreciation to the professors of the Department of Civil Engineering, University of Ottawa, for their guidance and instructions during the course work.

Grateful appreciations are extended to the National Research Council of Canada, NRCC, for providing laboratory facilities, equipment, and technical assistance during the course of the experimental work.

Special thanks are addressed to R. Jerome, NRCC, for his assistance, patience, and help during the experimental work.

Deep appreciations are expressed to the Natural Sciences and Engineering Research Council of Canada, NSERC, and the Government of Ontario for their financial support. Without this financial assistance both the graduate studies and this thesis would have been impossible.

SUMMARY

In the literature, most quoted mathematical models for ice were developed to describe the mechanical behaviour of ice samples subjected to uniaxial monotonically increasing loading conditions. A close examination of ice-structure interaction problems, however, indicates that ice fails under a complex state of stress and the use of uniaxial mathematical models to analyze such problems results in unrealistic ice load predictions (Sodhi and Cox, 1987). The lack of existing of reliable, deterministic, and general 3-D mathematical models for ice is the stumbling block that hindered the development of accurate predictive numerical methods for ice loads.

The objective of the present work is to develop and evaluate a three dimensional mathematical model for fresh water ice. The model serves as a mathematical base that can be extended to include the mechanical behaviour of sea-ice.

A series of creep compression tests were carried out on columnar grained S-2 fresh water ice samples. The tests were conducted at the National Research Council of Canada, NRCC, laboratory using a commercial closed-loop servo-hydraulic material testing system, MTS. During each test, a series of loading, unloading and reloading cycles were performed. The objective of this experimental work is to investigate the rate of accumulation of the permanent strains generated in ice undergoing creep deformations for non-cracking conditions.

The equations for the practical elastic moduli (Young's modulus, shear modulus, and Poisson's ratio) for ice are reviewed. These moduli are needed for the calculation of the elastic strains using Hooke's law. Sinha's (1989a) equations for Young's modulus and shear modulus are presented. New equations for Poisson's ratio for columnar grained ice are proposed.

All Sinha's (1989a) equations as well as the equations derived in this work (equations for the practical elastic moduli for ice) are based on the Reuss' averaging method. Many averaging methods have been developed to calculate the practical elastic moduli for polycrystals from the elastic moduli of monocrystals. In order to assess which averaging method is appropriate for polycrystalline ice, equations for the practical elastic moduli for granular ice are developed using three averaging methods. These equations are used to predict the values of both Young's modulus and Poisson's ratio for granular ice, and the predictions are compared with some experimental data. The comparison indicates that the Reuss averaging method is most appropriate for polycrystalline ice.

A three dimensional mathematical model for polycrystalline fresh water ice is developed on the basis of analysis of the experimental results obtained in this study as well as experimental results taken from the literature. The model describes the mechanical behaviour of ice subjected to any loading path in the three dimensional stress space, including cyclic loading. The model formulations take into account the observed material non-linearity, time and temperature dependency, plasticity, material anisotropy, stress path dependency, and hysteresis behaviour of ice subjected to cyclic loading.

The model is made up of the sum of two sub-models: A Non-cracking model and a Crack-activity model. The Non-cracking model describes the mechanical behaviour of intact ice while the Crack-activity model describes the effect of the structural deterioration (due to the formation of cracks) of ice on its mechanical behaviour. The two models are dependent on each other, their material constants and internal variables are interconnected.

Upon loading, ice undergoes both elastic and plastic deformations simultaneously. The total strains are presented as the sum of four strain components. These are the instantaneous elastic strains, the visco-plastic strains, the visco-elastic strains, and the strains generated by cracks.

The instantaneous elastic behaviour of polycrystalline ice results from the lattice deformation of its crystals. Hooke's law is used to relate the strains to the stresses.

A three dimensional visco-plastic constitutive relation is developed on the basis of the concepts of the classical theory of plasticity. However, the theory of plasticity was developed for time independent behaviour of isotropic metals undergoing deformations at low temperatures, ignoring the effect of time, temperature, and anisotropy on the plastic behaviour of the material. In this work, modifications of the classical theory of plasticity were made so that the theory could be used to model the behaviour of ice and accommodate time, temperature, and material anisotropy in the constitutive equations.

The visco-plastic constitutive equations developed in this work are based on the concept of the plastic work. Since the

model describes the creep behaviour of ice (time dependent material behaviour), a plastic power formulation is proposed. A plastic potential function is formulated on the basis of the experimental results, and the normality rule of plasticity is used to relate the plastic strain increments to the stresses.

The visco-elastic deformation of ice results from the grain boundary sliding. It is recognized that the grain boundary sliding is a non-uniform process of deformation, and this non-uniformity is induced by the visco-plastic deformations. Moreover, as the plastic strains accumulate with time, ice crystals undergo structural changes which affect the magnitude of the grain boundary sliding.

Sinha's (1979) equation for the delayed elastic strains is used to calculate the visco-elastic strains. However, Sinha's equation is modified to include the effect of the structural changes of the material (due to its visco-plasticity) on the grain boundary sliding. Sinha's equation is complemented by a structural change function, The latter, however, is formulated on the basis of the results of the creep tests carried out in this research work.

A constitutive relationship relating the stresses to the strains induced by grain boundary cracks are developed on the basis of long term creep tests carried out by Sinha (1989c). The formulation of this constitutive relationship is based on a concept similar to that of the rate theory presented by Krausz and Eyring (1975). It is assumed that the shear stresses contribute to the formation of the grain boundary cracks while the compressive hydrostatic pressure opposes the formation of these cracks. On the basis of this assumption, a

multi-axial energy barrier for crack formation and healing is developed. This energy barrier is used to develop an equation for the rate of the formation of grain boundary cracks. A crack potential function is formulated from the rate equation and the energy needed to create new surfaces (due to crack opening). Both shear and volumetric strains generated by grain boundary cracks are derived from the crack potential function.

A comprehensive evaluation of the proposed mathematical model is conducted to verify the versatility and accuracy of the model in predicting the observed ice behaviour. The model is used to predict the behaviour of laboratory fresh water ice samples subjected to various loading conditions. The data base used for the model evaluation includes the results of monotonic and cyclic uniaxial and triaxial tests, creep tests, and stress relaxation tests. The model predictions are compared with the actual test results.

The model predictions of the results of the monotonic uniaxial and triaxial tests are in excellent agreement with the measured stress strain curves. The failure stresses are predicted accurately (over 90% degree of accuracy), and the model is successful in predicting the softening behaviour of ice (post failure behaviour).

The model predictions of the results of the cyclic tests are in good agreement with the experimental data. The measured stress strain curves generated during unloading-reloading cycles in triaxial as well as uniaxial tests are predicted well, and the model is able to reproduce the observed hysteresis behaviour of ice subjected to cyclic loading.

The model predictions of the results of the creep tests are in good agreement with the experimental measurements. Both axial and volumetric strains generated during long term creep experiments are predicted well, and the effect of the grain size on the creep behaviour of ice is predicted properly.

Additional evaluation of the model includes theoretical predictions of tensile tests and predictions of the effect of stress rate and initial confining pressure on the behaviour of ice. In the light of all these predictions, recommendations for future research are suggested.

TABLE OF CONTENTS

TABLE OF CONTENTS (continued)

CHAPTER Page

TABLE OF CONTENTS (continued)

CHAPTER Page

TABLE OF CONTENTS (continued)

CHAPTER Page

TABLE OF CONTENTS (continued)

CHAPTER Page

LIST OF APPENDICES

APPENDIX Page

LIST OF APPENDICES (continued)

APPENDIX Page

LIST OF TABLES

LIST OF FIGURES

Figure No. Page

LIST OF FIGURES (continued)

Figure No. Page

LIST OF FIGURES (continued)

Figure No. Page

LIST OF FIGURES (continued)

Figure No. Page

LIST OF FIGURES (continued)

Figure No. Page

LIST OF FIGURES (continued)

Figure No. Page

LIST OF FIGURES (continued)

Figure No. Page

LIST OF FIGURES (continued)

Figure No. Page

GLOSSARY OF NOTATIONS

T and T_m	Current and melting temperatures, respectively,
d	Average grain size,
a_T	Inverse relaxation time,
t	Duration of loading,
$S_{1,2}$	Temperature shift function,
Q	Activation energy,
R	Gas constant,
X	Average grain boundary sliding displacement,
X_c	Critical grain boundary sliding displacement,
N	Crack density,
E	Young's modulus,
G	Shear modulus,
υ	Poisson's ratio,
B_m	Bulk modulus,
K_c	Compressibility coefficient,
dW^p	Plastic work increment per unit volume,
W^p	Plastic power per unit time of loading,
α_p and β_p	Plastic model parameters,
A, and D	Visco-elastic model parameters,
Ψ_c and χ	Cracking model parameters,

GLOSSARY OF NOTATIONS (continued)

f	Plastic loading function,
H^*	Hardening function,
g	Plastic potential function,
$\Delta\lambda$	Structural change function,
σ_{ij}	Stress tensor,
S_{ij}	deviatoric Stress tensor,
q	Shear stress,
p	Hydrostatic pressure,
J_{2D}	Second invariant of deviatoric stress tensor,
$I_{1\sigma}$	First invariant of the stress tensor,
τ_{oct}	Octahedral shear stress,
ε_{ij}	Strain tensor,
$\bar{\varepsilon}$	Generalized (or equivalent) shear strain,
ε^e_{ij}	Elastic strain tensor,
ε_{rv}	Reference visco-elastic strain,
ε^{ve}_{ij}	Visco-elastic strain tensor,
$\bar{\varepsilon}_{ve}$	Generalized visco-elastic shear strain,
ε^p_{ij}	Plastic strain tensor,
$d\varepsilon^p_{ij}$	Plastic strain increment,
de^p_{ij}	Plastic shear strain increment,

GLOSSARY OF NOTATIONS (continued)

ε_v^p	Plastic volumetric strain,
$d\varepsilon_v^p$	Plastic volumetric strain increment,
ε_{ij}^c	Tensor for the strains induced by crack,
e_{ij}^c	Shear strains induced by cracks,
ε_v^c	Volumetric strain induced by cracks,
V_c	Velocity of the crack growth,
ϕ_{RC}	Elementary rate constant for crack propagation,
ϕ_{gbc}	Net rate of grain boundary cracking,
G_b	Activation energy for grain boundary fracture,
W	Work needed to generate grain boundary cracks,
η	Activation volume,
U	Energy needed to create new surfaces,
γ_s	Surface energy,
A_c	Area created by crack opening.

CHAPTER 1

INTRODUCTION

1.1 General

During ice-structure interactions, the relative motion between the ice and the structure results in the development of forces known as "ice forces". Fixed offshore structures constructed in an ice infested environment must be strong enough to withstand the forces generated by ice. Many empirical and analytical methods (Appendix A) have been developed to compute the forces generated by ice on offshore structures. However, their application to solve general prototype ice-structure interaction problems may result in unsafe design of the structure against ice loads (Sodhi and Cox, 1987).

Jefferies and Wright (1988) presented field measurements of ice forces exerted on Gulf's Molikpad structure at Amauligak. They reported that ice exerted forces in excess of the design ice load (500 MN) and generated structural vibrations which led to the liquefaction of the sand in the core of the structure. Sanderson (1988) indicated that, during the impact of ice with offshore installations, complex ice force histories (ice force versus time) are generated at the ice-structure interface. The trace of these ice force histories can be periodic (cyclic) or sporadic (irregular).

In the present work, it is recognized that the method of predicting ice loads on offshore installations should be numerical. However, numerical methods (such as finite element and discrete element methods) require mathematical models for the description of the mechanical behaviour of the materials involved in the interaction problem. Therefore, in order to carry out a reliable analysis, and subsequently a safe design of the structure, realistic mathematical models for ice, structural material, and soils of the foundation are necessary.

A literature review indicated that most existing mathematical models for ice were developed to describe its mechanical behaviour under uniaxial, monotonically increasing loading. Therefore, there is a need for a three dimensional mathematical model capable of describing the mechanical behaviour of ice subjected to complex loading conditions. This stems from the fact that during ice-structure interactions, complex stress states are induced within the ice, and hence, a multiaxial mathematical model for ice should be used in conjunction with a numerical method (finite element) to analyze the interaction problem.

1.2 Statement of the Problem

A literature survey revealed that many methods for the calculation of ice forces on offshore structures have been developed (Appendix A). This section, however, presents a critical examination of these methods. The efforts are aimed to highlight the common drawbacks of these methods so that the need for numerical ice load models, and subsequently the need for general 3-D mathematical models for ice, is justified.

The most important drawbacks of the existing methods for the calculation of ice forces on offshore structures are listed as follows:

1) Although both empirical and analytical methods are widely used to solve ice engineering problems, they neglect all together the process of deformation undergone by ice prior to its failure. Moreover, the failure conditions (for ice) are randomly postulated ignoring the ice anisotropy, visco-plasticity, hysteresis behaviour, and stress path dependency.

2) Empirical methods are valid for rather limited conditions and restrictive geometries corresponding to those of the experimental setups. Their application to solve general prototype ice-structure interaction problems is underlined by a number of uncertainties, primarily the uncertainty of estimating the proper coefficients for the empirical equation that is used to solve the interaction problem at hand. The extrapolation of the parameters of an empirical equation from those originally measured in the laboratory may result in unsafe design of the structure against ice loads.

3) Most existing analytical methods are merely ad hoc formulations developed originally for the solution of trivial elastic-perfectly plastic problems with over simplified boundary conditions and presupposed failure criteria for ice.

4) Both empirical and analytical methods use the uniaxial strength of ice to compute the forces generated by ice on offshore structures. However, close examination of the ice-structure interaction problems indicates that ice fails

under a complex state of stress and the use of the uniaxial compressive strength to compute ice forces results in unrealistic ice load estimation (Sodhi and Cox, 1987).

5) In the literature, most quoted mathematical models for ice are developed for the description of its uniaxial behaviour (Chapter 2). The lack of reliable, deterministic, and general 3-D mathematical models for ice is the stumbling block that has hindered the development of accurate predictive numerical methods for ice loads.

1.3 Research Objectives

The objective of the present work is to develop and evaluate a three dimensional mathematical model for granular and columnar grained fresh water ice. The model serves as a mathematical base that can be extended to include the mechanical behaviour of sea-ice.

A series of laboratory creep tests are carried out on columnar grained S-2 fresh water ice samples. On the basis of the results of these experiments, a three dimensional visco-elasto-plastic model for ice is developed. Basically, the model is formulated for the description of the behaviour of ice subjected to any loading path in the three dimensional stress space, including cyclic loading conditions. The model formulation takes into consideration the observed material non-linearity, time and temperature dependency, plasticity, material anisotropy, stress path dependency, and hysteresis behaviour under cyclic loading conditions.

The objective of the model evaluation, however, is to assess the merits as well as shortcomings of the model. Within this general framework, it is aimed to achieve the following objectives:

1. Investigate the versatility and accuracy of the model in predicting the observed ice behaviour,

2. Evaluate the accuracy of the model in predicting the failure stresses (failure criteria),

3. Investigate the ability of the model to simulate the softening behaviour of ice after the peak of the stress strain curve has been reached,

4. Examine the performance of the model in simulating the cyclic behaviour of ice, and

5. Study the effect of strain rate, stress rate, material anisotropy and initial confining pressure on the predicted stress-strain curves.

These objectives are achieved by comparing the model predictions with actual test data. The later, however, includes the results of the tests carried out in the present study as well as the results of various tests taken from the open literature.

1.4 Scope of the Research

The steps that are followed in this work to achieve its objectives are listed as follows:

1. Literature review,
2. Laboratory testing of fresh water ice samples,
3. Review of the practical elastic moduli for ice,
4. Development of a mathematical model for ice using the results of the experimental work (step 2),
5. Development of numerical procedures for the calculation of the creep strains,
6. Evaluation of the performance of the model (step 4) in simulating the observed behaviour of ice, and
7. Conclusions and recommendation for future research.

The details regarding the above mentioned steps are given in the following subsections.

1.4.1 Literature Review

This literature review (Chapter 2) is focused on Sinha's (1978b, 1979, 1988a, 1990) mathematical model since it is used in the present work extensively. A brief review of the recent developments in ice mechanics modeling is also given in Chapter 2.

1.4.2 Laboratory Testing of Ice Samples

In this work, a series of creep compression tests were carried out on fresh water columnar grained S-2 ice samples. The tests were conducted at the National Research Council of Canada, NRCC, laboratory using a commercial closed-loop servo-hydraulic material testing system, MTS. During each test, a series of loading, unloading and reloading cycles were performed. The objective of this experimental work is to investigate the rate of accumulation of the plastic (permanent) strains induced in ice undergoing creep deformations for non-cracking conditions.

Brief descriptions of the method used to grow the ice, thin sectioning, and sample preparation are presented in Chapter 3. Also, descriptions of the testing system, testing procedure, and test results are given in the same chapter.

1.4.3 Review of the Practical Elastic Moduli for Ice

In this review, mathematical expressions for the practical (engineering) elastic moduli for ice such as Young's modulus, shear modulus, and Poisson's ratio are presented. These moduli are needed for the calculation of the instantaneous elastic strains using Hooke's law. Sinha's (1989a) equations for Young's modulus and shear modulus for granular and columnar grained ice are reviewed. New equations for Poisson's ratio for columnar grained ice are proposed.

The practical elastic moduli for polycrystalline ice are calculated from those corresponding to single ice crystals

using various averaging methods. In order to assess which averaging method is appropriate for polycrystalline ice, equations for the practical elastic moduli for granular ice are developed using three averaging methods, Voigt (1910), Reuss (1929), and Hill's (1952) methods. These equations are used to predict the values of both Young's modulus and Poisson's ratio for granular (isotropic) ice and the predicions are compared with experimental measurements taken from the open literature.

1.4.4 Development of a Mathematical Model for Ice

A mathematical model for polycrystalline ice is developed on the basis of analysis of the experimental results obtained in this study as well as experimental results obtained from the open literature. The model is made up of the sum of two sub-models: A Non-cracking model and a Crack-activity model. The Non-cracking model describes the mechanical behaviour of intact (non-cracked) ice while the Crack-activity model describes the effect of the structural deterioration (due to the formation of cracks) of ice on its mechanical behaviour. The two sub-models are dependent on each other, their material constants and internal variables are interconnected.

Upon loading, ice undergoes both elastic and plastic deformations simultaneously. The total strains (ε_t) are viewed as the sum of four strain components. These are: instantaneous elastic strains, ε_e, visco-plastic strains, ε_p, visco-elastic strains, ε_{ve}, and the strains generated by cracks, ε_c.

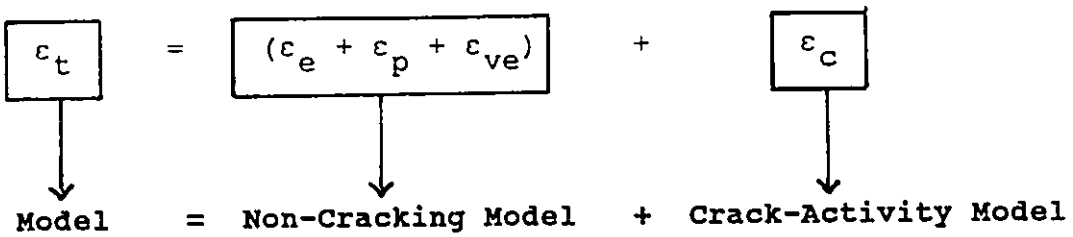

The details regarding these four strain components are given as follows:

1) The instantaneous elastic behaviour of polycrystalline ice represents an average elastic behaviour of single ice crystals. The latter, however, results from the lattice deformation. The generalized Hooke's law is used to relate the strains to the stresses. The stress-strain relations are given in Chapter 4.

2) A general 3-D visco-plastic constitutive relationship is developed using the concepts of the classical theory of plasticity. A brief review of the classical theory of plasticity is given in Appendix C. Since the model describes the creep behaviour of ice (time dependent material behaviour), a plastic power formulation is proposed. A plastic potential function is formulated on the basis of the experimental results, and the normality rule of plasticity is used to relate the plastic strain increments to the stresses.

3) The visco-elastic deformation in ice results from the grain boundary sliding. In this thesis, it is recognized that the plastic strains induce structural changes in ice and

affect the magnitude of the grain boundary sliding. Sinha's (1979) equation for the delayed elastic strain is used to calculate the visco-elastic strains. However, Sinha's equation is modified to include the effect of the structural changes of the material (due to its plasticity) on the grain boundary sliding. The structural change function is formulated on the basis of the results of creep tests carried out in this research work, Chapter 3.

4) During creep deformation, ice undergoes structural deterioration due to the formation of cracks, particularly at the grain boundaries. A constitutive relationship relating the applied stresses to the strains induced by cracks is developed on the basis of long term creep tests carried out by Sinha (1989c). This constitutive relationship is based on a concept similar to that of the rate theory (Krausz and Eyring, 1975). A review of the rate theory as well as a detailed presentation of the Crack-activity model are given in Chapter 6.

1.4.5 Numerical Procedures for the Calculation of the Creep Strains

The proposed mathematical model (Non-cracking + Crack-activity sub-models) is developed to calculate the creep strains generated in polycrystalline ice subjected to constant loading. Numerical procedures are used in conjunction with the model formulations to calculate the strains induced in ice subjected to arbitrary loading paths (variable loading). Boltzmann (1876) superposition principle is used to calculate the visco-elastic strains. A numerical procedure is proposed for the calculation of the visco-plastic strains, Chapter 7.

1.4.6 Evaluation of the Model

A comprehensive evaluation of the proposed mathematical model is necessary before it is used to solve boundary value problems. This stems from the fact that the constitutive equations determine whether or not the solution obtained for the boundary problem is realistic. Indeed, it should emphasized that even the solution provided by the most complex numerical computer program will never be more realistic than the constitutive equations implemented in the program to model the material behaviour.

In this research work, the efforts are made to verify the capability of the proposed model to predict the observed behaviour of laboratory ice samples. The model is coded into a stress point computer program. Subsequently, the program is used to predict the behaviour of ice samples subjected to various types of loading conditions. The comparisons of the model predictions with the experimental data are presented in Chapter 8.

CHAPTER 2

LITERATURE REVIEW

2.1 Introduction

In nature, the temperature of ice rarely goes below -40^0C for any extended period of time. Therefore, the working temperatures of ice are, usually, greater than the homologous temperature of 0.85 T_m ($T/T_m = 0.85$), where T and T_m are the current and melting temperatures in Kelvin scale. High temperatures, for metals and alloys, are considered to be around 0.4 T_m or above. Hence, in nature, ice exists at high temperature states (Sinha, 1981b).

Only one microscopic type of ice is found in nature. That is the 1h ice type (h refers to hexagonal) which exists under normal temperature and pressure (Michel, 1978). Under laboratory conditions, however, at least seven other atomic configurations of ice exist at high pressure (greater than 200 MPa) or low temperature (below -110°C). In nature, even at the bottom of the Antarctic ice cap (the thickness reaches 4000 m in some places), the hydrostatic pressure (35 MPa) is insufficient to allow for other ice types (other than 1h ice type) to exist in stable conditions (Sanderson, 1988).

Ice forms, of course, from liquid water and preserves some of the geometric features of the water molecules. The

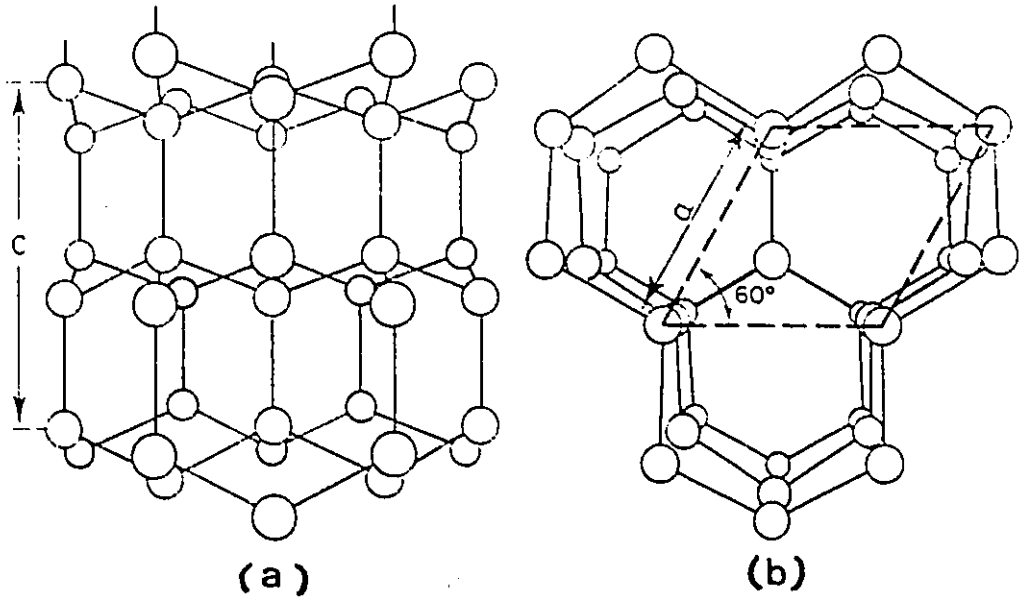

Figure 2.1: Molecular structure of ice. The lines joining the oxygen atoms (open circles) represent bounds. The hydrogen atoms are not shown: a) View perpendicular to the c-axis b) View along the c-axis (After Michel, 1978).

geometric configuration of 1h ice crystals is presented in Fig. 2.1. The oxygen atoms are arranged in layers of hexagonal geometry. The plane parallel to the layer structure is known as the basal plane. The direction perpendicular to the basal plane is known as the c-axis (or optic axis) of the crystal.

In nature, ice forms in variety of ways which depend on the growth processes, thermal, and mechanical histories. A classification system for fresh water river and lake ice on the basis of its genesis, structure, and texture was given by Michel and Ramseier (1971). Because this thesis deals with granular and columnar grained (S-1 and S-2) ice, brief identification of these two types of ice is given as follows:

Granular ice (snow ice or consolidated slush ice) is a conglomerate of randomly oriented grains which can be rounded, equiaxed, or angular. Granular ice is also known as equiaxed or random polycrystalline ice. Columnar grained ice, however, is an arrangement of ice crystals whose c-axes preferentially lie in a plane. In the case of columnar grained S-2 ice, the c-axes of the crystals are randomly oriented in the horizontal plane (plane parallel to the water surface) while for columnar grained S-1 ice, the c-axes of the crystals are in the vertical plane (perpendicular to the water surface).

The global orientation of the c-axes of individual grains influences greatly the mechanical behaviour of polycrystalline ice, and dictates the state of the material anisotropy. This is due to the fact that the practical elastic moduli (such as Young's modulus, shear modulus, and Poisson's ratio) as well as the plastic deformations depend on the preferred global

orientation of the c-axis. A random orientation of the c-axis (such as in the case of granular ice) dictates that the material is isotropic. In the case of columnar grained S-2 ice, for example, there is a random orientation of the c-axes of the grains in the horizontal plane, resulting in a transverse isotropic material (or cross anisotropic material).

At high temperatures, when loaded, polycrystalline materials, including ice, undergo pronounced creep deformations and grain-boundary embrittlement (Sinha et al. 1987). Under constant loads, the deformation history (strain versus time, creep curves) of polycrystalline ice shows 4 distinct stages; an instantaneous stage resulting from the instantaneous elastic deformations, a primary (or transient) creep stage, a secondary (or steady state) creep stage, and with time, the strain history may show a tertiary creep stage. Typical creep curves for polycrystalline ice are presented in Fig. 2.2

Over the years, much experimental work has been carried out to investigate the mechanical behaviour of polycrystalline ice. Literature reviews of the laboratory work on ice are given by Sanderson (1988) and Cammaert and Muggeridge (1988). Most of the reported work has been directed towards investigating the behaviour of ice subjected to: 1) constant loading (creep tests) or 2) monotonically increasing loading (constant strain rate tests). In general, the results of the creep tests are used to determine the parameters for Glen's (1955) power equation for the steady state creep while the results of the constant strain rate tests are used to develop empirical equations relating the strength of ice (peak of the stress-strain curves) to the strain rate. Very little experimental work has been reported on the cyclic behaviour of ice.

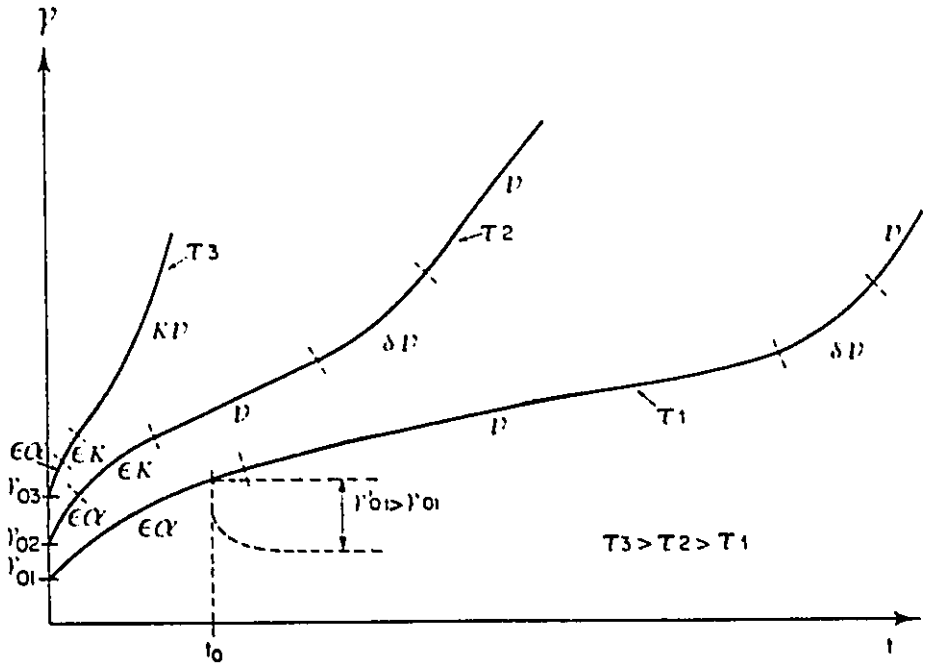

Figure 2.2: Typical creep curves for polycrystalline ice under constant stresses τ_1, τ_2, τ_3. The primary creep strains are represented by the symbols $\varepsilon\alpha$ and εk. The secondary creep strains are represented by the symbol υ. The tertiary creep strains are represented by the symbols $k\upsilon$ and $\delta\upsilon$ (After Michel, 1978).

A number of mathematical models have been developed to describe the mechanical behaviour of ice. Among these models are those developed by Michel (1978), Sinha (1978b, 1979, 1988a, 1990), Spring and Morland (1983), Szyszkowski et al. (1985), Ting and Sunder (1985), Pulkkinen (1988) and Santaoja (1990). Most of the existing mathematical models for ice are developed for the description of the behaviour of ice subjected to monotonic increasing loading where the behaviour of ice under cyclic loading conditions is not formulated. More importantly, most the existing models are developed to describe the behaviour of ice under uniaxial loading. Up to now, the author is not aware of any existing 3-D, realistic, visco-elasto-plastic mathematical model capable of describing the behaviour of ice subjected to cyclic loading conditions.

In the following sections, a review of Sinha's mathematical model is given. Sinha's model is used extensively in this thesis. Brief reviews of both Pulkkinen's (1988) and Santaoja's (1990) 3-D models are presented as examples of the most recent three dimensional mathematical modelling of ice.

2.2 Sinha's Model

Sinha(1978b, 1979, 1988a, 1990) developed a mathematical model to describe the mechanical behaviour of polycrystalline ice subjected to uniaxial compressive loading conditions. The model takes into account the effect of grain size, temperature, and crack activity (crack initiation and accumulation) on the creep behaviour of ice. Its ability to predict the results of both monotonically increasing loading as well as creep tests was demonstrated (Sinha, 1988a and 1989c).

2.2.1 Basic Equations

Ice undergoes both elastic and permanent deformations simultaneously upon loading. As shown in Fig. 2.3, the total strain is viewed as the sum of three strain components. These are an instantaneous elastic strain, ε_e, a delayed elastic strain (time dependent recoverable strain), ε_d, and a permanent viscous creep strain, ε_v.

$$\varepsilon_t = \varepsilon_e + \varepsilon_d + \varepsilon_v \tag{2.1}$$

1) Hooke's law is used to relate the instantaneous elastic strain to the applied stress.

$$\varepsilon_e = \frac{\sigma}{E} \tag{2.2}$$

where E is Young's modulus in the plane of loading. It varies linearly as a function of temperature (Sinha, 1989a).

2. The delayed elastic strain results from the grain boundary sliding. It was given by Sinha (1979):

$$\varepsilon_d = \frac{C_1 . d_1}{d} \left[\frac{\sigma}{E} \right]^s (1 - \exp(-(a_T\, t)^b)\ ) \tag{2.3}$$

where d is the average grain size. The parameter a_T is the inverse relaxation time, and t is the duration of loading. The parameters a_T, C_1, d_1, s, and b are given in Table 2.1.

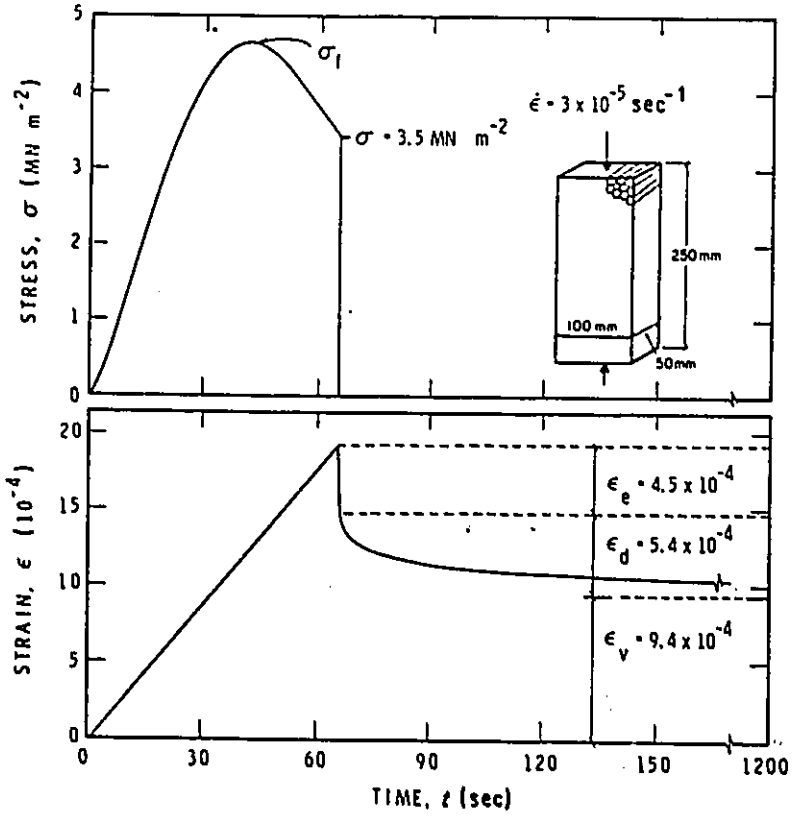

Figure 2.3: Stress and strain histories for columnar grained S-2 ice, average grain diameter of 5.0 mm at $-10^{o}C$ (0.96 T_m) under closed-loop controlled constant strain rate of 3 10^{-5} sec. (Sinha, 1988a)

Table 2.1: Sinha's Model Parameters

$C_1 = 9 \times 10^{-3}$ $d_1 = 1.$ m $s = 1.$ $n = 3.$ $b = 0.34$ $K = 1.$	$M_1 = 1.67 \times 10^{-6}$ $m_1 = 4.55 \times 10^{-9}$ K^{-1} $N_c = 550$ m^{-2} $a_T = 2.5 \times 10^{-4}$ S^{-1} $\psi = 1.33 \times 10^{7}$ m^{-1} $\dot{\varepsilon}_{vo} = 1.76 \times 10^{-7}$ S^{-1} ($\sigma_o = 1$ MN.m^{-2})
$Q = 67$ KJ/mol (16 Kcal/mol or 0.70 eV)	

Note: Both a_T and $\dot{\varepsilon}_{vo}$ correspond to temperature T = 263 K

3. The viscous creep strain results from the intra-granular deformation processes, particularly the movement of dislocations. It was expressed as follows (Sinha, 1978b):

$$\varepsilon_v = \dot{\varepsilon}_{vo}.t.\left[\frac{\sigma}{\sigma_o}\right]^n \qquad (2.4)$$

where $\dot{\varepsilon}_{vo}$ is the viscous strain rate for the reference stress σ_o and the parameter n is a material constant (Table 2.1).

The total strain is obtained by substituting Eqs. 2.4, 2.3, and 2.2 into equation 2.1:

$$\varepsilon_t = \frac{\sigma}{E} + \frac{C_1.d_1}{d}\left[\frac{\sigma}{E}\right]^s (1-\exp(-(a_T\ t)^b) + \dot{\varepsilon}_{vo}.t\left[\frac{\sigma}{\sigma_o}\right]^n \qquad (2.5)$$

In order to include the effect of temperature on the creep behaviour of ice, both parameters a_T and $\dot{\varepsilon}_{vo}$ (in Eq. 2.5) were made a function of the current temperature (Sinha, 1978b):

$$a_T(T_2) = a_T(T_1).S_{1,2} \quad \text{and} \quad \dot{\varepsilon}_{vo}(T_2) = \dot{\varepsilon}_{vo}(T_1).S_{1,2} \tag{2.6}$$

where the values of $a_T(T_1)$ and $\dot{\varepsilon}_{vo}(T_1)$ for $T_1 = -10^{o}C$ are given in Table 2.1. The shift function $S_{1,2}$ is given as:

$$S_{1,2} = \exp\left\{ \frac{Q}{R}\left[\frac{1}{T_1} - \frac{1}{T_2} \right] \right\} \tag{2.7}$$

where Q is the activation energy (Table 2.1) and R is the gas constant.

Equation 2.5 does not include any crack formulation. In the following section, a general form of Eq. 2.5 which incorporates the effect of cracking activity on the creep behaviour of ice is presented.

2.2.2 Crack Enhanced Matrix Creep

The strain induced by the grain boundary sliding is expressed as follows (Sinha, 1979):

$$\varepsilon_{gbs} = \frac{K.X}{d} \tag{2.8}$$

where the symbol **gbs** means grain boundary sliding and K is a material constant (Table 2.1). The parameter X is the average grain boundary sliding displacement.

The delayed elastic strains are attributed to the grain boundary sliding:

$$\varepsilon_d = \varepsilon_{gbs} \tag{2.9}$$

The grain boundary sliding results in stress concentrations at triple points (points at which three grains meet) or at irregularities on the grain boundaries. This stress concentration initiates cracks when the grain boundary sliding displacement reaches a critical value, (Sinha, 1984b):

$$X_c = (M_1 - m_1 T) \frac{d_1}{K} \tag{2.10}$$

where X_c is the critical value of the grain boundary sliding displacement, and T is the absolute temperature. Both parameters M_1 and m_1 are material constants which are given in Table 2.1.

Equations 2.8, 2.9, and 2.10 indicate that cracks initiate when the delayed elastic strain reaches its critical value:

$$\varepsilon_d^c = \frac{K.X_c}{d} = (M_1 - m_1 T) \frac{d_1}{d} \tag{2.11}$$

As the specimen deforms, the number of cracks increases. The crack density is expressed as follows (Sinha, 1984a):

$$N = N_c \left[\exp(\psi (X - X_c)) \right] \tag{2.12}$$

where N is the crack density at a given time, temperature, and stress. The parameters N_c and ψ are given in Table 2.1.

The presence of cracks enhances only the permanent viscous creep strain (Sinha, 1988a). The effect of the crack activity (crack initiation and accumulation) was added to the viscous creep strain component, ε_v. The term $\dot{\varepsilon}_{vo}$ (in Eq. 2.5) was modified as follows:

For Columnar Ice:

$$\dot{\varepsilon}_{vc} = \dot{\varepsilon}_{vo}\left[1 + \frac{\pi^2}{12\sqrt{3}} N d^2 n^{1/2}\right] \qquad (2.13)$$

For Granular Ice:

$$\dot{\varepsilon}_{vc} = \dot{\varepsilon}_{vo}\left[1 + \left\{\frac{\pi}{16.497}\right\}^{3/2} N d^3 n^{1/2}\right] \qquad (2.14)$$

where $\dot{\varepsilon}_{vc}$ is the viscous strain rate at the time and after cracks initiate. All other parameters in Eqs 2.13 and 2.14 were defined previously.

If the condition for crack initiation was fulfilled, Eq. 2.11. the stress-strain relationship, Eq. 2.5, has to be modified to include the continuous structural deterioration of the material as the number of cracks increases. This can be achieved by replacing the term $\dot{\varepsilon}_{vo}$ in Eq. 2.5 by $\dot{\varepsilon}_{vc}$ in Eq. 2.13 or Eq. 2.14 depending on the type of material whether it is columnar grained or granular ice (Sinha, 1990).

2.3 Pulkkinen's (1988) Model

Pulkkinen (1988) proposed a three dimensional mathematical model for polycrystalline ice. The model was made up of two separate sub-models: A rate dependent creep damage model and a rate dependent cracking model. The first sub-model was based on the theory proposed by Murakami and Ohno (1981) supplemented with an equation for damage evolution. The second sub-model was based on the crack concept presented by Rots et al. (1985) for concrete (two dimensional).

Pulkkinen's (1988) model includes the effect of the strain rate, anisotropy, and cracking on the mechanical behaviour of ice. However, the model was developed, purely, on a mathematical basis. It represents only a general, theoretical, picture of ice behaviour subjected to monotonic loading conditions. Consequently, its capability to predict the observed ice behaviour has to be demonstrated (Pulkkinen's recommendations in his Ph.D. thesis)

2.4 Santaoja's (1990) Model

Santaoja (1990) developed a three dimensional mathematical model for the mechanical behaviour of ice. The total strain was presented as the sum of the instantaneous elastic, delayed elastic, and permanent strains (similar to Eq. 2.1). He assumed that the instantaneous elastic strains induced in ice can be decomposed into two components. These are the instantaneous elastic strain generated in the non-cracked material, and the strain generated by instantaneous microcracks.

For the calculation of the instantaneous elastic strains, Santaoja (1990) assumed that the material is isotropic and obeys Hooke's law. The cracks formed during deformation are assumed to be penny shaped, and the interactions among cracks are neglected. The stress at the crack tip is not influenced by the existing neighbouring cracks, and each crack is treated under a uniform stress field.

Santaoja (1990) generalized the uniaxial equations for delayed elastic and permanent strains in the modified Sinha's model by Ashby and Duval (1985) to three dimensions. The total strains were calculated by adding the instantaneous elastic, delayed elastic and permanent strains (similar to Eq. 2.1).

CHAPTER 3

LABORATORY EXPERIMENTS ON COLUMNAR GRAINED S-2 ICE

3.1 Introduction

In the present work, a series of creep compression tests were carried out on fresh water columnar grained S-2 ice samples. The tests were conducted at the National Research Council of Canada, NRCC, laboratory under the supervision of Dr. N.K. Sinha. The tests were carried out at temperature of $-10^{\circ}C$ on samples with an average grain size of about 4.5 mm. During each test, a series of loading, unloading and reloading cycles were performed. The main objective of this experimental work was to investigate the rate of accumulation of the plastic (permanent) strains induced in columnar grained ice undergoing creep deformations for non-cracking conditions. The test results were used to formulate the visco-plastic strains in the Non-cracking model. However, the results of long term creep tests carried out by Sinha (1989c) were used to formulate the Crack-activity model.

In this Chapter, brief descriptions of the method used to grow the ice, thin sectioning, and sample preparation are presented. Also, descriptions of the testing system as well as the testing procedure are given. The results of the tests that were used to formulate the Non-cracking model are presented in Appendix D. Other test results are given together with the model predictions in Appendix G.

3.2 Preparation of Ice

Ice was prepared in a cold room at -10°C from deaerated tap water in a galvanized tank. The water was allowed to cool down for about 2 - 3 days in an insulated plastic container (1 X 0.6 X 0.3 m). The container was equipped with a pressure relief system to minimize the possibility of generating any deformation in the ice during its growing period. Freezing was initiated by spreading a very fine crushed and aged ice (using No. 18 U.S. standard sieve) on the water when its surface temperature was just above freezing. The plate of ice (obtained after 2 weeks) was about 150 mm thick with visible air bubbles formed in the bottom layer (20 - 30 mm).

Because the method of freezing was unidirectional, the ice had a columnar grained structure. Ice crystals in the top layer (about 20 mm) were randomly oriented because the seed ice was initially scattered randomly over the surface of the water. Since the crystals have a tendency to grow in the direction perpendicular to c-axis rather than parallel to it, the grains that were favorably oriented (grains with their c-axes normal to the direction of the growth) grew at the expense of the less favorable oriented grains. Because of this, some of the grains were tapered and the average grain size increased gradually in the direction of the growth.

3.3 Thin Sectioning

The grain size and crystallographic orientation of individual grains, in both normal and parallel planes to the columns, were studied by making thin sections and examining

them with a transmitted polarized light. The thin sections (about 0.5 mm thick) were microtomed from thick sections (about 15 mm thick) cut from the central area of an ice block using a band saw. The ice block, itself, was cut from the ice plate from which the ice samples were machined for testing. Each thick section was mounted on a clear clean glass plate by freezing drops of water at its edges. First, the top surface of the thick section was microtomed just to remove the cutting marks induced by the band saw. About 3 mm was cut off the surface in 10 μm layers. Second, a 0.5 mm was microtomed off the surface in 5 μm layers. This was followed by removing another 0.3 mm in 2 - 1 μm layers and cleaning the microtome blade (before cutting off each layer) with soft tissue paper. This procedure resulted in a smooth, clean, and light reflecting surface. The ice section was, then, dismounted from the first glass plate and mounted on an-other clean clear glass plate such that the finished surface of the ice section was facing the glass plate. The ice section was mounted on the glass plate by freezing drops of water along all its sides, and applying a slight pressure on it to ensure that no water enters between the glass plate and the ice section. The microtoming of the exposed surface was, then, continued until the thickness of the ice section was about 2 mm removing off the surface 10 μm layer during each microtome pass. This was followed by microtoming off about 1 mm in 5 μm layers. Finally, the microtoming continued in 1 - 2 μm layers accompanied with cleaning the microtome blade before each pass until the thickness of the ice reached about 0.4 - 0.5 mm.

For viewing and analyzing the crystallographic orientation of the individual grains, the thin section was placed between crossed polaroid sheets illuminated with a white light. Since ice has a birefringent crystals, the grains with the same

crystallographic orientation had a different brightness and a different color than the neighboring grains with different crystallographic orientations. Therefore, the grain structure can be, easily, seen. Figure D.1 shows a typical horizontal and vertical thin sections.

For the analysis of the grain size and shape, a picture of the thin section (as seen between the crossed polaroids) was taken. A 100 X 125 mm black and white film was used. The film provided an immediate positive and negative. The positive was kept for the record. The negative, however, was placed in a microfiche viewer to measure the size of the grains and to analyze their shapes.

3.4 Sample Preparation

Rectangular samples (typical dimensions 80 X 100 X 220 mm) were prepared in a cold room at -10°C such that the long direction of the grains was perpendicular to the 100 X 220 mm surface, as shown in Fig. D.2a. Both top and bottom layers of the ice block (ice block from which the samples were made) were removed to obtain a uniform columnar grained ice with a random orientation of the c-axis in the plane parallel to the top surface of the ice plate and without any visible air bubbles. The samples were rough-cut from the ice block using a band saw to dimensions slightly larger than their final values. The samples were machined to their final dimensions by milling and lathing. The 80 X 220 mm and 100 X 220 mm surfaces were milled, and any imperfections or cutting marks induced by the band saw were removed. The 80 X 100 mm end surfaces were lathed to remove any imperfections produced by the band saw and to ensure a right angle between the side and the end

surfaces of the sample. Following the lathe cutting, the end surfaces were, also, polished using a fine sand paper to ensure the smoothness of the ends and to remove any cutting marks produced by the lathe machine. The final dimensions were measured and the rectangularity of the specimen was checked. Then, all surfaces of the sample were given a final polish with a fine tissue paper moistened with alcohol. This sample preparation procedure resulted in transparent ice samples with clean, smooth, and light reflecting surfaces. The samples were stored in sealed plastic bags to prevent sublimation, and the tests were conducted in the following 1 to 5 days.

3.5 Testing System

A commercial closed-loop, servo-hydraulic material test system (MTS) was used to carry out the tests. The test machine was situated inside a cold room near an observation window. The hydraulic pump, the control panel of the machine, and the data recording system were kept outside the cold room. The frame of the machine was designed for load capacity of 1 MN. The loading train consists of two 152 mm diameter compression platens, a 250 KN capacity load cell, and a 250 KN capacity actuator. The lower platen was equipped with a liquid circulation system (refrigeration system) to maintain it at a cold room air temperature, and subsequently isolate it from any warming effect generated by the actuator.

The machine is a single channel type testing system. It has one actuator and one servo-controller. Therefore, only uniaxial compression and tension tests can be carried out. Both strain and stress controlled tests can be conducted. The stress or strain histories (variation of stress or strain with time) can be controlled by setting the desired load or

displacement history on the control panel situated outside the cold room. During testing, the recording system provides an instantaneous strip chart which shows the history of both applied load (or displacement) and the measured displacements (or load) so that an exact record of the experiment history is known at the time of testing. The test results can be recorded at any desired time intervals and stored on a digital magnetic tape recorder.

3.6 Testing Procedure

As shown in Fig. D.2, the experiments were carried out such that the load was applied parallel to the long axis of the specimen, hence it was perpendicular to the columns. The axial (vertical) and lateral (horizontal) strains were measured by using commercial extensometers attached (frozen) to the central area of the surfaces of the specimen. For each test, three extensometers were used to measure one axial and two lateral strains. Figure D.2b presents a picture of the experimental setup showing the loading train, ice sample, and the extensometers.

3.7 Test Results

The compressive stresses are considered to be positive. The axial and lateral strains are denoted as ε_i (i =1,3). The directions 1 and 2 are those corresponding to the directions perpendicular to the columns while direction 3 corresponds to the direction along the columns, as depicted in Fig. D.2a.

In this section, the results of three creep experiments are reported. The experiments are carried out for applied

stress values of 0.5 MPa, 1.0 MPa, and 1.5 MPa. Figure D.3 shows a schematic description of the stress history followed during testing. This type of stress history allows for the measurement of the plastic strains generated during testing (the plastic strains are measured at the end of the recovery time). The rate of accumulation of the plastic strains, however, is obtained from the measured plastic strains and the accumulated duration of loading.

Because it was aimed to avoid the development of cracks in the ice specimen during testing, both the applied stresses and the duration of loading were kept small. During creep tests on columnar grained S-2 ice samples, Gold (1972a, 1976) recorded the time for the formation of the first three cracks at temperatures of -5°C, -10°C, -15°C, and -31°C. Sinha (1984b) used Gold's experimental work and his equation for the delayed elastic strain to establish the conditions (stress, duration of loading, and temperature) required for crack initiation. Using Sinha's work, it was found that for an applied stress of 1.0 MPa (temperature of -10°C), the first cracks occur for a duration of loading of about 1000 sec. For an applied stress of 1.5 MPa (temperature of -10°C), the first cracks occur for a duration of loading of about 130 sec, and no cracks form for an applied stress of 0.5 MPa. Gold (1972a) did not observe any cracking below 0.5 MPa, and Sinha (1984b) computed the minimum stress required for crack activity to be 0.47 MPa for temperature of -5°C and 0.59 MPa for temperature of -30°C.

3.7.1 Creep Test No. 1

A constant stress of 1.0 MPa was applied for a duration of loading, Δt, of 60 sec., then the load was removed. This was

followed by a waiting time period (t_r in Fig. D.3a) until all elastic strains were recovered. The waiting time period needed for the elastic strains to recover was decided upon during testing by examining the strip chart. When the curve of axial strain versus time (on the strip chart) appeared to be parallel to the time axis, all elastic strains were considered to be fully recovered. The sample was reloaded up to 1.0 MPa for an-other 60 sec, then, the load was removed. A total of 34 cycles of loading (loading up to 1.0 MPa), unloading, and reloading were performed.

The measured axial and lateral strain histories are shown in Fig. D.4. These measurements correspond to the strain values at the time of unloading. Figure D.5 shows the measured axial and lateral plastic strain histories. The examination of Fig. D.5 indicates that the plastic strains generated in directions 1 and 2 (directions perpendicular to the columns) vary linearly with time, and a very small amount of the plastic strains is generated in direction 3 (direction along the columns). Therefore, within the accuracy of the experiment, it can be concluded that the absolute values of the plastic strain rates in directions 1 and 2 are equal, and the plastic strain rate in direction 3 is zero. Consequently, at any given period of time, the plastic volumetric strain (sum of axial and lateral plastic strains) is zero.

During the experiment, it was observed that the waiting time period for the elastic strains to recover, t_r, is not equal to the duration of loading, Δt. As shown in Figs. D.6 and D.7, the elastic strains generated during each cycle (duration of loading of 60 sec.) did not recover during a waiting time period of 60 seconds. Moreover, from both figures, it can be seen that the recovery time of the elastic

strains increases as both time of loading and plastic strains increase. In this thesis, it is hypothesized that the increase of the recovery time of the elastic strains with the increase of the plastic strains is due to the following:

Upon loading, ice undergoes structural changes to accommodate the plastic strains. Slip bands, pile ups, grain boundary migration, small angle boundaries, distortion of the grain boundaries, ...etc, have been observed by a number of investigators: Gold (1963, 1972b), Levi and Suraski (1965), and Sinha (1977, 1978a, 1987a). Therefore, in the present study, it is assumed that the increase of the recovery time of the elastic strains with the increase of the plastic strains results from the structural changes that manifest within the material to accommodate the plastic strains.

3.7.2 Creep Tests No. 2 and 3

The stress histories followed during these two experiments are similar to that of the previous test (creep test No. 1). The applied axial stresses were 0.5 MPa, for creep test No. 2, and 1.5 MPa, for creep test No. 3. The test results are given in Fig. D.8 (for creep test No. 2) and Fig. D.9 (for creep test No. 3), respectively. The objective of these tests is to investigate the influence of the stress magnitude on the rate of accumulation of the plastic strains (as it will be explained in Chapter 4, formulation of the Non-cracking model)

3.8 Conclusions

The following conclusions have been drawn on the basis of analyses of the experimental results reported above. It is important to note that these conclusions are valid only for ice undergoing creep deformations for no-cracking conditions.

1) The plastic strains generated in an ice specimen undergoing creep deformation vary linearly with the loading time.

2) There are very small (negligible) amounts of plastic (permanent) strains developed in the direction along the columns, $\varepsilon_3^p = 0$.

3) There is no plastic volumetric strains generated in the ice samples ($\varepsilon_v^p = \varepsilon_1^p + \varepsilon_2^p + \varepsilon_3^p = 0.$).

4) During the experiments, it was observed that the waiting time period for the recovery of the elastic strains is not equal to the duration of loading.

5) As the plastic strains accumulate, the recovery time of the elastic strains increases.

CHAPTER 4

PRACTICAL ELASTIC MODULI FOR ICE

4.1 Introduction

The correct determination of the practical (engineering) elastic moduli for polycrystalline ice such as Young's modulus, shear modulus and Poisson's ratio is very important in solving ice boundary value problems. In general, these moduli are determined by performing standard static tests such as compression, tensile, and bending tests. At high temperatures ($T > 0.4\ T_m$), however, depending on the stress, temperature, and the time needed to apply the full load, the results of the static tests can become inaccurate for the determination of the elastic properties of the material. Both the visco-elasticity and visco-plasticity of the material can contribute to the deformation of the specimen to the extent that the measured stresses and strains do not correspond to its true instantaneous elastic bahaviour.

On the basis of the results of creep tests carried out on columnar grained S-2 ice samples, loaded in the direction normal to the length of the columns, Sinha (1978b) reported that the value of the effective modulus (ratio of the stress to the strain) at 5 sec after application of full load (for loads less than 0.5 MPa) is lower than its zero-time value by 6 percent at temperature of $-45^{o}C$, 12 percent at $-30^{o}C$, 23 percent at $-10^{o}C$, and about 30 percent at temperatures near the freezing point. At 30 sec after application of the full

load (also for loads less than 0.5 MPa), the value of the effective modulus is lower than its zero-time value by 10 percent at $-45^{o}C$, 20 percent at $-30^{o}C$, 35 percent at $-10^{o}C$, and more than 50 percent at temperatures just below the freezing point. In fact, these are the error percentages involved in the measured values of Young's modulus if the times needed to apply the full load are 5 sec and 30 sec, respectively.

An alternative to the static tests is the use of ultrasonic methods whereby the practical elastic moduli for a given polycrystalline material are determined from the velocity of sound within the material and its density. Using these methods (ultrasonic methods) the elastic moduli are obtained for single crystals. The elastic moduli for polycrystals, however, are calculated from those corresponding to monocrystals using various averaging methods such as Voigt (1910), Reuss (1929), and Hill's (1952) methods.

Dantl (1969) determined the elastic moduli for single ice crystals using a supersonic method (pulse-echo method). On the basis of Dantl's experimental data, Sinha (1989a) formulated mathematical equations for Young's modulus and shear modulus for polycrystalline ice. This chapter is a continuation of Sinha's (1989a) work. Equations for Poisson's ratio for columnar grained (S-1 and S-2) ice are proposed.

All Sinha's (1989a) equations as well as the equations proposed in this chapter (equations for the practical elastic moduli for ice) are based on the Reuss' averaging method. Historically, many averaging methods have been developed to calculate the practical elastic moduli for polycrystals from the elastic moduli of monocrystals (Ledbetter, 1990). In order to assess which averaging method is appropriate for

polycrystalline ice, equations for the practical elastic moduli for granular ice are derived using three averaging methods (Voigt, Reuss, and Hill's methods). These equations are used to predict the values of both Young's modulus and Poisson's ratio for granular ice, and the predictions are compared to laboratory measurements taken from the literature.

4.2 Elastic Stress-Strain Relationship

The instantaneous elastic strains in polycrystalline materials are calculated by using the generalized Hooke's law:

$$\varepsilon_{ij} = s_{ijkl}\,\sigma_{kl} \tag{4.1a}$$

The inverse of equation 4.1a is given as:

$$\sigma_{ij} = c_{ijkl}\,\varepsilon_{kl} \tag{4.1b}$$

where the c_{ijkl}'s are 81 components of a fourth order tensor which represent the elastic stiffness of the material while s_{ijkl}'s are the elastic compliancies. The consideration of the symmetry conditions ($c_{ijkl} = c_{ijlk}$ and $c_{ijkl} = c_{jikl}$) reduce the 81 components of the tensor c_{ijkl} to 36. Similarly, the number of the components of the tensor s_{ijkl} is reduced to 36 (Nye, 1985, reprint of the original publication in 1957).

In matrix notation, the stress strain relations (Eqs. 4.1a and 4.1b) are given as:

$$\varepsilon_i = s_{ij}\,\sigma_j \quad (i, j = 1, 2, \ldots, 6) \tag{4.1c}$$

$$\sigma_i = c_{ij}\,\varepsilon_j \quad (i, j = 1, 2, \ldots, 6) \tag{4.1d}$$

The elements of the matrices c_{ij} and s_{ij} must have the same orientations as the stresses and strains. Experimentally, for single crystals, the elements c_{ij}'s (and s_{ij}'s) are measured with respect to the crystal axes (standard orientation). Their values in the standard orientation are called the characteristic elastic constants of the crystal and they are represented by capital letters C_{ij} and S_{ij} (Nowick and Berry, 1972). The existence of the strain energy functions ($C_{ij} = C_{ji}$ and $S_{ij} = S_{ji}$) reduce the 36 elements of the matrix C_{ij} (and the matrix S_{ij}) to 21. (Nye, 1985).

4.3 Characteristic Elastic Constants for Single Ice Crystals

Ice belongs to the family of hexagonal crystals which are orthotropic material (transverse isotropic). Its plane of isotropy is the basal plane. According to Nye (1985), hexagonal crystals have 12 elements in the matrix S_{ij} (similarly 12 elements in the matrix C_{ij}) of which only five are completely independent. These are C_{11}, C_{12}, C_{13}, C_{33}, and C_{44} for the stiffness coefficients (similarly, S_{11}, S_{12}, S_{13}, S_{33}, and S_{44} for the compliancies).

Matrix C_{ij}

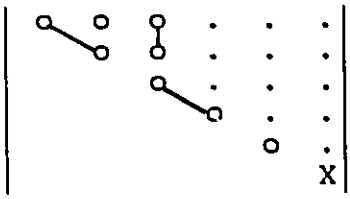

Matrix S_{ij}

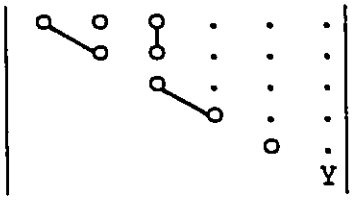

The symbols used in the above matrices are defined as follows:

o is a non-zero element,

. is a zero element,

o — o equal elements,

$$X = \frac{1}{2}(C_{11} - C_{12}), \qquad \text{and} \qquad Y = 2(S_{11} - S_{12})$$

Note: both matrices (C_{ij} and S_{ij}) are symmetrical with respect to the main diagonal.

Measurements of the characteristic elastic constants for single ice crystals have been made by Jona and Scherrer (1952) using ultrasonic waves (frequencies 15 - 18 MHz). The same method was used by Zaremboviteh and Kahane (1964) over a temperature range of -2 to -180°C (frequencies 6 - 14 MHz). Green and Mackinnon (1956), and Bogorodskii (1964) used the direct pulse propagation method to determine the values of the constants C_{ij}'s. These constants (C_{ij}'s) were, also, measured by Gagnon et al. (1988) using Brillouin spectroscopy.

According to Sinha (1989a), the most complete and probably the most accurate values of the characteristic elastic constants (C_{ij} and S_{ij}) were given by Dantl (1969). Dantl measured the velocity of sound within single ice crystals by means of the pulse-echo supersonic method. In this method, short supersonic pulses travel the bulk of the ice crystal and the corresponding transit time is measured. The ratio of the path length to the transit time yields the velocity of sound within the ice. The characteristic elastic constants were calculated from the velocity of sound and the desity of ice.

Dantl (1969) investigated the dependence of the characteristic elastic constants on the frequency over a range of 5 to 190 MHz. Within the experimental accuracy, no frequency dependence was observed. The dependency of the characteristic elastic constants on temperature was determined at 30 MHz (for

longitudinal waves) and 28.75 MHz (for transversal waves) over a range of 0 to -140°C in intervals of 5°C. The results showed that the elastic constants vary as function of temperature:

$$S_{ij} = S^{o}_{ij} \left[1 + a.T + b.T^2\right] \tag{4.2a}$$

$$C_{ij} = C^{o}_{ij} \left[1 + \bar{a}.T + \bar{b}.T^2\right] \tag{4.2b}$$

where the S_{ij}'s and the C_{ij}'s are the five independent elements of the matrices S_{ij} and C_{ij}, respectively. These elements are those corresponding to a given temperature, T. The S^{o}_{ij}'s and C^{o}_{ij}'s are the values of S_{ij}'s and C_{ij}'s corresponding to the melting temperature, T_m. The numerical values of S^{o}_{ij}'s, and C^{o}_{ij}'s and the constants a, b, $\bar{a}$, and $\bar{b}$ are given in Tables 4.1 and 4.2.

Table 4.1: Values of S^{o}_{ij} and the parameters a and b for the five non-zero compliancies (Dantl, 1969)

S_{ij} (1/MPa)	S^{o}_{ij} (1/MPa)	a	b	Error (%)
S_{11}	10.40×10^{-11}	1.070×10^{-3}	1.87×10^{-6}	$\mp$ 1
S_{33}	8.48×10^{-11}	1.405×10^{-3}	4.66×10^{-6}	$\mp$ 1
S_{44}	33.42×10^{-11}	1.505×10^{-3}	4.04×10^{-6}	$\mp$ 1
S_{12}	-4.42×10^{-11}	0.463×10^{-3}	-2.06×10^{-6}	$\mp$ 6
S_{13}	-1.89×10^{-11}	1.209×10^{-3}	6.15×10^{-6}	$\mp$ 20

Table 4.2: Values of C^{o}_{ij} and the parameters $\bar{a}$ and $\bar{b}$ for the five non-zero stiffness constants (Dantl, 1969)

C_{ij} (1/MPa)	C^{o}_{ij} (1/MPa)	$\bar{a}$	$\bar{b}$	Error (%)
C_{11}	12.904×10^{-11}	-1.489×10^{-3}	-1.85×10^{-6}	$\bar{+}0.3$
C_{33}	14.075×10^{-11}	-1.629×10^{-3}	-2.93×10^{-6}	$\bar{+}0.4$
C_{44}	2.819×10^{-11}	-1.601×10^{-3}	-3.62×10^{-6}	$\bar{+}0.7$
C_{12}	6.487×10^{-11}	-2.072×10^{-3}	-3.62×10^{-6}	$\bar{+}2.0$
C_{13}	5.622×10^{-11}	-1.874×10^{-3}	0.000	$\bar{+}7.0$

4.4 Practical Elastic Moduli for Polycrystalline Ice

For a general 3-D anisotropic case, the elastic stress strain relation is given as:

$$\begin{vmatrix} \varepsilon_x \\ \varepsilon_y \\ \varepsilon_z \\ \gamma_{xy} \\ \gamma_{zx} \\ \gamma_{zy} \end{vmatrix} = \begin{vmatrix} 1/E_x & -\upsilon_{yx}/E_y & -\upsilon_{zx}/E_z & 0 & 0 & 0 \\ -\upsilon_{xy}/E_x & 1/E_y & -\upsilon_{zy}/E_z & 0 & 0 & 0 \\ -\upsilon_{xz}/E_x & -\upsilon_{yz}/E_y & 1/E_z & 0 & 0 & 0 \\ 0 & 0 & 0 & 1/G_{xy} & 0 & 0 \\ 0 & 0 & 0 & 0 & 1/G_{zx} & 0 \\ 0 & 0 & 0 & 0 & 0 & 1/G_{zy} \end{vmatrix} \begin{vmatrix} \sigma_x \\ \sigma_y \\ \sigma_z \\ \tau_{xy} \\ \tau_{zx} \\ \tau_{zy} \end{vmatrix} \tag{4.3}$$

The coordinate system <xyz> is presented in Fig. E.1a. For columnar grained ice, the columns are in the vertical direction (O-Z direction, Figs. E.1c, and E.1d).

For hexagonal crystals, both Young's modulus and shear modulus are determined from the characteristic compliancies (S_{ij}'s) and Euler transformations (Nowick and Berry 1972):

$$E^{-1} = (1 - l_3^2)^2 S_{11} + l_3^4 S_{33} + l_3^2(1 - l_3^2)(2S_{13} + S_{44}) \qquad (4.4a)$$

$$G^{-1} = S_{44} + (S_{11} - S_{12} - 0.5\, S_{44})(1 - l_3^2) +$$

$$+ \quad 2(S_{11} + S_{33} - 2\, S_{13} - S_{44})\, l_3^2(1 - l_3^2) \qquad (4.4b)$$

where l_3 = cos ø; ø is the angle between any arbitrary direction and the c-axis of the crystal.

Since both E and G (in Eqs. 4.4a and 4.4b) depend on the orientation of the c-axis of the crystals in the <xyz> coordinate system, the practical elastic moduli are discussed, in the following subsections, separately for each ice type. The equations for the practical elastic moduli are derived with respect to the horizontal and the vertical planes. In the coordinate system <xyz>, Fig. E.1a, the horizontal plane corresponds to the plane xoy while the vertical plane corresponds to the planes xoz and yoz.

4.4.1 Columnar Grained S-1 Ice

In S-1 ice, the c-axis tends to be vertical, Fig. E.1c. In the vertical plane, the values of $E^{s-1}_{(v)}$ and $G^{s-1}_{(v)}$ are calculated from Eqs. 4.4a and 4.4b for $l_3 = 1$. In the horizontal plane, however, $E^{s-1}_{(h)}$ and $G^{s-1}_{(h)}$ are those corresponding to $l_3 = 0$.

Sinha (1989a) calculated both E and G using Eqs. 4.4a, 4.4b, and Dantl's data (Table 4.1). He suggested the following equations for both E and G in the horizontal plane:

$$E^{s-1}_{(h)T} = 9.61 + 1.1\ 10^{-2}\ (T_m - T) \quad \text{(GPa)} \tag{4.5a}$$

$$G^{s-1}_{(h)T} = 3.17 + 4.1\ 10^{-3}\ (T_m - T) \quad \text{(GPa)} \tag{4.5b}$$

In this thesis, similar calculations to those of Sinha's (1989a) are performed to formulate equations for both E and G in the vertical plane:

$$E^{s-1}_{(v)T} = 11.8 + 1.43\ 10^{-2}\ (T_m - T) \quad \text{(GPa)} \tag{4.6a}$$

$$G^{s-1}_{(v)T} = 3.00 + 4.1\ 10^{-3}\ (T_m - T) \quad \text{(GPa)} \tag{4.6b}$$

The values of Poisson's ratio (in both horizontal and vertical planes) are calculated by using the bulk modulus, B_m, and the compressibility coefficient, K_c:

$$K_c = \frac{1}{B_m} = S_{iijj} \tag{4.7}$$

where S_{iijj} is the second invariant of the characteristic elastic compliancies (Nye, 1985).

From the elastic relations, the values of Poisson's ratio (in the horizontal and vertical planes) are given as:

$$\upsilon^{s-1}_{(h)T} = \frac{1}{2}\left\{1 - \frac{E^{s-1}_{(h)T}}{3\ B}\right\} \tag{4.8a}$$

$$\upsilon^{s-1}_{(v)T} = \frac{1}{2}\left\{ 1 - \frac{E^{s-1}_{(v)T}}{3\ B} \right\} \qquad (4.8b)$$

Using Eqs. 4.4a, 4.7, 4.8a, 4.8b, and Dantl's data (Table 4.1), the following equations are proposed for Poisson's ratio in the horizontal and vertical planes:

$$\upsilon^{s-1}_{(h)T} = 0.308 + 1.03\ 10^{-4}\ (T_m - T) \qquad (4.9a)$$

$$\upsilon^{s-1}_{(v)T} = 0.275 + 8.60\ 10^{-5}\ (T_m - T) \qquad (4.9b)$$

For temperature of -10°C, equations 4.9a and 4.9bb predict values of 0.309 and 0.276 for $\upsilon^{s-1}_{(h)}$ and $\upsilon^{s-1}_{(v)}$, respectively. For temperature of -20°C, values of 0.31 for $\upsilon^{s-1}_{(h)}$ and 0.277 for $\upsilon^{s-1}_{(v)}$ are predicted. These predictions agree well with the measured values of Poisson's ratio as it will be shown later.

Figure E.2 shows the variation of Young's modulus, shear modulus, and Poisson's ratio (for S-1 ice) with temperature. In the range of 0°C to -60°C, the values of $E^{s-1}_{(h)}$ and $E^{s-1}_{(v)}$ increase by about 7 percent, the values $G^{s-1}_{(h)}$ and $G^{s-1}_{(v)}$ increase by about 8 percent, and the values $\upsilon^{s-1}_{(h)}$ and $\upsilon^{s-1}_{(v)}$ increase by about 2 percent. Obviously, the increase of the practical elastic moduli for ice with the decrease of temperature is very small. Measurements by Yamaji and Kuroiwa (1958), temperature range of 0°C to -100°C, and Gold (1958) in the range of -5°C to -40°C indicate that Young's modulus for ice vary very little (few percent) with temperature.

4.4.2 Columnar Grained S-2 Ice

In S-2 ice, the c-axis is in the horizontal plane, Fig. E.1d. In the vertical plane ($l_3 = 0$), both $E^{s-2}_{(v)}$ and $G^{s-2}_{(v)}$ are calculated from Eqs. 4.4a and 4.4b, respectively.

$$E^{s-2}_{(v)T} = E^{s-1}_{(h)T} = \text{Eq. 4.5a} \qquad \text{and} \qquad G^{s-2}_{(v)T} = G^{s-1}_{(h)T} = \text{Eq. 4.5b}$$

In the horizontal plane, the c-axes are randomly oriented. Sinha (1989a) suggested the following equations:

$$E^{s-2}_{(h)T} = 9.39 + 1.30\ 10^{-2}\ (T_m - T) \qquad \text{(GPa)} \qquad (4.10a)$$

$$G^{s-2}_{(h)T} = 3.37 + 4.70\ 10^{-3}\ (T_m - T) \qquad \text{(GPa)} \qquad (4.10b)$$

Equations for Poisson's ratio (for S-2 ice, in the horizontal and vertical planes) are formulated by using Eqs. 4.5a, 4.10a, 4.7, 4.8a, and 4.8b:

$$\upsilon^{s-2}_{(v)T} = \upsilon^{s-1}_{(h)T} = \text{Eq. 4.9a}$$

$$\upsilon^{s-2}_{(h)T} = 0.313 + 3.80\ 10^{-5}\ (T_m - T) \qquad (4.11)$$

For temperature of -10°C, equations 4.11a and 4.11b predict values of 0.309 and 0.313 for $\upsilon^{s-2}_{(v)}$ and $\upsilon^{s-2}_{(h)}$, respectively. For temperature of -20°C, values of 0.31 for $\upsilon^{s-2}_{(v)}$ and 0.314 for $\upsilon^{s-2}_{(h)}$ are predicted.

Figure E.3 shows the variation of Young's modulus, shear modulus, and Poisson's ratio (for S-2 ice) with temperature.

4.4.3 Granular Isotropic Ice

Macroscopically, granular ice is isotropic. The c-axes of its crystals are randomly oriented in all directions, Fig. E.1b. For isotropic materials, the elastic stress-strain relationship is given as:

$$\begin{vmatrix} \varepsilon_x \\ \varepsilon_y \\ \varepsilon_z \\ \gamma_{xy} \\ \gamma_{zx} \\ \gamma_{zy} \end{vmatrix} = \begin{vmatrix} 1/E & -\upsilon/E & -\upsilon/E & 0 & 0 & 0 \\ -\upsilon/E & 1/E & -\upsilon/E & 0 & 0 & 0 \\ -\upsilon/E & -\upsilon/E & 1/E & 0 & 0 & 0 \\ 0 & 0 & 0 & 1/G & 0 & 0 \\ 0 & 0 & 0 & 0 & 1/G & 0 \\ 0 & 0 & 0 & 0 & 0 & 1/G \end{vmatrix} \begin{vmatrix} \sigma_x \\ \sigma_y \\ \sigma_z \\ \tau_{xy} \\ \tau_{zx} \\ \tau_{zy} \end{vmatrix} \qquad (4.12)$$

For isotropic polycrystalline materials, equations for E, G, and υ were given by Hirth and Lothe (1968):

$$E^{-1} = \frac{1}{15}(2I_1 + I_2) \qquad (4.13a)$$

$$G^{-1} = \frac{1}{15}(6I_1 - 2I_2) \qquad (4.13b)$$

$$\upsilon = \frac{E}{15}(I_1 - 2I_2) \qquad (4.13c)$$

where I_1 and I_2 are the first and 2nd invariants of the characteristic elastic constants, respectively. For a hexagonal system, I_1 and I_2 are given as:

$$I_1 = S_{ijij} = 3S_{11} + S_{33} + S_{44} - S_{12} \qquad (4.14a)$$

$$I_2 = S_{iijj} = 2S_{11} + S_{33} + 2S_{12} + 4S_{13} \qquad (4.14b)$$

Sinha (1989a) calculated E, G and υ using Eqs. 4.13a, 4.13b, 4.13c and Dantl's data (Table 4.1). His calculations resulted in the following equations:

$$E_T = 8.93 + 1.2\ 10^{-2}\ (T_m - T) \quad \text{(GPa)} \tag{4.15a}$$

$$G_T = 3.41 + 4.5\ 10^{-3}\ (T_m - T) \quad \text{(GPa)} \tag{4.15b}$$

$$\upsilon_T = 0.308 + 7.0\ 10^{-5}\ (T_m - T) \tag{4.15c}$$

4.5 Appropriate Averaging Method for Polycrystalline Ice

All equations derived above (for both columnar grained and granular ice) are based on the Reuss' (1929) averaging method. This method is based on the assumption that the stress is the same in all crystals (constant state of stress) and the practical elastic moduli are formulated as function of the characteristic elastic compliancies, S_{ij}. Voigt's (1910) averaging method, however, is based on the assumption that the strain is the same in all crystals (constant state of strain) and the practical elastic moduli are formulated as function of the characteristic elastic stiffness coefficients, C_{ij}. Hill (1952) suggested that an arithmetic or a geometric mean of the two methods (Voigt and Reuss methods) should be taken.

In the following, the efforts are made to asses which averaging method is appropriate for polycrystalline ice. Equations for the practical elastic moduli (for granular ice) are developed using three averaging methods. These are Reuss, Voigt, and Hill's methods. These equations are used to predict the values of Young's modulus and Poisson's ratio for granular ice, and the predictions are compared with some measurements.

Reuss method: The equations for E, G, and υ for granular ice were given by Sinha (1989a) (Eqs. 4.15a, 4.15b, and 4.15c).

Voigt method: For isotropic material, the equations for E, G, and υ were given by Hirth and Lothe (1968):

$$E_T^V = \frac{I_{2c}(3I_{1c} - I_{2c})}{3\,(I_{1c} + 3\,I_{2c})} \qquad (4.16a)$$

$$G_T^V = \frac{1}{30}\,(3I_{1c} - I_{2c}) \qquad (4.16b)$$

$$\upsilon_T^V = \frac{(2I_{2c} - I_{1c})}{(I_{1c} + 3\,I_{2c})} \qquad (4.16c)$$

where the letter V (in Eqs. 4.16) is used to refer to Voigt method. Both I_{1c} and I_{2c} are the first and second invariant of the characteristic stiffness coefficients:

$$I_{1c} = C_{ijij} = 3C_{11} - C_{12} + C_{33} + 4\,C_{44} \qquad (4.17a)$$

$$I_{2c} = C_{iijj} = 2C_{11} + C_{33} + 2C_{12} + 4\,C_{13} \qquad (4.17b)$$

Equations for the practical elastic moduli (E, G, and υ) for granular ice are obtained by using Eqs. 4.16a, 4.16b, 4.16c, 4.17a, 4.17b, and Dantl's data (Table 4.2):

$$E_T^V = 6.47 + 7.0\ 10^{-3}\ (T - T_m) \quad \text{(GPa)} \qquad (4.18a)$$

$$G_T^V = 2.40 + 2.44\ 10^{-3}\ (T - T_m) \quad \text{(GPa)} \qquad (4.18b)$$

$$\upsilon_T^V = 0.345 + 8.1\ 10^{-5}\ (T - T_m) \qquad (4.18c)$$

Hill's (1952) method: Hill's (1952) arithmetic mean yields:

$$E_T^a = 7.71 + 8.8\ 10^{-3}\ (T - T_m) \quad \text{(GPa)} \qquad (4.19a)$$

$$G_T^a = 2.91 + 3.2\ 10^{-3}\ (T - T_m) \quad \text{(GPa)} \qquad (4.19b)$$

$$\upsilon_T^a = 0.327 + 7\ 10^{-5}\ (T - T_m) \qquad (4.19c)$$

where the superscript a (in Eqs. 4.19) refers to "average".

Values of E, G, and υ obtained by using all three averaging methods (over a temperature range of $0^{\circ}C$ to $-60^{\circ}C$) are plotted together in Fig E.4.

Sinha (1978b) presented experimental results for Young's modulus obtained from creep tests carried out on columnar grained S-2 ice samples, loaded in the direction normal to the length of the columns. He obtained values for E (in the horizontal plane) between 9.1 GPa and 9.8 GPa at temperatures between $-40^{\circ}C$ and $-45^{\circ}C$, with an average of 9.3 GPa. He indicated that his values are in the same range as the values of Young's modulus (for fresh water polycrystalline ice) measured by Yamaji and Kuroiwa (1958) using high frequency sonic methods over a range of temperature of $0^{\circ}C$ to $-100^{\circ}C$.

Values of Poisson's ratio in the range of 0.31 to 0.37 for fresh water ice were tabulated by Gold (1958). Lin'Kov's (1958) in-situ seismic measurements (sea ice) ranged from 0.36 to 0.39. Langleben and Pounder (1963) reported a dynamic (seismic) value of 0.29 for sea ice. Sinha (1987b) indicated that, irrespective of ice type, there is only a little discrepancy in the reported dynamic (seismic) measurements of υ.

Values of Young's modulus are calculated using three averaging methods (Eqs. 4.15a, 4.18a, and 4.19a) for temperature of -40°C. The computed values of E are presented together with Sinha's (1987b) data in Table 4.3. Also, a comparison between the computed and observed values of Poisson's ratio is included in Table 4.3.

The comparisons presented in Table 4.3 indicate that the equations based on the Reuss method predict well the measured values of Young's modulus. However, all three averaging methods yield acceptable predictions for Poisson's ratio. Judging from the predictions of Young's modulus, it is concluded that the Reuss averaging method is the appropriate one for polycrystalline ice.

Table 4.3: Comparison between measured and calculated values of Young's modulus, E, and Poisson's ratio, υ.

	Reuss	Voigt	Hill	Experimental
E	9.41 (GPa)	6.75 (GPa)	8.06 (GPa)	9.1 - 9.8 (average is 9.3 GPa) T = -40°C to -45°C (Sinha, 1978b)
υ	0.308 (-10°C)	0.346 (-10°C)	0.327 (-10°C)	0.31 - 0.37 (Gold, 1958) 0.31 - 0.32 (Sinha, 1988b) 0.29 (Langleben & Pounder, 1963)

CHAPTER 5

FORMULATION OF THE NON-CRACKING MODEL

5.1 Introduction

The objective of this chapter is to present a mathematical model for fresh water granular and columnar grained (S-1 and S-2) polycrystalline ice undergoing creep deformations for non-cracking conditions. The formulation of the model is based on the analysis of the experimental results presented previously in Chapter 3. The model describes the non-linearity, elasto-plasticity, time and temperature dependency, and material anisotropy of polycrystalline ice subjected to three dimensional loading conditions.

5.2 Basic Formulation

Ice undergoes both elastic and plastic deformations simultaneously upon loading. The total strain is viewed as the sum of an instantaneous elastic strain, ε_e, a visco-plastic strain (time dependent permanent strain), ε_p, and a visco-elastic strain (time dependent recoverable strain), ε_{ve}.

$$\varepsilon_t = \varepsilon_e + \varepsilon_p + \varepsilon_{ve} \tag{5.1}$$

The formulations of these strain components are given in the following sections.

5.3 Instantaneous Elastic Strains

The instantaneous elastic behaviour of polycrystalline ice represents an average elastic behaviour of single ice crystals. The latter, however, results from the lattice deformation. The generalized Hooke's law is used to relate the strains to the stresses. The stress-strain relations are given in Chapter 4.

5.4 Visco-Plastic Strains

The stress parameters used in the following formulations are the shear stress, q, and the hydrostatic pressure, p. The stress and strain invariants used in this thesis are presented in Appendix B.

The visco-plastic strains result from intra-crystalline deformation processes, particularly the movement of dislocations. The formulation of ε_p (Eq. 5.1) is based on the classical theory of plasticity. A brief review of the classical theory of plasticity is given in Appendix C to provide the necessary theoretical background needed for the formulation of the present model.

5.4.1 General Visco-Plastic Stress-Strain Relationship

The plastic work, dW^p, done per unit volume on a material during a plastic strain increment, $d\varepsilon^p_{ij}$, was given by (Hill, 1950):

$$dW^p = \sigma_{ij}\, d\varepsilon^p_{ij} \tag{5.2}$$

The experimental results shown in Figs. F.1, F.2, and F.3, indicate that under constant loading, ice undergoes continuous plastic creep deformation with a constant rate of straining. Therefore, in order to accommodate the concept of the plastic work (Eq. 5.2) to describe such a behaviour, it is necessary to introduce a concept relating the plastic work to the rate of the plastic strains, $\dot{\varepsilon}^p_{ij}$. The following equation is used:

$$\dot{W}^P = \sigma_{ij}\, \dot{\varepsilon}^p_{ij} \tag{5.3}$$

where $\dot{W}^p$ is the plastic power which is defined as the work done per unit volume on a material undergoing plastic creep deformation for a unit time of loading.

As shown in Fig. F.4, the relation between the applied external stresses and their corresponding (measured) plastic power can be described as:

$$\dot{W}^P = \sigma\, \dot{\varepsilon}^p = \alpha_p \exp(\beta_p\, \sigma) \tag{5.4}$$

where ($\alpha_p = 4.4 \times 10^{-9}$ MPa/sec) and ($\beta_p = 3.7$ MPa^{-1}) are material constants.

Equation 5.4 indicates that for a given state of stress and plastic strain, an equilibrium mechanical plastic state is achieved if the following condition is satisfied.

$$\alpha_p\, t \exp(\beta_p\, \sigma) - W^P = 0 \tag{5.5}$$

In a general form, equation 5.5 can be rewritten as:

$$F = f(\sigma_{ij}, t) - H^*(W^p) = 0 \qquad (5.6)$$

where $f = f(\sigma_{ij}, t)$ can be viewed as a loading function, and $H^*(W^p)$ is a hardening parameter which is a function of the plastic work in agreement with the work hardening hypothesis in the classical theory of plasticity.

The hardening parameter, $H^*(W^p)$, can be expressed as a function of the stress and the plastic strains. Thus, Eq. 5.6 becomes:

$$F = f(\sigma_{ij}, t) - H(\sigma_{ij}, \varepsilon^p_{ij}) = 0 \qquad (5.7a)$$

The formulation of the present model is independent of the plastic volumetric strains (the reasons are explained below). Hence, Eq. 5.7a can be rewritten as:

$$F = f(\sigma_{ij}, t) - H(\sigma_{ij}, \bar{\varepsilon}^p) = 0 \qquad (5.7b)$$

where $\bar{\varepsilon}^p$ is the generalized plastic shear strain (Appendix B).

A plastic potential function, g, of an exponential form is proposed as follows:

$$g = g(\sigma_{ij}) = \alpha_p \exp(\beta_p \sigma_{ij}) \qquad (5.8)$$

Thus, equation 5.7b becomes:

$$F = g(\sigma_{ij}).t - H(\sigma_{ij}, \bar{\varepsilon}^p) = 0 \qquad (5.9)$$

According to the normality rule of plasticity (Eq. C.1, in Appendix C), the plastic strain increment is expressed as:

$$d\varepsilon^p_{ij} = \Lambda \frac{\partial g}{\partial \sigma_{ij}} \tag{5.10}$$

where Λ is a positive scalar factor of proportionality.

The plastic strain increment ($d\varepsilon^p_{ij}$) is decomposed into a plastic shear strain increment (de^p_{ij}) and a plastic volumetric strain increment ($d\varepsilon^p_v$):

$$d\varepsilon^p_{ij} = de^p_{ij} + \frac{1}{3}\delta_{ij}(d\varepsilon^p_{ii}) = de^p_{ij} + \frac{1}{3}(d\varepsilon^p_v) \tag{5.11}$$

where δ_{ij} is the Kronecker delta.

A mathematical expression for $d\varepsilon^p_v$ (in Eq. 5.11) is derived from the normality condition (Eq. 5.10) as:

$$d\varepsilon^p_v = d\varepsilon^p_{ii} = \Lambda \frac{\partial g}{\partial p} \tag{5.12}$$

The expression for de^p_{ij} is obtained from Eqs. 5.10, 5.11 and 5.12:

$$de^p_{ij} = d\varepsilon^p_{ij} - \frac{1}{3}\delta_{ij}(d\varepsilon^p_{ii}) = \Lambda \frac{\partial g}{\partial \sigma_{ij}} - \frac{1}{3}\delta_{ij}\Lambda \frac{\partial g}{\partial p} \tag{5.13}$$

The value of $\partial g/\partial \sigma_{ij}$ (in Eq. 5.13) is given as:

$$\frac{\partial g}{\partial \sigma_{ij}} = \frac{\partial g}{\partial p}\frac{\partial p}{\partial \sigma_{ij}} + \frac{\partial g}{\partial q}\frac{\partial q}{\partial \sigma_{ij}} \tag{5.14}$$

It was concluded (in Chapter 3) that there is no plastic volumetric strains developed in the material during testing. The condition of zero volumetric plastic strains is satisfied as follows:

$$d\varepsilon_v^p = d\varepsilon_{ii}^p = \Lambda \frac{\partial g}{\partial p} = 0. \qquad (5.15)$$

Since Λ is a positive quantity, the value $(\partial g/\partial p)$ should be zero. Therefore, Eq. 5.13 takes the following form:

$$de_{ij}^p = \Lambda \frac{\partial g}{\partial \sigma_{ij}} = \Lambda \frac{\partial g}{\partial q} \frac{\partial q}{\partial \sigma_{ij}} \qquad (5.16)$$

The parameter Λ (Eq. 5.16) is determined from the normality and consistency conditions. The later, however, dictates that the condition required by the equilibrium of the mechanical plastic state (in Eq. 5.7) must be satisfied as long as the material is in plastic state:

$$dF = \frac{\partial f}{\partial \sigma_{ij}} d\sigma_{ij} + \frac{\partial f}{\partial t} dt - \frac{\partial H}{\partial \sigma_{ij}} d\sigma_{ij} - \frac{\partial H}{d\bar{\varepsilon}^p} d\bar{\varepsilon}^p = 0. \qquad (5.17)$$

In the present study, it is assumed that there is no effect of the hydrostatic pressure on the plastic strains. On the basis of laboratory experiments, Rigsby (1958) reported that the plastic deformation in single ice crystals is independent of the hydrostatic pressure. The effect of the hydrostatic pressure on the creep rate of polycrystalline ice, however, was investigated by Haefeli et al. (1968) who carried

out compressive creep tests with a 30 MPa superimposed hydrostatic pressure. They showed that the hydrostatic pressure increased the creep rate. Simonson et al. (1975) carried out triaxial tests on ice samples (temperature of $-10^{\circ}C$), and they reported a decrease in the strength of ice with the increase of the confining pressure. Jones (1978, 1982) investigated the effect of confining pressure on the compressive behaviour of polycrystalline (granular) ice over a wide range of strain rates (10^{-7} to 10^{-1} sec^{-1}) and with confining pressures ranging from 0.1 to 85 MPa (temperature of $-11^{\circ}C$). His results indicated that, at high strain rates, the strength of ice increases at low confining pressures and decreases at high confining pressures. Nadreau and Michel (1986a) reported that, for confining pressures of 20 to 40 MPa, the maximum deviatoric stress increases with the increase of the strain rate.

In this thesis, as indicated earlier, the plastic (intragranular) deformation of ice crystals are induced by microstructure dependent mechanisms, particularly the movement of dislocations. The conclusion of Rigsby's (1958) experimental work on single ice crystals is considered. His results are those corresponding to single ice crystals which are independent of the effect of the hydrostatic pressure on the grain boundary sliding as well as grain boundary cracking.

The condition that no plastic strains can be generated by the hydrostatic pressure dictates that Eq. 5.17 should be reduced to:

$$dF = \frac{\partial f}{\partial q} dq + \frac{\partial f}{\partial t} dt - \frac{\partial H}{\partial q} dq - \frac{\partial H}{d\bar{\varepsilon}^{p}} d\bar{\varepsilon}^{p} = 0 \qquad (5.18)$$

From the normality rule of plasticity, Eq. 5.10, the plastic shear strain increment, $d\bar{\varepsilon}^p$, is expressed as:

$$d\bar{\varepsilon}^p = \Lambda \frac{\partial g}{\partial q} \tag{5.19}$$

The scalar Λ is determined from Eqs. 5.18 and 5.19:

$$\Lambda = \frac{\frac{\partial f}{\partial q} dq + \frac{\partial f}{\partial t} dt - \frac{\partial H}{\partial q} dq}{\frac{\partial H}{\partial \bar{\varepsilon}^p} \frac{\partial g}{\partial q}} \tag{5.20}$$

By substituting Eq. 5.20 into Eq. 5.10, the plastic strain increment is given as follows:

$$d\varepsilon^p_{ij} = \frac{\frac{\partial f}{\partial q} dq + \frac{\partial f}{\partial t} dt - \frac{\partial H}{\partial q} dq}{\frac{\partial H}{\partial \bar{\varepsilon}^p} \frac{\partial g}{\partial q}} \frac{\partial g}{\partial \sigma_{ij}} \tag{5.21}$$

5.4.2 Simplification for Constant Loading Condition

Equation 5.21 is a general visco-plastic stress strain relationship. It can be applied to model the behaviour of ice subjected to any loading conditions. However, for ice undergoing visco-plastic deformations under constant loading, dq = 0, equation 5.21 is simplified to:

$$\varepsilon^{p}_{ij} = \frac{3}{2}\, t\, \frac{\alpha_p \exp(\beta_p . q)}{(q)^2}\, S_{ij} \qquad (5.22)$$

Equation 5.22 is valid, only, for isotropic materials. Macroscopically, granular ice is isotropic, and therefore, Eq. 5.22 can be used to describe its visco-plastic behaviour. However, columnar structured ice is an anisotropic material. This material anisotropy should be taken into consideration. The following subsection presents a generalization of Eq. 5.22 to include the effect of the material anisotropy on the visco-plastic behaviour of columnar grained ice.

5.4.3 Effect of Material Anisotropy on the Visco-Plastic Strains

Ice is a cross anisotropic material. Its plane of isotropy is the basal plane. Sinha (1987a) reported that at high temperature, a single crystal of ice deforms, when loaded, primarily by slip on the basal plane because non-basal slip is significantly more difficult. Steinemann (1954), Glen and Perutz (1954), and Nakaya (1958) have observed that slip occurs predominantly on the basal plane and no evidence has been found of slip on the prismatic plane.

For polycrystalline columnar grained S-1 ice, the c-axes of the crystals tend to be vertical. As shown in Fig. E.1c, the c-axes are in the long direction of the grains. Since ice crystals deform primarily by slip on the basal plane, the deformation of this type of ice (S-1 ice) is two dimensional. The plastic deformation in the long direction of the columns is considered to be zero, $\varepsilon^{p}_{3} = 0$.

For polycrystalline columnar grained S-2 ice, the results of the creep tests (given in Chapter 3) showed that the samples undergo very small (negligible) plastic deformations in the direction parallel to the columns, and hence, it was concluded (in Chapter 3) that the plastic strain in the long direction of the columns is practically zero, $\varepsilon_3^p = 0$.

For columnar grained S-2 ice, Gold (1963, 1972b) reported that the resolved shear stress on the basal plane in the long direction of the grains tends to be zero. Consequently, the deformation of this type of ice (columnar grained S-2 ice) is essentially two dimensional. The deformation in the long direction of the grains is much smaller than perpendicular to it for at least 2% axial strain. This is in agreement with the results of the creep tests given in Chapter 3 for non-cracking condition (very small amount of deformation is generated in the long direction of the grains).

Gold (1963) indicated that a combination of the geometric configuration of the grains and the applied stress resulted in very small deformations in the long direction of the grains. Each grain had only one independent slip system for deformation when the load was applied. This system operated in the basal plane in the direction perpendicular to the long axis of the grains. Some grains had no operative slip plane, and they were oriented so that their basal planes were either parallel or perpendicular to the principal stress axes. These grains are considered to be "**hard sites**" within the aggregate. Their neighbouring grains must deform around these hard sites. Upon loading, the material tends to flow away from these hard sites in the direction perpendicular to the applied stress.

In this thesis, for mathematical modelling purposes, columnar grained (S-1 and S-2) ice is considered to undergo plastic deformations only on the basal plane in the direction perpendicular to the long axes of the grains, and no plastic strains can be induced in any other plane. This anisotropy is included in the model formulation as:

$$\varepsilon^{p}_{ij} = \frac{3}{2}\, t\, \frac{\alpha_p \exp(\beta_p . \bar{q})}{(\bar{q})^2}\, \bar{S}_{ij} \qquad (5.23)$$

where $\bar{q}$ and $\bar{S}_{ij}$ are the shear stress and the deviatoric stress tensor for an anisotropic material, respectively. The development of the mathematical equations for both $\bar{q}$ and $\bar{S}_{ij}$ are given in Appendix B.

5.4.4 Effect of Temperature on the Visco-Plastic Strains

Creep of polycrystalline materials involves thermally activated processes, and show a rate dependency on temperature (Garafalo, 1965). For polycrystalline ice, the temperature dependence of the steady state creep rate, $\dot{\varepsilon}_{st}$, has been commonly represented after Glen (1955):

$$\dot{\varepsilon}_{st} = A_{st} \exp(-Q/RT) \qquad (5.24a)$$

where the subscript st is used to indicate the steady state. The parameter A_{st} is a constant for a given stress, Q and R are the activation energy and gas constant, respectively.

Sinha (1978b) formulated a shift function ($S_{1,2}$, Eq. 2.7) to model the variation of both delayed elastic and viscous creep strains with temperature. He obtained the same activation energy value for both delayed elastic and viscous creep strains.

In this thesis, Sinha's (1978b) shift function (Eq. 2.7) is used to model the variation of the visco-plastic strains (ε_p, Eq. 5.23) with temperature. The dependency of the visco-plastic strain rate on temperature is expressed as:

$$\ln S_{1,2} = \ln (\dot{\varepsilon}_p^{(T2)} / \dot{\varepsilon}_p^{(T1)}) = \frac{Q}{R} \left(\frac{1}{T_1} - \frac{1}{T_2}\right) \qquad (5.24b)$$

where $\dot{\varepsilon}_p^{(T1)}$ and $\dot{\varepsilon}_p^{(T2)}$ are the visco-plastic strain rates at temperatures T_1 and T_2, respectively.

Substituting the visco-plastic strain rates, $\dot{\varepsilon}_p$ (obtained from Eq. 5.23) into Eq. 5.24b, the parameter α_p can be expressed as follows:

$$\alpha_p(T_2) = \alpha_p(T_1) . \exp\left[\frac{Q}{R}\left(\frac{1}{T_1} - \frac{1}{T_2}\right)\right] \qquad (5.24c)$$

where $\alpha_p(T_1)$ and $\alpha_p(T_2)$ are the values of α_p(in Eq. 5.23) at temperatures T_1 and T_2, respectively. The value of α_p (T_1) for temperature $T_1 = 263^{\circ}K$ is $4.4\ 10^{-9}$ MPa/sec (Eq. 5.4).

5.5 Visco-Elastic Strains

5.5.1 Source of the Visco-Elastic Strains

During creep of polycrystalline materials, the interaction between adjacent grains generates intergranular deformation (ε_{ve}, in Eq. 5.1) which adds to the instantaneous elastic, ε_e, and visco-plastic, ε_p, strains as far as the external measurements are concerned. Zener (1941, 1948) offered a physical explanation for the grain boundary sliding process. He argued that the sliding of a given crystal over another evokes an elastic deformation at the ends of the adjoining grains. This elastic deformation, however, develops a back stress opposing the movement of the sliding. The back stress continues to build up in the form of stored elastic energy as the sliding of the grain boundaries continues. When the back stress reaches the magnitude of the imposed stress, the sliding stops. Therefore, the strain rate due to the grain boundary sliding is a decreasing one. Upon removing the external load, the back stress (stored energy) reverses the process of sliding and drives back the boundaries towards their initial positions. Thus, the strains generated by the grain boundary sliding are elastic (recoverable).

5.5.2 Effect of Plastic Deformation on Grain Boundary Sliding

For polycrystalline metals, Garofalo (1965) stated that sliding of the grain boundaries is induced to accommodate the plastic (intra-granular) deformations. A similar argument was offered by McLean and Farmer (1956), and Martin et al. (1957) who observed that a sudden structural change within copper and

β-brass crystals coincided with a sudden change in the rate of the grain boundary sliding. Therefore, it was concluded that the grain boundary sliding is a deformation process controlled by the plastic (intra-granular) deformation.

5.5.3 Non-Uniformity of the Grain Boundary Sliding

For polycrystalline metals, Conrad (1961) reported that, at early stages of loading, uniform grain boundary sliding occurs in the immediate vicinity of the boundaries. With time, sliding takes place in larger zones around the boundaries, and it becomes gradually non-uniform.

In the present study, it is assumed that two ice crystals do not slide over each other uniformly. This stems from the fact that, at the time of sliding, each crystal is undergoing intra-granular (visco-plastic) deformations of its own. These plastic deformations are not necessarily the same in both crystals, resulting in different deformations on the two sides of the boundary. Thus, it is hypothesized, that the non-uniformity of the plastic deformations results in a non-uniform grain boundary sliding. However, at early stages of loading when the visco-plastic deformations are not significant, uniform grain boundary sliding takes place.

5.5.4 Formulation of the Visco-Elastic Strains

During creep deformation, with time, the plastic strains accumulate, and subsequently ice crystals undergo structural changes. These structural changes affect the magnitude of the grain boundary sliding and, consequently, the visco-elastic

behaviour of the material. The following equation is proposed for the calculation of the visco-elastic strain, ε_{ve}:

$$\varepsilon_{ve} = (1 + \Delta\lambda)\ \varepsilon_{rv} \tag{5.25}$$

where $\Delta\lambda$ is a structural change function, ε_{rv} is the reference visco-elastic strains. It is defined as follows:

The reference visco-elastic strain is the visco-elastic strain generated in the material without the influence of the structural changes induced by the intra-granular deformations:

$$\varepsilon_{rv} = C_o\ (e_{ij}) \left\{ 1 - \exp \left[-(a_T\ t)^b \right] \right\} \tag{5.26}$$

where $C_o = C_1 d_1/d$. The parameters C_1, d_1, a_T, and b are given in Chapter 2, Table 2.1. The strains e_{ij} are the instantaneous elastic shear strains.

Equation 5.26 is a modified version of Sinha's (1979) equation for the delayed elastic strain (ε_d, in Eq. 2.3). It dictates that the grain boundary sliding generates only visco-elastic shear strains: No visco-elastic volumetric change is generated by the grain boundary sliding. Sinha (1987b, 1988b) indicated that, in the absence of any crack activity, the grain boundary sliding involves no appreciable volume change.

5.5.5 Determination of the Structural Change Function

In order to determine the structural change function ($\Delta\lambda$, Eq. 5.25), the experimental visco-elastic strains generated in the creep tests No. 1, 2, and 3 (Chapter 3) are used. The

values of these (experimental) visco-elastic strains are obtained by using Eq. 5.1:

$$\varepsilon_{ve} = \varepsilon_t - (\varepsilon_e + \varepsilon_p) \tag{5.27}$$

where ε_t and ε_p are the measured total and plastic strains, respectively. The instantaneous elastic strain, ε_e, is calculated from Eq. 2.2 (Chapter 2).

The histories of the visco-elastic strains corresponding to four loading cycles, for each test (creep tests No. 1, 2, and 3) are presented in Figs. F.5a, F.6a, and F.7a. Also, the figures include the calculated reference visco-elastic strain histories. The reference visco-elastic strains were computed, using Eq. 5.26, for an average grain size of 4.5 mm and temperature of -10°C.

The discrepancy between the visco-elastic strains and the reference visco-elastic strains (Figs. F.5a, F.6a, and F.7a) is attributed to the structural changes of the material induced by the visco-plastic strains. The structural change function is, then, determined from Eq. 5.25:

$$\Delta\lambda = \frac{\varepsilon_{ve} - \varepsilon_{rv}}{\varepsilon_{rv}} \tag{5.28}$$

The key hypothesis of the present model is that the structural changes of the material (induced by the visco-plastic strains) influence the magnitude of the grain boundary sliding. The visco-plastic strains, however, are taken as the measure of the structural changes. Therefore, the formulation

of the structural change equations should be made as function of the visco-plastic strains, ε_p.

Taking into account the cyclic loading situations, the structural change equations should be formulated as function of the initial and current visco-plastic strains (ε^p, ε^p_o). Both quantities (ε^p and ε^p_o) are taken as the measures of the initial and current structural states of the material.

$$\Delta\lambda = \Delta\lambda(\varepsilon^p, \varepsilon^p_o) \tag{5.29}$$

The results of the creep experiments, creep tests No. 1, 2, and 3 in Chapter 3, were used to formulate a function relating $\Delta\lambda$ to the visco-plastic strains. This was achieved following two steps:

Step 1: For a given loading cycle (for a given creep test), both ε_{ve} and ε_{rv} were calculated at n time intervals.

Step 2: For each time interval, the values of $\Delta\lambda$ and λ were computed: $\Delta\lambda$'s were calculated using Eq. 5.28, and λ's were calculated according the following summation:

$$\lambda = \sum_{i=1}^{n} \Delta\lambda_i \tag{5.30}$$

where n is the number of the time intervals.

Figures. F.5b, F.6b, and F.7b show plots of λ versus the visco-plastic strain difference ($\varepsilon^p - \varepsilon^p_o$) for various loading cycles, where ε^p_o is the visco-plastic strain at the start of

the loading cycle. An equation is proposed to describe the variation of λ versus $(\varepsilon^p - \varepsilon^p_o)$:

$$\lambda = A\,(\varepsilon^p - \varepsilon^p_o) + \frac{D}{\ln(\varepsilon^p/\varepsilon^p_o)}\,(\varepsilon^p - \varepsilon^p_o) \qquad (5.31)$$

where $(A = 7.5 \times 10^5)$ and $(D = 1.9 \times 10^4)$ are material parameters.

For most loading cycle, in all three creep tests, it was found that the ratio $\frac{\Delta\lambda}{\lambda}$ varies linearly with the inverse of t^{2b}, where t is the loading time, and b = 0.34 is the constant given in Table 2.1.

Figures F.8, F.9, F.10 show plots of $\frac{\Delta\lambda}{\lambda}$ versus $1/t^{2b}$ obtained from the results of the creep tests No.1, 2, and 3, respectively. All plots of $\frac{\Delta\lambda}{\lambda}$ versus t^{2b} (for 12 loading cycles, 3 creep tests) are presented together in Fig. F.11a. It is apparent (From Fig. F.11a) that a unique linear relationship exists between $\Delta\lambda/\lambda$ and t^{2b}. As shown in Fig. F.11b, a linear best-fit curve is obtained for the results presented in Fig. F.11a. This best fit curve is described by the following equation:

$$\frac{\Delta\lambda}{\lambda} = \frac{1}{t^{2b}} \qquad (5.32)$$

Finally, The structural change function, $\Delta\lambda$, is formulated from Eqs. 5.31 and 5.32 as:

$$\Delta\lambda = \frac{A}{t^{2b}}\,(\varepsilon^p - \varepsilon^p_o) + \frac{1}{t^{2b}}\,\frac{D}{\ln(\varepsilon^p/\varepsilon^p_o)}\,(\varepsilon^p - \varepsilon^p_o) \qquad (5.33)$$

So far, the structural change function, Eq. 5.33, is valid only for uniaxial loading conditions. As a consequence of the fact that, during loading, ice undergoes only plastic shear distortions (no plastic volumetric strains), equation 5.33 is generalized to 3-D loading situations as follows:

$$\Delta\lambda = \frac{A}{t^{2b}} (\bar{\varepsilon}^p - \bar{\varepsilon}^p_o) + \frac{1}{t^{2b}} \frac{D}{\ln(\bar{\varepsilon}^p/\bar{\varepsilon}^p_o)} (\bar{\varepsilon}^p - \bar{\varepsilon}^p_o) \qquad (5.34)$$

where $\bar{\varepsilon}^p$ and $\bar{\varepsilon}^p_o$ are the current and initial generalized plastic shear strains, respectively.

5.6 Summary of the Non-Cracking Model Formulation

For no-cracking conditions, the creep behaviour of ice is described as follows:

$$\varepsilon_t = \varepsilon_e + \varepsilon_p + \varepsilon_{ve}$$

where the strain components ε_e, ε_p, and ε_{ve} are the instantaneous elastic, visco-plastic, and visco-elastic strains, respectively. They are given as follows:

Instantaneous Elastic Strains

$$\varepsilon^e_{ij} = s_{ijkl}\, \sigma_{kl}$$

(the formulation of the elastic stress strain relations is given in Chapter 4).

Visco-Plastic Strains

$$\varepsilon^{p}_{ij} = \frac{3}{2}\, t\, \frac{\alpha_p \exp(\beta_p . q)}{(q)^2}\, S_{ij}$$

(the formulation of the visco-plastic strains is given in Section 5.4 of this Chapter).

Visco-Elastic Strains:

$$\varepsilon^{ve}_{ij} = (1 + \Delta\lambda)\; C_o\; (e_{ij}) \left\{ 1 - \exp \left[-(a_T\, t)^b \right] \right\}$$

where $\Delta\lambda$ is given as:

$$\Delta\lambda = \frac{A}{t^{2b}} (\bar{\varepsilon}^p - \bar{\varepsilon}^p_o) + \frac{1}{t^{2b}} \frac{D}{\ln(\bar{\varepsilon}^p / \bar{\varepsilon}^p_o)} (\bar{\varepsilon}^p - \bar{\varepsilon}^p_o).$$

(the formulation of the visco-elastic strains is given in Section 5.5 of this Chapter).

CHAPTER 6

FORMULATION OF THE CRACK-ACTIVITY MODEL

6.1 Introduction

At elevated temperatures, polycrystalline materials, including ice, exhibit pronounced creep deformation and grain boundary embrittlement (Sinha et al., 1987). A consequence of creep deformation is the formation of cavities at the grain boundaries. The growth of the cavities leads to inter-granular fracture (Garafalo, 1965). Several mechanisms have been proposed to explain the cause of inter-granular fracture (Gifkins, 1959). Among these mechanisms are those of Zener (1948) and Greenwood (1952). Zener's mechanism is based on the idea that the grain boundary sliding may be blocked at triple points and built up to large stresses (stress concentrations) that produce cracks. Greenwood (1952) suggested that the concentration of vacancies at the grain boundaries leads to the formation of cavities. These cavities link up to form grain boundary cracks. The vacancies, however, are supplied by intra-granular deformation generated by the movement of dislocations.

The objective of this chapter is to develop a constitutive relationship relating the applied stresses to the strains generated by the formation of grain boundary cracks. The formulation of this constitutive relationship (Crack-activity model) is based on a concept similar to that of the rate theory (Krausz and Eyring, 1975). A brief review of the rate

theory is presented first. Then, a detailed derivation of the Crack-activity model formulation is given second.

6.2 Brief Review of the Rate Theory

The rate theory was built on the idea that crack growth results from a succession of inter-atomic bond breaking. Upon loading, the inter-atomic distances stretch. If the load is sufficient to break the atomic bonds, the crack moves forward. Backward movement of the crack (crack healing) is possible if the atoms are brought close to each other enough to restore the broken bonds.

The process of bond breaking occurs in steps known as activations. During each activation, the crack moves forward (or backward) by one or more atomic distances. The numbers of activations per unit time is called the elementary rate constant.

In its simplest form, the rate theory relates the velocity of the crack growth, V_c, to the elementary rate constant, ϕ_{RC} (Krausz and Krausz, 1989):

$$V_c = n\, a_o\, \phi_{RC} \tag{6.1}$$

where n is an integer indicating the number of atomic bonds broken during each activation, and a_o is the atomic distance. The elementary rate constant, ϕ_{RC}, was given by Krausz and Krausz (1989):

$$\phi_{RC} = \frac{k\,T}{h} \exp\left[- \frac{\Delta G}{kT} \right] \tag{6.2}$$

where k is Boltzmann constant ($k = 1.38\ 10^{-23}$ J K^{-1}), h is Planck's constant ($h = 6.62\ 10^{-34}$ J sec), and T is the absolute temperature. The parameter ΔG is the apparent activation energy which is partly available from the true activation energy, G_t, and partly from an energy supplied by external loads, w:

$$\Delta G = G_t - w \tag{6.3}$$

To produce a crack growth of one step, an energy barrier should be overcome. A schematic representation of an energy barrier is given in Fig. 6.1. In the absence of the energy supplied by external loads (solid line in Fig. 6.1), a state of equilibrium exists: The number of forward activations is equal to that in the opposite direction, and the crack growth appears stationary. When the external load is applied (dashed line in Fig. 6.1), the energy required for crack growth (forward activations) is $(G_t - w)$ while the energy needed for crack healing (backward activations) is $(G_t + w)$. Thus, the net elementary rate constant is the sum of the forward and backward activations (Krausz and Krausz, 1989):

$$\phi_{RC} = \frac{k\,T}{h}\left\{ \exp\left[- \frac{G_t - w}{k\,T} \right] - \exp\left[- \frac{G_t + w}{k\,T} \right] \right\} \tag{6.4}$$

6.3 Formulation of the Crack-Activity Model

During creep deformation, polycrystalline ice undergoes structural deterioration, resulting in the formation of grain boundary cracks. It is assumed that each grain boundary can be broken, or healed, by a single activation. The net rate of the grain boundary cracking is expressed by an equation similar to that of the net elementary rate constant, Eq. 6.4:

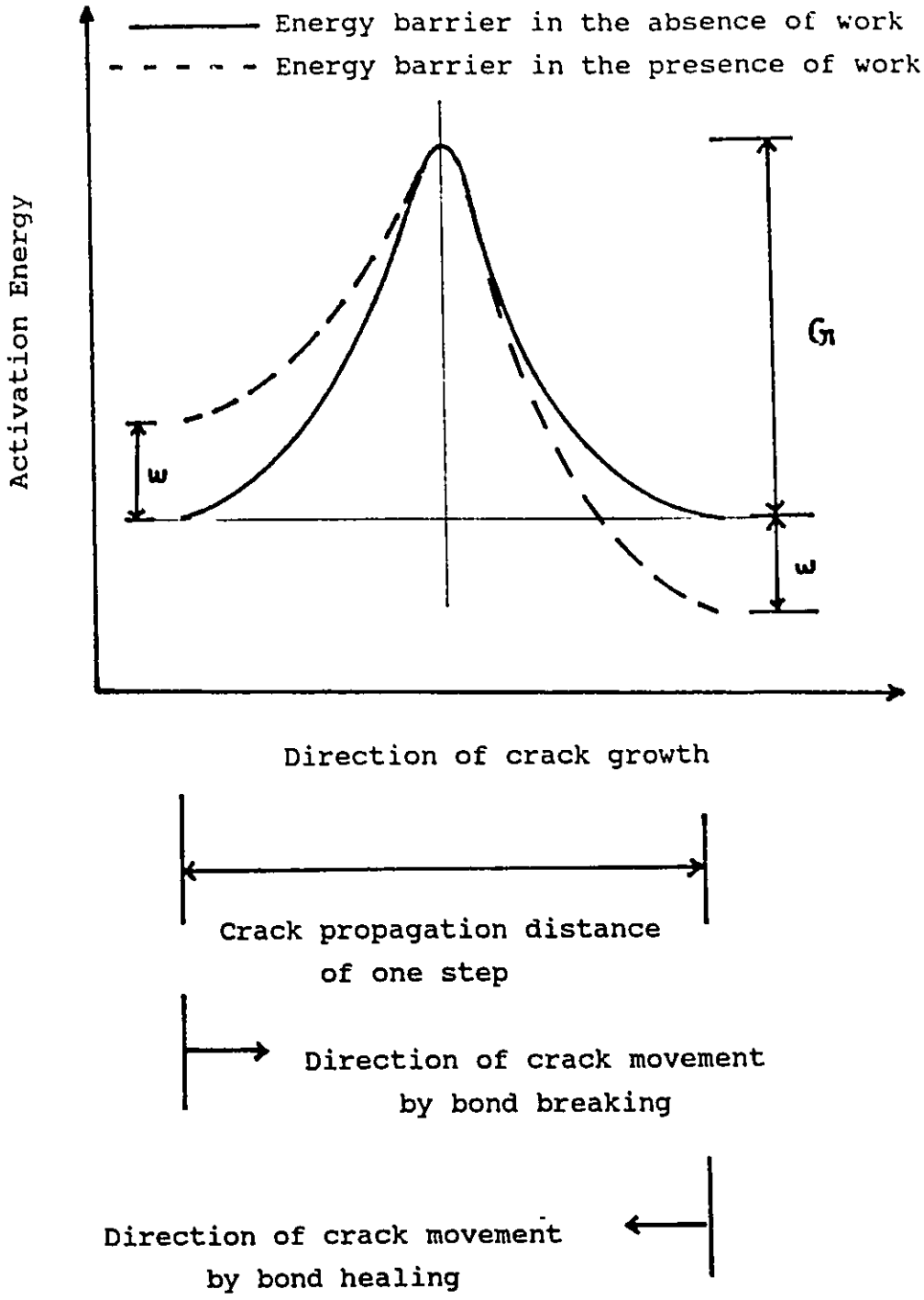

Fig.6.1: Schematic representation of the energy barrier (Krausz and Krausz, 1989)

$$\phi_{gbc} = \frac{k\,T}{h}\left\{\exp\left[-\frac{G_b}{R\,T} + \frac{W}{k\,T}\right] - \exp\left[-\frac{G_b}{R\,T} - \frac{W}{k\,T}\right]\right\} \qquad (6.5)$$

where ϕ_{gbc} is the net rate of the grain boundary cracking, G_b is the activation energy for grain boundary fracture, and R is the gas constant. The work, W, can be expressed as a function of the activation volume, η:

$$W = \eta\,\sigma \qquad (6.6)$$

The stress σ (in Eq. 6.6) is divided into a shear stress, q, and a hydrostatic pressure, p. Due to the fact that the hydrostatic tension enhances cracking of the material while the hydrostatic compression opposes it, equation 6.6 can be written as:

$$W = \eta(q - p) \qquad (6.7)$$

As shown in Fig. 6.2a, equation 6.7 is formulated by considering an energy barrier for a multi-axial compression loading situation. The underlying concept of this energy barrier is that the shear stress, q, contributes to the formation of the grain boundary cracks. However, the compressive hydrostatic pressure, p, opposes the formation of these cracks. Therefore, the energy needed for the formation of grain boundary cracks is $\left[G_b - \eta(q - p)\right]$. For crack healing, the compressive hydrostatic pressure contributes to the healing process while the shear stress opposes it. Thus, the energy required for crack healing is $\left[G_b + \eta(q - p)\right]$. This concept is, also, valid for loading situations with tensile hydrostatic pressure, Fig. 6.2b.

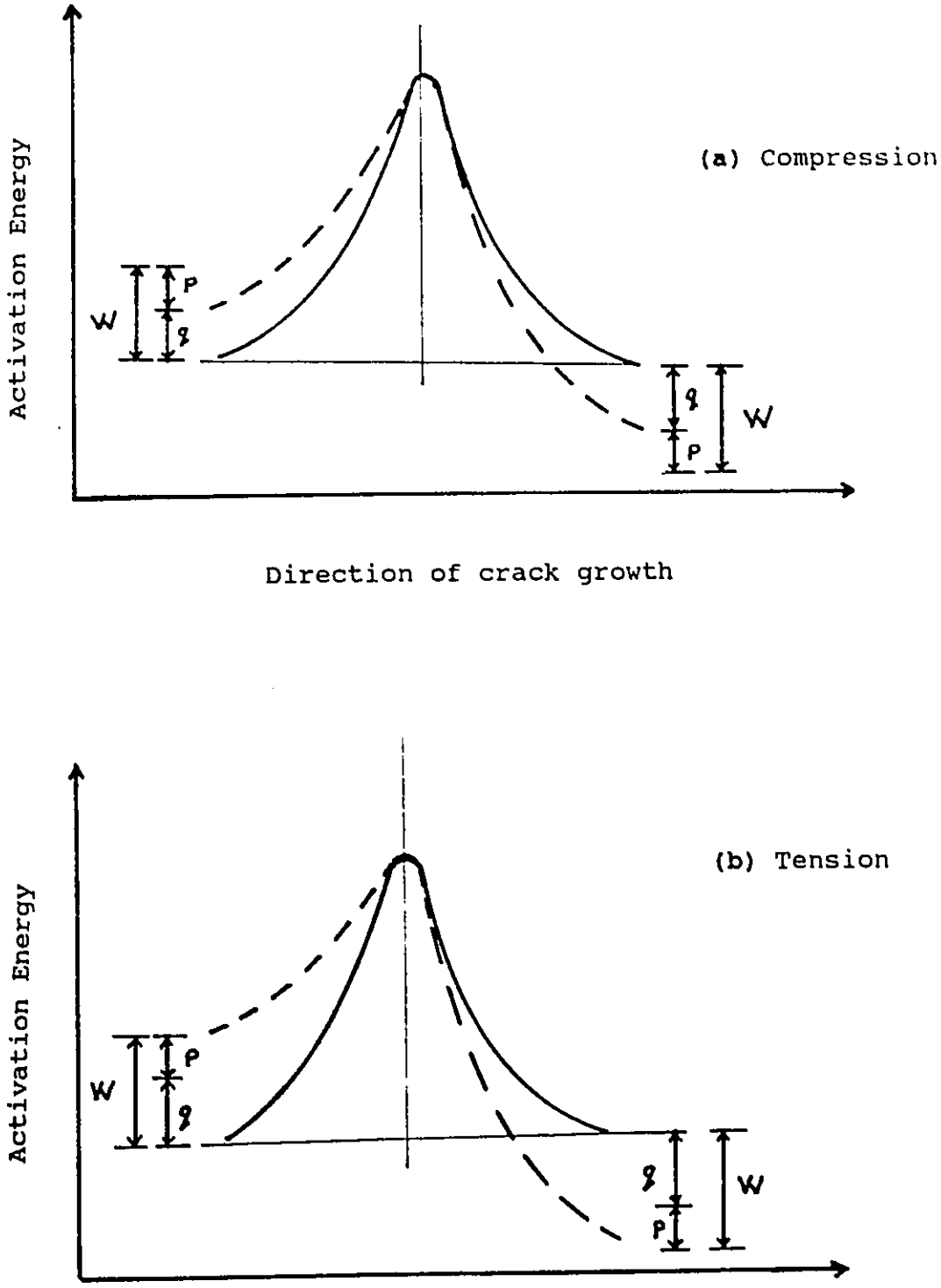

Figure 6.2: Schematic of a multiaxial energy barrier, q is the shear stress and p is the hydrostatic pressure.

For a given time increment, Δt, the energy needed to create new surfaces due to the opening of the grain boundary cracks is expressed as:

$$U = 2\ \gamma_s\ A_c\ \phi_{gbc}\ \Delta t \tag{6.8a}$$

where γ_s is the surface energy and A_c is the area of the crack opening.

Substituting Eqs. 6.5 and 6.7 into Eq. 6.8a, the energy needed to create new surfaces is expressed as:

$$U = 4\ \gamma_s\ A_c\ \Delta t\ \ \frac{k\ T}{h}\ \exp\left[-\frac{G_b}{R\ T}\right]\ \text{Sinh}\ \left[\frac{\eta(q\ -\ p)}{k\ T}\right] \tag{6.8b}$$

$$\text{where Sinh} = \frac{1}{2}\ \left\{\exp\left[\frac{\eta(q\ -\ p)}{k\ T}\right]\ -\ \exp\left[\ -\ \frac{\eta(q\ -\ p)}{k\ T}\right]\right\}$$

The equation for the energy needed to create new surfaces, U, represents a crack potential function. The strains induced by cracks, ε^c_{ij}, are calculated as follows:

$$\varepsilon^c_{ij}\ \ =\ \ \Psi\ \frac{\partial U}{\partial \sigma_{ij}} \tag{6.9}$$

where Ψ is a factor of proportionality.

Alternatively, the strains generated by cracks, ε^c_{ij}, can be represented by two strain components: 1) crack shear strains, e^c_{ij}, and 2) crack volumetric strains, ε^c_v:

$$e_{ij}^{c} = \Psi \frac{\partial U}{\partial q} \frac{\partial q}{\partial \sigma_{ij}} \tag{6.10a}$$

$$\varepsilon_{v}^{c} = \Psi \frac{\partial U}{\partial p} \frac{\partial p}{\partial \sigma_{ij}} \tag{6.10b}$$

After the derivations of the equations (Eqs. 6.10a and 6.10b), the following expressions are obtained:

$$e_{ij}^{c} = 6\ \Psi\ \Delta t\ \gamma_s\ A_c \frac{\eta}{h} \exp\left[-\frac{G_b}{R\ T}\right] \mathrm{Cosh}\left[\frac{\eta(q - p)}{k\ T}\right] \frac{S_{ij}}{q} \tag{6.11a}$$

$$\varepsilon_{v}^{c} = -\frac{4}{3}\ \Psi\ \Delta t\ \gamma_s\ A_c \frac{\eta}{h} \exp\left[-\frac{G_b}{R\ T}\right] \mathrm{Cosh}\left[\frac{\eta(q - p)}{k\ T}\right] \tag{6.11b}$$

The work contributing to the formation of grain boundary cracks (W, Eq. 6.5) is related to the work done at the grain boundaries. The latter, however, is formulated as function of the external stresses (q, p) and the grain boundary sliding displacement. The ratio (W/kT, in Eq. 6.5) is expressed as:

$$\frac{W}{k\ T} = \frac{\eta(q - p)}{k\ T} = \chi\ d\ \bar{\varepsilon}_{ve}(q - p) \tag{6.12}$$

where d is the average grain size, $\bar{\varepsilon}_{ve}$ is the generalized visco-elastic shear strain, and χ is a material parameter determined by trial and error, as it will be explained in the next section.

The area of the crack opening, A_c, can be calculated from the crack width and length. Both parameters (crack width and length) can be expressed as function of the average grain size, d. If the cross sectional geometry of the grains is hexagonal, the width of the crack is equal to the grain facet, as formulated by Sinha (1989d). For columnar structured ice, the length of the crack can be taken as a multiple of the grain size (10d - 20d).

In the present model, for a simple representation of the constitutive equations (Eqs. 6.11a, 6.11b), and without loss of generality, the ratio, A_p, is used:

$$A_p = \frac{A_c}{d^2} \tag{6.13}$$

whre A_c is the area of the crack opening and d is the average grain size. The value of A_c is, then, $A_c = A_p\ d^2$

Substituting Eq. 6.12 and the value of A_c into Eqs. 6.11a, 6.11b, the stress-strain relationships for the Crack-activity model take the following form:

$$e_{ij}^c = 6\ \Psi_c\ \Delta t\ \gamma_s\ d^2\ \frac{\eta}{h}\ \exp\left[-\frac{G_b}{R\ T}\right]\ \mathrm{Cosh}\left[\chi\ d\ \bar{\varepsilon}_{ve}(q - p)\right]\ \frac{S_{ij}}{q} \tag{6.14a}$$

$$\varepsilon_v^c = -\frac{4}{3}\ \Psi_c\ \Delta t\ \gamma_s\ d^2\ \frac{\eta}{h}\ \exp\left[-\frac{G_b}{R\ T}\right]\ \mathrm{Cosh}\left[\chi\ d\ \bar{\varepsilon}_{ve}(q - p)\right] \tag{6.14b}$$

where Ψ_c is equal to $\Psi\ A_p$.

6.4 Determination of the Parameters, Ψ_c and χ.

The parameters Ψ_c and χ (Eqs. 6.14a and 6.14b) are determined by trial and error (curve fitting) as follows:

The present model (Non-cracking model + Crack-activity model) was used to predict the volumetric dilation as well as the axial strain observed during long term creep tests conducted by Sinha (1989c). The tests (Fig. G.7) were carried out at temperature of -10°C on columnar grained S-2 ice samples with an average grain size of 2 mm. The volumetric strain history associated with the creep test of 1.6 MPa was selected, randomly, for the predictions. The value of G_b is taken to be equal to the activation energy Q (Table 2.1) and the value of the surface energy γ_s is 0.02 J m^{-2}. Trial values of Ψ_c and χ were used in the calculations. The best prediction was obtained for:

$$\Psi_c = (1/\alpha_p) \qquad \text{and} \qquad \chi = A/3$$

where (α_p = 4.4 10^{-9} MPa/sec for T = 263°K, and A = 7.5 10^5) are the material parameters given in Chapter 5.

CHAPTER 7

NUMERICAL PROCEDURES FOR THE CALCULATION OF THE CREEP STRAINS

7.1 Introduction

The proposed mathematical model (Non-cracking + Crack-activity sub-models) is developed to calculate the creep strains generated in polycrystalline ice subjected to constant loading. This chapter, however, presents the numerical procedures that are used in conjunction with the model formulations to calculate the strains induced in ice subjected to arbitrary loading paths (variable loading). Boltzmann (1876) superposition principle is used to calculate the visco-elastic strains. A numerical procedure is proposed for the calculation of the visco-plastic strains needed for the computation of the structural change functions. The instantaneous elastic strains and the strains generated by cracks are calculated by using Eqs. 4.1c, and 6.14, respectively.

For the sake of clarity, a stress history, Figs. 7.1 and 7.2, is used as an illustrative example to show the method for the calculation of the creep strains generated in polycrystalline ice subjected to monotonically increasing loading. The formulations presented in this chapter are, also, valid for general loading conditions, including cyclic loading events.

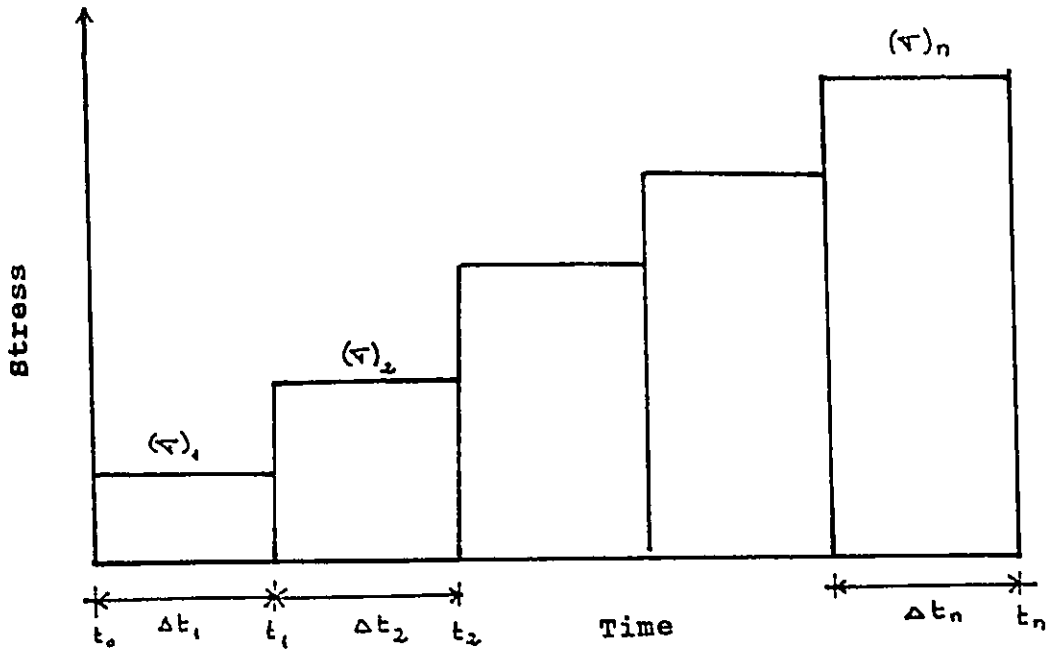

Figure 7.1: Schematic of a monotonic stress history

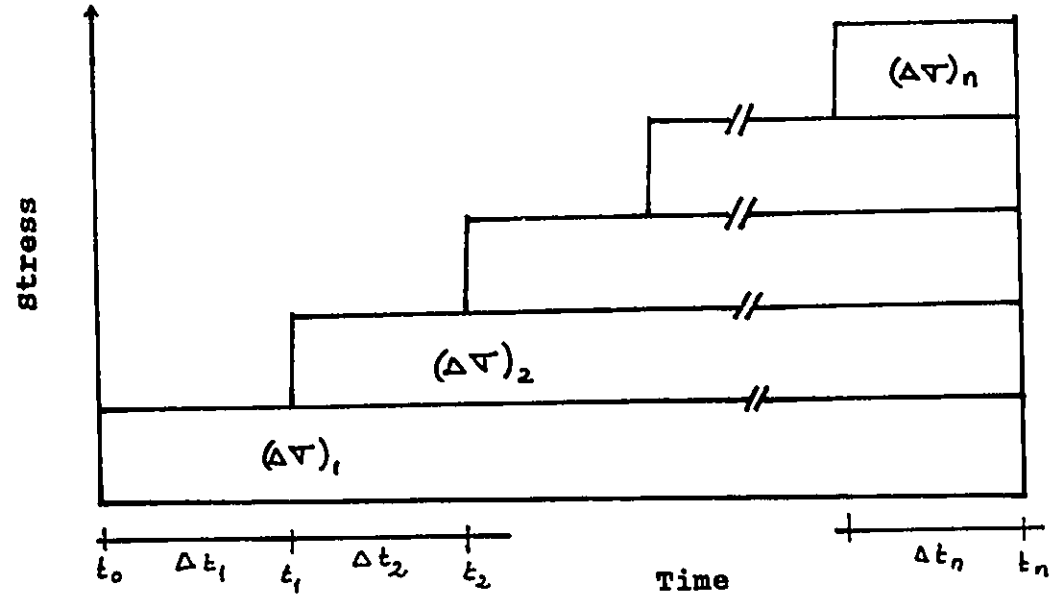

Figure 7.2: Schematic of a monotonic stress history, representation of strees increments versus time.

As shown in Fig. 7.1, the time period (over which the creep strains are calculated) is divided into n time intervals (time steps). The external loading is applied in the form of stress steps, $(\sigma)_1$, $(\sigma)_2$, $\ldots(\sigma)_n$ corresponding to time intervals Δt_1, Δt_2, $\ldots\Delta t_n$. Any change in the external loading is assumed to occur at the beginning of the time step. Therefore, the external stresses remain constant during each time step.

7.2 Calculation of the Visco-Plastic Strains

The equations needed for the calculations of the visco-plastic strains generated over two time steps are presented. Also, a generalised equation for the calculation of the visco-plastic strains generated over n time steps is formulated.

Time Step No. 1: As shown in Fig. 7.1, the stress $(\sigma)_1$ is applied over the time step Δt_1. The plastic strains generated during this time step are given by Eq. 5.22:

$$(\varepsilon^p_{ij})_1 = \frac{3}{2}\alpha_p \Delta t_1 \left[\frac{\exp(\beta_p . q_1)}{(q_1)^2} \right] (S_{ij})_1 \qquad (7.1)$$

Time Step No. 2: The stress $(\sigma)_2$ is applied over the time step Δt_2. The plastic strains generated over this time step are given by Eq. 5.22:

$$(\varepsilon^p_{ij})_2 = \frac{3}{2}\alpha_p \Delta t_2 \left[\frac{\exp(\beta_p . q_2)}{(q_2)^2} \right] (S_{ij})_2 \qquad (7.2)$$

General Equation: The total plastic strains generated during the time period t_2 ($t_2 = \Delta t_1 + \Delta t_2$) are calculated by adding Eqs. 7.1 and 7.2:

$$(\varepsilon^p_{ij}) = \frac{3}{2}\,\alpha_p\left\{\Delta t_1\left[\frac{\exp(\beta_p \cdot q_1)}{(q_1)^2}\right](S_{ij})_1 + \right.$$

$$\left. + \Delta t_2\left[\frac{\exp(\beta_p \cdot q_2)}{(q_2)^2}\right](S_{ij})_2\right\} \qquad (7.3)$$

After n time steps, the visco-plastic strains are calculated according to the following summation:

$$(\varepsilon^p_{ij}) = \frac{3}{2}\alpha_p \sum_{k=1}^{n} \Delta t_k \left[\frac{\exp(\beta_p \cdot q_k)}{(q_k)^2}\right](S_{ij})_k \qquad (7.4)$$

Note: All equations presented in this section are those of granular (isotropic) ice. For columnar grained (anisotropic) ice, the values of q and S_{ij} (in Eqs. 7.1, 7.2, 7.3, and 7.4) should be replaced by $\bar{q}$ and $\bar{S}_{ij}$, as explained in Chapter 5.

7.3 Calculation of the Visco-Elastic Strains

Boltzmann (1876) superposition principle is used to calculate the visco-elastic strains. This principle states that, in a linearly visco-elastic system, the total response to a stress history is equivalent to the sum of the responses

to a sequence of incremental stress histories. The material is considered to be linearly visco-elastic if the following two conditions are satisfied: a) the stress is proportional to the strains, b) the linear superposition principle holds. The details regarding these two requirements are given by Findley et al. (1976), and Lockett (1972).

In this section, the equations needed for the calculations of the visco-elastic strains generated over two time steps are presented. Also, a generalized equation for the calculation of the visco-elastic strains induced over n time steps is given.

Time Step No. 1: As shown in Fig. 7.2, the stress increment $\Delta(\sigma)_1$ is applied at time t_o. The visco-elastic strains developed over the time step Δt_1 are given by Eqs. 5.25 and 5.26:

$$(\varepsilon_{ij}^{ve}) = (1 + \Delta\lambda_1)\, C_o \left[(e_{ij}^{e})_1\right] \left\{1 - \exp\left[-(a_T\, \Delta t_1)^b\right]\right\} \qquad (7.5)$$

where $(e_{ij}^{e})_1$ are the elastic shear strains generated by the stress increment $\Delta(\sigma)_1$. The structural change function, $\Delta\lambda_1$, is calculated according to the procedure outlined in the next section.

Time Step No. 2: The stress increment $\Delta(\sigma)_2$ is applied at time t_1 (Fig. 7.2). The visco-elastic strains developed over the time period t_2 ($t_2 = \Delta t_1 + \Delta t_2$) are given as follows:

$$(\varepsilon_{ij}^{ve}) = (1 + \Delta\lambda_1)\ C_o\left[(e_{ij}^{e})_1\right] \left\{1 - \exp\left[-(a_T\ (\Delta t_1 + \Delta t_2)\ )^b\right]\right\} +$$

$$+ \quad (1 + \Delta\lambda_2)\ C_o\ \left[(e_{ij}^{e})_2\ \right] \left\{1 - \exp\left[-(a_T\ \Delta t_2)^b\right]\ \right\} \qquad (7.6)$$

where the structural change functions $\Delta\lambda_1$ and $\Delta\lambda_2$ are those corresponding to to the stress increments $\Delta(\sigma)_1$ and $\Delta(\sigma)_2$, respectively. All parameters in Eq. 7.6 are given, previously, in Chapter 5.

General Formulation: After n time steps the visco-elastic strains are calculated as follows:

$$(\varepsilon_{ij}^{ve}) = C_o \sum_{k=1}^{n} (1 + \Delta\lambda_k) \left[(e_{ij}^{e})_k\right] \left\{1 - \exp\left[-(a_T \sum_{j=k}^{n} \Delta t_j)^b\right]\right\} \qquad (7.7)$$

7.4 Calculation of the Structural Change Functions

The procedure presented in Section 7.2 gives the value of the visco-plastic strains induced by the stress magnitude, $(\sigma)_i$, and not the value of the visco-plastic strains induced by the stress increment, $\Delta(\sigma)_i$. For the calculation of the structural change function ($\Delta\lambda$, Eq. 5.34), however, the visco-plastic strains induced by each stress increment should be known. The reason is that the visco-plastic strains generated by a given stress increment, $\Delta(\sigma)_i$, are used to calculate the structural change function, $\Delta\lambda_i$, which affects only the visco-elastic strains induced by $\Delta(\sigma)_i$.

The plastic strain induced by a given stress, $(\sigma)_i$, over a time step, Δt_i, is divided into elementary plastic strains. Each elementary plastic strain is generated by its corresponding stress increment. In the following, the equations needed for the calculations of the elementary plastic strains and their respective structural change functions induced over two time steps are presented. Also, a generalized equation for the calculation of the elementary plastic strains generated over n time steps is given.

Time Step No. 1: As shown in Fig. 7.2, the stress $(\sigma)_1$ is applied at time t_o. For the first time step, the stress $(\sigma)_1$ is equal to the stress increment $\Delta(\sigma)_1$, and therefore the elementary plastic strains are given by Eq. 7.1.

The elementary plastic strains generated over the first time step (Eq. 7.1) are used to calculate the generalized plastic shear strain, $\bar{\varepsilon}$ in Appendix B. Subsequently, the structural change function, $\Delta\lambda_1$, is calculated using Eq. 5.34.

Time Step No. 2: The stress $(\sigma)_2$ is applied at time t_1 (Fig. 7.2). The plastic strains generated over the second time step are given by Eq. 7.2.

The plastic strains generated over time step Δt_2 (Eq. 7.2) are the sum of two elementary plastic strains induced by the stress increments $\Delta(\sigma)_1$ and $\Delta(\sigma)_2$, respectively. Since the plastic strain rate is constant for a given constant stress, it is assumed that the elementary plastic strains induced by the first stress increment, $\Delta(\sigma)_1$, over the time step Δt_2 are: given as follows:

$$(\varepsilon^p_{ij})_{1-2} = \frac{3}{2}\alpha_p \Delta t_2 \left[\frac{\exp(\beta_p \cdot q_1)}{(q_1)^2}\right] (S_{ij})_1 \qquad (7.8)$$

However, the elementary plastic strains generated by the second stress increment $\Delta(\sigma)_2$ over the time step Δt_2 are calculated by subtracting Eq. 7.8 from Eq. 7.2:

$$(\varepsilon^p_{ij})_{2-2} = \frac{3}{2}\alpha_p \Delta t_2 \left\{ \left[\frac{\exp(\beta_p \cdot q_2)}{(q_2)^2}\right] (S_{ij})_2 - \left[\frac{\exp(\beta_p \cdot q_1)}{(q_1)^2}\right] (S_{ij})_1 \right\} \qquad (7.9)$$

The total plastic strains developed over the time period t_2 ($t_2 = \Delta t_1 + \Delta t_2$) are given by Eq. 7.3. In terms of elementary visco-plastic strains, equation 7.3 can be written as the sum of Eqs. 7.8 and 7.9:

$$(\varepsilon^p_{ij}) = \frac{3}{2}\alpha_p (\Delta t_1 + \Delta t_2) \left[\frac{\exp(\beta_p \cdot q_1)}{(q_1)^2}\right] (S)_1 + \frac{3}{2}\alpha_p \Delta t_2 \left\{ \left[\frac{\exp(\beta_p \cdot q_2)}{(q_2)^2}\right] (S)_2 - \left[\frac{\exp(\beta_p \cdot q_1)}{(q_1)^2}\right] (S)_1 \right\} \qquad (7.10)$$

Equation 7.10 has the form of (ε^p = **A** + **B**) where **A** is the elementary plastic strains induced by $\Delta(\sigma)_1$ over time steps ($\Delta t_1 + \Delta t_2$), and **B** is the elementary plastic strains induced by $\Delta(\sigma)_2$ over time step Δt_2. The value of **A** is used to compute the structural change, $\Delta\lambda_1$, induced by the first stress increment, and the value of **B** is used to calculate the structural change, $\Delta\lambda_2$, induced by the second stress increment.

General Equation: The procedure of dividing the total plastic strains into elementary plastic strains is repeated for all time steps. After n time steps, the elementary plastic strains generated by a given stress increment $(\Delta\sigma)_k$ are:

$$(\varepsilon^p_{ij})_{k-n} = \frac{3}{2}\alpha_p \sum_{j=k}^{n} \Delta t_k \left\{ \left[\frac{\exp(\beta_p \cdot q_k)}{(q_k)^2}\right](S_{ij})_k - Z \right\} \qquad (7.11)$$

$$\text{For } k = 1,\ Z = 0. \quad \text{For } k > 1,\ Z = \left[\frac{\exp(\beta_p \cdot q_{k-1})}{(q_{k-1})^2}\right](S_{ij})_{k-1}$$

Subsequently, both the plastic shear distortion, $(\bar{\varepsilon}^p)_k$, and the structural change parameter $\Delta\lambda_k$ are calculated using equations B. 11 and 5.34, respectively.

CHAPTER 8

EVALUATION OF THE MODEL

8.1 Introduction

In this Chapter, the efforts are made to demonstrate the capabilities of the model to predict the observed ice behaviour. The model was coded into a stress driven computer program where stress values are provided as input and the corresponding strains are calculated as output. The numerical procedures presented in Chapter 7 were used for the calculation of the creep strains. The program was used to predict the behaviour of ice samples subjected to various types of loading conditions. Comparisons of the model predictions with the experimental data are presented.

The data base used for the model evaluation includes the results of experiments carried out by the author as well as the results of tests taken from the literature. The data from the literature includes primarly the results of various tests carried out by Sinha. His data is considered to be reliable and qualified for the appraisal of the model. In this evaluation of the model, discrapancies between the model predictions and the test results are obtained. These discrapancies are function of 1) accuracy of the measurements during testing, 2) accuracy of the numerical procedure (Chapter 7) used in the computer program for predictions, and 3) actual performance of

the model. In this thesis, if the discrapancy between the model predictions and the test results is equal or less than 20%, the predictions are considered to be in good agreement with the experimental results.

8.2 Predictions of Uniaxial and Triaxial Tests

8.2.1 Tests on Anisotropic Ice Samples

Under constant strain rate conditions, Sinha (1982) carried out a series of uniaxial tests covering strain rates ranging from 5. 10^{-7} sec^{-1} to 3. 10^{-5} sec^{-1}. The tests were conducted at temperature of - 10°C on columnar grained S-2 (anisotropic) ice samples with an average grain size of about 4.5 mm. The test results are presented in Fig. G.1a

The model predictions of Sinha's (1982) test results are shown in Fig. G.1b. The predicted stress-strain curves are in excellent agreement with the experimental measurements. The initial stiffness of the material was predicted well. The peaks of the stress strain curves (failure loads) were predicted accurately. In general, for all tests, the model achieved a very high degree (over 90 %) of accuracy in predicting the test results.

In order to show the ability of the model to simulate the anisotropic behaviour of columnar grained S-2 ice, the predicted axial and lateral strains for a uniaxial test (strain rate = 3. 10^{-5} Sec^{-1}) are presented in Fig G.2. The strains generated in the directions perpendicular to the columns (ε_1 and ε_2) have approximately the same magnitude.

However, the lateral strain (ε_3) is much smaller than the axial one. According to the model formulation, this anisotropy results from two sources: 1) the elastic anisotropy, and 2) the hypothesis that the plastic strains along the columns are prohibited, $\varepsilon_3^p = 0$.

8.2.2 Tests on Isotropic Ice Samples

Stone et al. (1989) carried out a series of uniaxial as well as triaxial tests on laboratory prepared granular ice samples. The ice was isotropic (random orientation of the c-axis) with an average grain size of about 3.0 mm. The tests were conducted at temperature of -10°C using an MTS testing system. Two LVDT's were mounted on the samples to measure the axial strain and to provide the closed loop feedback control signal to the MTS servo-valve.

The tests were carried out for various axial strain rates ranging from 5. 10^{-5} sec^{-1} to 1. 10^{-3} sec^{-1}. During each test a series of unloading and reloading were performed. The test results are presented in Figs. G.3a, G.4a, G.5a, and G.6a.

The model predictions of Stone's et al. (1989) test results are shown in Figs. G.3b, G.4b, G.5b, and G.6b. The predicted stress-strain curves are in excellent agreement with the experimental data. The peaks of the stress strain curves (failure loads) were predicted well. The post peak behaviour of the material (softening of the stress-strain curves) was predicted accurately, and the model was successful to predict the strains generated during each unloading-reloading cycle.

8.3 Predictions of Creep Tests

8.3.1 Predictions of Axial and Volumetric Strains

The model was used to predict the axial and volumetric strains measured during creep tests carried out by Sinha (1989c). The tests were conducted at a temperature of -10°C on columnar grained S-2 ice samples with an average grain size of 2 mm. The test results are presented in Fig. G.7.

The model predictions of the Sinha's (1989c) creep test results are shown in Fig. G.8. Except for test of 1.7 MPa, the predictions agree well with the experimental measurements. Note that the test of 1.6 MPa was used for the determination of the parameters needed for the crack-activity Model. Thus, the comparison between the observed and measured volumetric strains is a direct evaluation of the crack-activity model formulation.

The model predictions of the tests at very early stages of loading are shown in Figs. G.9a and G.9b. It is apparent (from Fig. G.9a) that the model is capable of predicting the three stages of creep: primary, secondary, and tertiary creep.

Figure G.9b shows the transition from a compressive to an expansive volumetric behaviour. Upon loading, the model predicts an initial elastic compressive volumetric strain. With time, ice undergoes plastic as well as visco-elastic strains. Moreover, as the visco-elastic strain increases, ice undergoes structural deterioration due to the formation of grain boundary cracks. This structural deterioration of the material leads to its expansive volumetric behaviour.

8.3.2 Effect of the Grain Size on the Predicted Creep Curves

The model was used to predict the creep behaviour of two ice samples of granular (isotropic) ice with grain sizes of 1.5 mm and 4.4 mm, respectively. The predictions were calculated for an axial stress of 3.0 MPa and temperature of -10°C. The model predictions are shown in Fig. G.10b.

As shown in Fig. G.10b, at initial stages of loading, a higher axial strain is predicted for the sample with the small grain size (1.5 mm) as compared to that of the large grain size (4.4 mm). With time, ice undergoes cracking activity, and the sample with the large grain size generates more axial strain than that of the small grain size. This type of prediction is in agreement with the experimental observation reported by Sinha (1989b), Fig G.10a.

The ability of the model to predict the effect of the grain size on the creep behaviour of anisotropic ice is demonstrated in Fig. G.11. The model was used to predict the creep behaviour of three columnar grained S-2 ice samples with average grain sizes of 2, 5 and 10 mm, respectively. The predictions were computed for an axial stress value of 3.0 MPa and temperature of -10°C. The model predictions of the axial as well as volumetric strain histories are shown in Figs. G.11a and G.11b, respectively. These predictions indicate that, with time, the increase of the average grain size leads to an increase of the axial and volumetric strain rates. This stems from the fact that the crack-activity model is formulated as a function of the grain size, and consequently the increase of the grain size value enhances the creep strains generated by cracks. In general, the model predictions

of the creep behaviour of anisotropic ice (for various average grain sizes) are in agreement with the experimental observations reported by Sinha (1989b).

8.4 Predictions of Stress Relaxation Tests

In this study, a stress relaxation test was carried out at temperature of -10^0C on columnar grained S-2 ice sample with an average grain size of 4.5 mm. The test was carried out as follows: A constant axial strain of $1.30\ 10^{-4}$ was applied, and the variation of the stress with time was recorded. When the change in the measured stress became negligible, an increment of axial strain was applied. Again, the variation of the stress with time was recorded. When the change in the measured stress was negligible, an-other axial strain increment was applied. This strain history was repeated covering an axial strain range from $1.3\ 10^{-4}$ to $2.9\ 10^{-3}$.

The model predictions of the test results for an applied axial strain of $2.48\ 10^{-3}$ are shown in Figs. G.12 and G.13. The predicted and measured axial stress histories are plotted together in Fig. G.12. The model predictions are in excellent agreement with the experimental data.

According to the model formulation, during a stress relaxation test, the macroscopic (measured) axial strain is kept constant while its components (instantaneous elastic, visco-elastic, and visco-plastic strains) undergo changes. The decrease of the magnitude of the axial stress leads to a decrease of the instantaneous elastic strains. With time, however, an increase of both the visco-elastic and visco-plastic strains is calculated. Figure G.13 shows the predicted

histories of the axial and lateral strain components for the test shown in Fig. G.12. Note that due to the fact that the axial stress decreases, during testing as well as during predictions, the rate of the strain components decreases as well.

8.5 Predictions of Cyclic Tests

In this study, a cyclic test was carried out on columnar grained S-2 ice sample with an average grain size of 4.5 mm. The test was conducted at temperature of -10^0C and frequency of 0.0167 Hz (1/60 sec^{-1}). During testing, the sample was subjected to a cyclic excitation by increasing the axial stress from 0 MPa to 0.5 MPa, then, reducing it to 0. MPa in a sinusoidal manner as a function of time. The applied stress history is shown in Fig. G.14. The measured strain history and the measured stress-strain curve are presented in Figs. G.15a and G.16a, respectively.

The predicted strain history as well as the predicted stress strain curve are presented in Figs. G.15b and G.16b, respectively. The model predictions are in good agreement with the experimental data. Although the model seems to under-estimate the axial strain at early stages of loading, it was successful in predicting the hysteresis stress-strain behaviour of ice and the accumulated strains as the number of cycles increased.

8.6 Predictions of Tensile Tests - Shortcoming of the Model

In this section, a shortcoming of the model is discussed. The ability of the present model to predict accurately the results of tensile tests is uncertain. The model was used to

predict a series of uniaxial tensile tests over strain rates ranging from 2.0 10^{-7} sec^{-1} to 5.0 10^{-5} sec^{-1}. The predictions were made for granular (isotropic) ice samples with an average grain size of 3.0 mm and temperature of -10°C. The model predictions are shown in Fig. G.17. The predicted maximum tensile stresses are compared to tensile strength values taken from the open literature.

Hawks and Mellor (1972) conducted a series of tensile tests at a temperature of -7°C on samples (dumb-bell) of granular ice with an average grain size of 0.7 mm. The tests were carried out under quasi-constant cross head rates, and the ice was described as bubbly. Their measurements are plotted together with the model predictions of the maximum tensile stress in Fig. G.18.

Sinha (1983) hypothesized that the tensile strength of ice is equivalent to the compressive stress magnitude needed to generate the first few large micro-cracks in uniaxial compression tests. He carried out a series of uniaxial compression tests on columnar grained ice samples. During each test, he measured the axial stress, time, and axial strain at the time of the formation of the first large internal cracks. (σ_{fc}, t_{fc}, ε_{fc}, respectively). He plotted the stress (σ_{fc}) versus the strain rate (ε_{fc}/t_{fc}). Then, he compared his findings with Hawks' and Mellor results, Sinha's measurements are also given in Fig. G.18.

As shown in Fig G.18, the comparison of the model predictions with the experimental data indicates that the model over-estimates the tensile strength of ice at strain rates over 5. 10^{-6} sec^{-1}. and hence, an improvement of the

model formulation is required. More than one solution may exist to improve the model formulations so that the results of the tensile tests can be predicted with acceptable degree of accuracy. The solution suggested in this thesis, however, is that the crack-activity model should be supplemented by a crack propagation formulation. This stems from the fact that when a crack forms, it propagates, particularly under applied tensile stresses. Sinha (1983) indicated that the nucleation of the first few large cracks in tension could dictate the ultimate strength of ice.

8.7 Additional Evaluation of the Model

Theoretical predictions are presented in this section to highlight the merits of the model to predict:

1. the effect of initial confining pressure on the stress-strain behaviour of ice, and

2. the behaviour of ice samples subjected to monotonically increasing loading under constant stress rate conditions.

8.7.1. Effect of the Initial Confining Pressure

The model was used to predict a series of triaxial compression tests for a constant axial strain rate of $1.0\ 10^{-4}$ sec^{-1}. The predictions were made for granular (isotropic) ice samples with an average grain size of 3.0 mm and temperature of $-10^{\circ}C$. The initial confining pressure was varied from 0. MPa to 40. MPa. Typical model predictions are shown Fig. G.19. As the initial confining pressure increases, the predicted

maximum deviatoric stress increases. The predicted volumetric strain history, Fig. G.19, indicates that the increase of the initial confining pressure leads to a decrease of the predicted volumetric dilatancy. This is due to the fact that the confining pressure hinders the formation of the grain boundary cracks, as hypothesized by the model. In other words, the increase of the initial confining pressure increases the resistance of the material towards the formation of cracks. Subsequently, the material at high confining pressure becomes stronger than that subjected to low confining pressure. Consequently, the increase of the initial confining pressure results in an increase of the shear strength of the material.

The predictions shown in Fig. G.19 indicate that ever increasing initial confining pressure results in ever increasing strength of ice. Experimental results of triaxial tests carried out by Jones (1978, 1982) indicate that the strength of ice increases at low confining pressures and decreases at high confining pressures. The application of the model is, therefore, limited to low confining pressures.

8.7.2 Effect of the Stress Rate

The model was used to predict a series of uniaxial compression tests for various constant stress rates ranging from 10^{-4} MPa/sec to 1. MPa/sec. The predictions were made for granular (isotropic) ice samples with an average grain size of 3.0 mm and temperature of -10°C. The model predictions are shown in Fig. G.20. As the stress rate increases, the tendency of the material to dilate decreases. In general, the predicted stress strain curves agree with Sinha's (1981a) work.

CHAPTER 9

CONCLUSIONS AND RECOMMENDATIONS

9.1 Conclusions Regarding the Experimental work

The following conclusions have been drawn on the basis of analyses of the experimental results reported in Chapter 3.

1- The plastic strains generated in an ice specimen undergoing creep deformation vary linearly with the loading time.

2- There are very small (negligible) amounts of total and visco-plastic strains developed in the direction along the columns.

3- There is no plastic (intra-granular) volumetric strains generated in the ice samples.

4- During the experiments, it was observed that the waiting time period for the recovery of the visco-elastic strains was not equal to the duration of loading.

5- As the plastic strains accumulate, with time, the recovery time of the visco-elastic strains increases.

9.2 Conclusions Regarding the Practical Elastic Moduli for Polycrystalline Ice

1- The practical elastic moduli (Young's modulus, shear modulus, and Poisson's ratio) for polycrystalline ice were determined from the characteristic elastic constants of single ice crystals using the Reuss averaging method.

2- New equations for Poisson's ratio for columnar grained (S-1 and S-2) ice are proposed.

3- Three averaging methods (Voigt, Reuss, and Hill's methods) were used to develop mathematical equations for the practical elastic moduli for granular ice. These equations were used to predict the values of both Young's modulus and Poisson's ratio for granular ice. The comparison between the predicted and measured values indicated that the Reuss method is the appropriate averaging method for polycrystalline ice.

9.3 Conclusions Regarding the Model Evaluation

1- The versatility and accuracy of the model in predicting the observed behaviour of ice were demonstrated. The model was used to predict the behaviour of ice samples subjected to various loading conditions. The predictions were in excellent agreement with the experimental data.

2- The model predicted the measured uniaxial as well as triaxial stress strain curves with high degree of accuracy (over 90 % accurate predictions were obtained).

3- The model predicted the observed failure stresses (peak of the stress-strain curves) accurately, over 90% degree of accurate predictions were obtained.

4- The model was successful in predicting the measured stress-strain curves generated during unloading-reloading cycles in triaxial and uniaxial tests.

5- The measured stress-strain curves generated during unloading-reloading cycles (in uniaxial and triaxial tests) for various strain rates were predicted very well.

6- The model was able to predict accurately the softening behaviour of ice after the peak of the stress strain curve has been reached (post peak behaviour).

7- The model was able to predict successfully the observed axial strain as well as the volumetric expansive behaviour of ice generated during long term creep experiments.

8- The model predicted the effect of the grain size on the creep behaviour of ice reasonably well. The comparison between the predicted and measured creep test results, for various grain sizes, indicated that the model took into account the effect of the grain size on the creep behaviour of ice properly.

9- The model predicted accurately the stress history generated during stress relaxation tests.

10- During the stress relaxation test simulations, the model predicted a decrease of the instantaneous elastic strain

history accompanied with an increase of the visco-elastic and visco-plastic strain histories.

11- The model was able to reproduce the observed hysteresis behaviour of ice generated during cyclic tests. Both the cyclic strain history as well as the stress strain curves were predicted reasonably well.

12- Although the model is able to predict the tensile stress-strain curves, the accuracy of its predictions is questionable. A shortcoming of the model is apparent in its ability to predict accurately the measured tensile strength values.

13- With ever increasing initial confining pressure, the model predicts ever increasing strength of ice. The model application is limited to low confining pressure situations.

9.4 Recommendations for Future work

1- The model formulation should be improved so that the results of the tensile tests can be predicted with acceptable degree of accuracy.

2- The model formulation should be generalized to include the effect of high confining pressure on the behaviour of ice.

3- At the present time, the lack of existence, in the literature, of 3-D experimental results (results of true triaxial tests) hinders the evaluation of the model with respect to its accuracy to predict the results of 3-D

tests for various stress paths. Further investigation is, then, needed to appraise the accuracy of the model predictions of the behaviour of ice subjected to arbitrary loading paths in the three dimensional stress space.

4- Three dimensional laboratory testing of ice samples is very much needed. Experimental investigations of the effect of initial hydrostatic pressure, initial and current density, crack propagation, etc. on the behaviour of ice are vital for the development of a realistic 3-D mathematical model that can be used, with confidence, to solve complex boundary value problems.

5- The present model should be implemented into a finite element computer program so that it can be used to solve ice engineering boundary value problems.

6- For the analysis of offshore structures constructed in sea-ice environments, the model should be extended to include the bahaviour of sea-ice.

7- The practical elastic moduli for anisotropic ice should be further investigated to establish whether or not their values could be approximated to those of isotropic material. The equations of the practical elastic moduli for anisotropic ice result in a non-symmetric elastic stiffness matrix. This increases both the computer CPU time and computer storage during computations.

REFERENCES

Afanas'ev V.P., 1972. Ice pressure on vertical structures. Technical Translation No. 1708, NRCC, Ottawa, Canada, 1978.

Ashby M.F. and Duval P., 1985. The creep of polycrystalline ice. Cold Regions Science & Technology, Vol. 11, pp. 285-300.

Bogorodskii V.V., 1964. Elastic moduli of ice crystals. Soviet Physics Acoustics, Vol. 10, pp. 124-126.

Cammaert A.B. and Muggeridge D.B., 1988. Ice Interaction with Offshore Structures. Van Nostrand Reinhold, New York, 431 p.

Conrad H., 1961. The role of grain boundaries in creep and stress rupture. Mechanical Behaviour of Materials at Elevated Temperatures, Chapter 9, pp. 218-269, **J.E Dorn** Editor, McGraw-Hill Inc., New York, 529 p.

Croasdale K.R., Morgenstern N.R., and Nutall J.B., 1977. Indentattion tests to investigate ice pressure on vertical structures. Journal of Glaciology, Vol. 19, No. 81, pp. 301-311.

Croasdale K.R., 1980. Ice forces on fixed rigid structures. U.S. Army Corps of Engineers, Cold Regions Research and Eng., Laboratory, CRREL, Special Report No. 80-24.

Dantl G., 1969. Elastic moduli of ice. Physics of Ice, N. **Riehl, B. Builemer, and H Engelhardt** Editors, Plenum Press, New York, pp. 223-230.

Dessai C.S. and Siriwardane H.J., 1984. Constitutive Laws for Engineering Materials. Prentice-Hall. Inc., 468 p.

Frederking R.M.W., 1977. Plane-strain compressive strength of columnar-grained and granular snow-ice. Journal of Glaciology, Vol. 18, No. 80, pp. 505-516.

Gagnon R.E., Kiethe H., Clouter M.J., and Whalley E., 1988. Pressure dependence of the elastic constants of ice 1h to 2.8 kbar by Brillouin spectroscopy. J. Chem. Phys., American Inst. of Physics, Vol. 89, No. 8, pp. 4522-4528.

Garofalo F., 1965. Fundamentals of Creep and Creep-rupture in Metals. The Macmillan Company, New York, 258 p.

Gifkins. R.C., 1959. Fracture. Proc. of Int. Conf. on Atomic Mechanisms of Fracture, Chapter 27, Swampscott, Massachusetts, April 12 - 16, pp. 579-627.

Glen J.W. and Perutz M.F., 1954. The growth and deformation of ice crystals. Journal of Glaciology, Vol.2, No.16, pp. 397-403.

Glen J.W., 1955. The creep of polycrystalline ice. Proc. of the Roy. Soc., London, A228, pp. 519-538.

Gold L.W., 1958. Some observations on the dependence of strain on stress for ice. Canadian Journal of Physics, Vol.36, No.10, pp. 1265-1275.

Gold L.W., 1963. Deformation mechanisms in ice. Proc. of Ice and Snow Conference. **W. D. Kingery** Editor, M.I.T. Press, Cambridge, Massachusetts. pp. 8-27.

Gold L.W., 1972a. The failure process in columnar-grained ice. Technical Paper No. 369 of the Division of Building Research, National Research Council, Ottawa, Ontario, Canada, 150 p.

Gold L.W., 1972b. The process of failure of columnar grained ice. Philosophical Magazine, Vol. 26, No. 2, pp. 311-328.

Gold L.W., 1976. Physics of Ice and Snow Conference edited by **H. Oura,** Hokkaido University, Japan, Part 1, pp. 359-370.

Green R.E and Mackinnon L., 1956. Determination of the elastic constants of ice single crystals by an ultrasonic pulse method. Journal of Acoustic Society, Vol. 28, pp. 169-170.

Hawks I. and Mellor M., 1972. Deformation and fracture of ice under uniaxial stress. Journal of Glaciology, Vol. 11, No. 61, pp. 103 - 131.

Hill R., 1950. Mathematical Theory of Plasticity, Oxford Clarendon Press, London, 355 p.

Hill R., 1952. The elastic behaviour of crystalline aggregate. Proc. of the Physical Society, Vol. A65, pp. 349-354.

Hirth J.P. and Lothe J., 1968. Theory of Dislocations. McGraw-Hill Inc., 780 p.

Hull D. and Bacon D.J., 1984. Introduction to Dislocations (3rd Edition). Pergamon Press, New York, 257 p.

Jefferies M.G. and Wright W.H., 1988. Dynamic response of Molikpaq to ice-structure interaction. Proc. 7th Int. Conf. on Offshore Mechanics and Arctic Engineering, OMAE/ASME, Houston, Texas, Vol. 4, pp. 201-220.

Jones S.J, 1978. Triaxial testing of polycrystalline ice. Proc. 3th Int. Conf. on Permafrost, Edmonton, Vol. 2, pp. 670-674

Jones S.J, 1982. The confined compressive strength of polycrystalline ice. Journal of Glaciology, Vol.28, No.98, pp. 171-177.

Kachanov M., 1980. Continuum model of medium with cracks. Journal of Engineering Mechanics, Vol. 106, pp. 1039-1051.

Korzhavin K.N., 1962. Action of ice on engineering structures. USSR Acad. Science, Siberian Branch. Technical Translation No. 260, CRREL, Hanover, USA, 1971.

Krausz A.S. and Eyring H., 1975. Deformation Kinetics. Wiley Inter-Science Publications, New York, 398 p.

Krausz A.S. and Krausz K., 1989. Fracture Kinetics of Crack Growth. Kluwer Academic Publishers, 180 p.

Levi E.M. and Suraski E., 1965. Experimental study of non-basal dislocations in ice crystals. Journal of Glaciology, Vol. 5, No. 41, pp. 691-699.

Michel B. and Ramseier R.D., 1971. Classification of river and lake ice. Canadian Geotech. Journal, Vol. 8, No. 1, pp. 38-45.

Michel B. and Toussaint N., 1977. Mechanisms and theory of indentation of ice plates. Journal of Glaciology, Vol. 19, No. 81, pp. 285-300.

Michel B., 1978. Ice Mechanics. Les Presses de l'Universite Laval, Quebec, Canada, 499 p.

Miller K.J., 1980. The application of fracture mechanics to ice problems. Proc. Conf. on Physics and Mechanics of Ice, Springer Verlag, Berlin, pp. 265-277.

Murakami S. and Ohno H., 1981. A continuum theory of creep and creep damage in structures. Creep in Structures, **A.R.S. Ponter & D.R. Hayhurst** Editors, Springer-Verlag, Berlin, pp. 422-444.

Murat J.R., 1976. Axisymmetric finite element formulation of non homogeneous floating ice sheets, Part II. Report EP. 76-R-37, Ecole Polytechnique de Montreal, Montreal, 83 p.

Nadreau J.P. and Michel B., 1986a. Secondary creep in Confined ice samples, Proc. of IAHR Symposium, Iowa City, Iowa, USA,

Nadreau J.P. and Michel B., 1986b. Yield and failure envelope for ice under multi-axial compressive stresses. Journal of Cold Regions Science and Technology, No. 13, pp. 75-82.

Nakaya U., 1958. Mechanical properties of single ice crystals. U.S. Army Corps of Engineers, Cold Regions Research and Eng. Laboratory, Research Report No. 28.

Neill C.R., 1976. Dynamic ice forces on piers and piles. Canadian Journal of Civil Eng., Vol. 3, No. 2, pp 305-341.

Nye J.F., 1985. Physical Properties of Crystals. Oxford Science Publications, Clarendon Press, Oxford, 329 p.

Nowick A.S. and Berry B.S, 1972. Anelastic Relaxation in Crystalline Solids. Acad. Press, New York, 550 p.

Palmer A.C., Goodman D.J., Ashby M.F., Evans A.G., Hutchinson J.W., and Ponter A.R.S., 1983. Fracture and its role in determining ice forces on offshore structures. Annals of Glaciology, No. 4, pp. 216-221.

Ponter A.R.S., Palmer A.C., Goodman D.J., Ashby M.F., Evans A.G., and Hutchinson J.W., 1983. The force exerted by a moving ice sheet on an offshore structure. Journal of Cold Regions Science and Technology, Vol. 8, pp. 109-118.

Prager A.W., 1949. Recent developments in mathematical theory of plasticity. Journal of App. Phy., Vol.20, No.3, pp. 235-241.

Pulkkinen E., 1988. Numerical modelling of ice behaviour. Ph.D. Thesis, University of Oulu, Dept. of Mech. Eng. 122 p.

Ralston T.D., 1978. An analysis of ice sheet indentation. Proc. IAHR, Symp. on Ice Problems, Lulea, Sweden, Vol. 1, pp. 13-31.

Read W.T., 1953. Dislocations in Crystals. McGraw Hill Inc., New York, 228 p.

Rice J.R., 1971. Inelastic constitutive relations for solids. Journal of the Mech. and Phy. of Solids, Vol.19, pp. 433-455.

Rigsby G.P., 1958. Effect of hydrostatic pressure on velocity of shear deformation of single ice crystals, Journal of Glaciology, Vol. 3, No. 24, pp. 271-278.

Sanderson T.J.O., 1986. A pressure-area curve for ice. Proc. of IAHR, Iowa City, Iowa, Vol. 2, pp. 361 - 384.

Sanderson T.J.O., 1988. Ice Mechanics, Risks to Offshore Structures. Graham & Trotman, London, UK., 253 p.

Santaoja K., 1990. Mathematical modelling of deformation mechanisms in ice. Technical Research Center of Finland. Research Report No. 676, 228 p.

Sinha N.K., 1977. Dislocations in ice as revealed by etching. Philosophical Magazine, Vol. 36, No. 6, pp. 1385-1404.

Sinha N.K., 1978a. Observation of basal dislocations in ice by etching and replicating. Journal of Glaciology, Vol.21, No. 85, pp. 385-395.

Sinha N.K., 1978b. Rheology of columnar grained ice. Experimental Mechanics, Vol. 18, No. 12, pp. 464-470.

Sinha N.K., 1979. Grain boundary sliding in polycrystalline materials. Philosophical Magazine, Vol. 40, No. 6, pp. 825-842.

Sinha N.K., 1981a. Constant stress rate deformation Modulus of ice. Proc. 6th Int. Conf. on Port and Ocean Eng. under Arctic Conditions, P.O.A.C, Quebec City, Quebec, pp. 216-224.

Sinha N.K., 1981b. Deformation behaviour of ice like material in engineering applications. Int. Symp. on the Mechanical Behaviour of Structured Media, Ottawa, Canada, pp. 419-430.

Sinha N.K., 1982. Constant strain and stress rate compressive strength of columnar grained ice. Experimental Mechanics, Vol. 17, pp. 785-802.

Sinha N.K., 1983. Does the strength of ice depend on the grain size at high temperatures? Scripta Metallurgica, Vol. 17, pp. 1269 - 1273.

Sinha N.K., 1984a. Delayed-elastic model for initiation and accumulation of creep cavitation at high temperatures. Proc. 6th Int. Conf. on Fracture, New Delhi, pp. 2295-2302.

Sinha N.K., 1984b. Intercrystalline cracking, grain-boundary sliding, and delayed elasticity at high temperatures. Journal of Materials Science, Vol. 19, pp. 359 - 376.

Sinha N.K., 1987a. Dislocation climb in ice observed by etching and replicating. Journal of Material Science letters, Vol. 6, No. 12, pp. 1406-1408.

Sinha N.K., 1987b. Effective Poisson's ratio for isotropic ice. Proc. 6th Int. Conf. on Offshore Mechanics and Arctic Eng., OMAE/ASME, Houston, Texas, Vol. 4, pp. 189-195.

Sinha N.K., Timco G.W. and Frederking R.M.W., 1987., Recent advances in ice mechanics in Canada. Applied Mechanics Review, Vol. 40, No. 9, pp. 1214-1231.

Sinha N.K., 1988a. Crack-enhanced creep in polycrystalline material: Strain-rate sensitive strength and deformation of ice. Jour. of Materials Science, Vol.23, No.12., pp. 4415-4428.

Sinha, N.K., 1988b. Experiments on anisotropic and rate sensitive strain ratio and modulus of columnar grained ice. Proc. 7th Int. Conf. on Offshore Mechanics and Arctic Engineering, OMAE/ASME, Houston, Texas, Vol. 4, pp. 55-62.

Sinha N.K., 1989a. Elasticity of natural types of polycrystalline ice. Cold regions Science and Technology, Vol. 17, No. 2, pp. 127-135.

Sinha N.K., 1989b. Ice and steel - A comparison of creep and failure. Conf. on Mechanics of Creep Brittle Materials. **A.C.F. COCKS** and **A.R.S. PONTER** Editors, Elsevier Applied Science Publishers, Vol. 1, pp. 201-212.

Sinha N.K., 1989c. Kinetics of micro-cracking and dilatation in polycrystalline ice. IUTAM/IAHR, Symposium on Ice-Structure Interaction, St. John's, Newfoundland, Canada.

Sinha N.K., 1989d. Microcrack enhanced creep in polycrystalline material at elevated temperature. Acta Metallurgica, Vol. 37, No. 11., pp. 3107-3118.

Sinha N.K., 1990. Microfracturing and creep dilatation in polycrystalline columnar-grained and equiaxed ice. Proc. 4th Int. Conf. on Creep and Fracture of Engineering Materials, Univ. College, Swansea, UK., pp. 345-354.

Sodhi D.S. and Cox G.F.N., 1987. Advances in sea ice mechanics in USA. Applied Mechanics Review, Vol.40, No.9, pp. 1232-1242.

Spring U. and Morland L.V., 1983. Integral representations for the visco-elastic deformation of ice. Journal of Cold Regions Science and Technology, Vol. 6, pp. 185-193.

Steinemann S., 1954. Results of preliminary experiments on the plasticity of ice crystals. Journal of Glaciology, Vol. 2, No. 16, pp. 404 - 416.

Stone B.M, Jordaan I.J., Jones S.J., and Mckenna R.F., 1989. Damage of isotropic polycrystalline ice under moderate confining pressures. Proc. 13th Int. Conf. on Port and Ocean Eng. under Arctic Conditions, P.O.A.C, pp. 408-419.

Szyszkowski V. Dost S., and Glockner G., 1985. A nonlinear constitutive model for ice. Journal of Solids and Structures, Vol. 21, No. 3, pp. 307-321.

Timco G.W. and Frederking R.M.W., 1986. Confined compression tests: Outlining the failure envelope of columnar sea ice. Jour. of Cold Regions Science & Technology, No. 12, pp. 13-28.

Ting S.K. and Sunder S.S., 1985. Constitutive modelling of sea ice with applications to interaction problems. CSBOE Research Report No. 3, M.I.T., Cambridge, Massachusetts, USA.

Vivatrat V. and Stomski S., 1983. A probabilistic basis for selecting design ice pressures for arctic offshore structures. Proc. of OTC, Houston, Vol. 1, pp. 121-132.

Zarembovitch A. and Kahane A. 1964. Determination des vitesses de propagation d'ondes ultrasonores longitudinales dans la glace. Acadimic Science, Paris, pp. 2529-2532.

Zener C., 1941. Theory of the elasticity of polycrystals with viscous grain boundaries, Physics Review, Vol. 60, pp. 906-908.

Zener C., 1948. Elasticity and Anelasticity of Metals. The University of Chicago Press, Illinois, 170 p.

APPENDIX A

REVIEW OF THE METHODS FOR THE CALCULATION OF ICE FORCES ON OFFSHORE STRUCTURES

APPENDIX A

METHODS FOR THE CALCULATION OF ICE FORCES ON OFFSHORE STRUCTURES

A.1 Introduction

Many methods for the calculation of ice forces exerted on offshore structures have been developed. A literature review reveals that these methods can be classified into four categories: Empirical, Semi-empirical, Analytical, and Numerical methods. Since it is not possible to report all existing methods, only few examples for each category are presented. Detailed information regarding these methods, however, can be found in various textbooks of ice engineering, such as Sanderson (1988) and Cammaert and Muggeridge (1988).

A.2 Empirical Methods

A.2.1 Korzhavin's (1962) Equation

For crushing mode of failure, Korzhavin (1962) proposed an equation relating the pressure, P, induced by ice on vertical structures to the uniaxial compressive strength of ice, σ_c.

$$P = I\, f_c\, m\, (V/V_o)^{-0.333}\, \sigma_c \qquad (A.1)$$

where I is the indentation factor, f_c is the contact

coefficient, and m is the shape factor. Both V_o and V are the reference velocity (1 m/sec) and the velocity of the ice sheet, respectively.

Korzhavin's (1962) equation is valid for strain rates ranging from 10^{-3} to 10^{-4} sec^{-1} (Neill, 1976). The general form of Eq. A.1 for all strain rates is given as follows:

$$p = I\ f_c\ m\ \sigma_c \qquad (A.2)$$

where the value of σ_c can be obtained for the appropriate strain rate from Fig. A.1.

A.2.2 Afanas'ev (1972) Equation

Afanas'ev (1972) proposed an equation relating the force of ice, F, to the apsect ratio (h/D):

$$F = m\ \sigma_c\ D\ h\ (1 + 5h/D)^{0.5} \qquad (A.3)$$

where D is the width of the indentor and h is the thickness of ice. The parameter m is the shape factor, and σ_c is the uniaxial compressive strength of ice.

A.2.3 Vivatrat and Stomski's (1983) Equation

Vivatrat and Stomski (1983) analyzed the results of 195 small and medium scale indentation tests, and they proposed the following equation for the calculation of indentation pressure, P:

$$p = f_T f_{\dot{\varepsilon}} p_r \qquad (A.4)$$

where f_T and $f_{\dot{\varepsilon}}$ are the temperature and the strain rate correction factors, respectively. p_r is a reference indentation pressure which is function of the contact area.

A.2.4 Sanderson's (1986) Curve

Based on a wide range of laboratory and field data, Fig. A.2, Sanderson (1986) produced a plot relating the indentation pressure, P, to the contact area, A. He indicated that an upper bound curve provides an empirical best-fit to the data for contact areas exceeding 0.1 m^2, Fig. A.3:

$$p = A^{-1/2} \qquad (A.5)$$

A.3 Semi-Empirical Methods

A.3.1 Michel and Toussaint (1977) Equations

Based on experimental indentation test results using fresh water columnar S-2 ice, Michel and Toussaint (1977) suggested a set of equations to compute ice pressure on vertical structures. Their equations are given as follows:

1. In the ductile zone (10^{-8} sec^{-1} < $\dot{\varepsilon}$ < 5 10^{-4} sec^{-1}):

$$p = I\ f_c\ m\ \sigma_{cmax}\ (\dot{\varepsilon}/\dot{\varepsilon}_o)^{0.32} \qquad (A.6a)$$

2. In the transition zone ($5\ 10^{-4}\ sec^{-1} < \dot{\varepsilon} < 10^{-2}\ sec^{-1}$):

$$p = I\ f_c\ m\ \sigma_{cmax}\ (\dot{\varepsilon}/\dot{\varepsilon}_o)^{-0.126} \qquad (A.6b)$$

3. In the brittle zone ($\dot{\varepsilon} > 10^{-2}\ sec^{-1}$):

$$p = I\ f_c\ m\ \sigma_{cb} \qquad (A.6c)$$

where $\dot{\varepsilon}_o = 5.10^{-4}\ sec^{-1}$, σ_{cmax} is the compressive strength of ice in the ductile range, and σ_{cb} is the compressive strength of ice in the brittle zone. The values of the parameters I, f_c and m are given by Michel and Toussaint (1977).

In the above equations (Eqs. A.6a, A.6b, and A.6c), the strain rate, $\dot{\varepsilon}$, is expressed as a function of the indentor width, D, and the indentation velocity, V.

$$\dot{\varepsilon} = V/4D \qquad (A.7)$$

Other equations have been proposed to compute the strain rate, $\dot{\varepsilon}$. For example, Ralston (1978) suggested $\dot{\varepsilon} = V/2D$, and Palmer et al. (1983) suggested the equation $\dot{\varepsilon} = V/D$.

A.4 Analytical Methods

Most analytical methods developed for the calculation of ice forces on offshore structures are based on the plastic limit equilibrium state concept, whereby the behaviour of the material (ice) is idealized as an elastic-perfectly plastic

isotropic material. During indentation, only the elasticity of the material is considered until the stress reaches a critical value defined by a prescribed failure criteria, after which the material flows plastically.

For an isotropic material behaviour, both Tresca and von Mises yield criteria have been used to compute ice forces on offshore structures. Recently, a number of failure envelopes have been proposed to account for the observed anisotropic behaviour of ice, for example the failure envelopes proposed by Nadreau and Michel (1986b) and Timco and Frederking (1986).

The plasticity bound solutions have been applied to solve ice indentation problems. Croasdale et al. (1977) suggested the following equation:

$$p = I \sigma_c \qquad (A.8)$$

where the indentation factor, I, is obtained from upper and lower bound plasticity analyses. Croasdale (1980) reported that a lower bound solution (I = 1) is obtained from the plane stress case (D >> h). Upper bound solutions, however, are obtained for both rough and smooth indentors as function of aspect ratio, D/h, Fig. A.4.

Other analytical methods have been proposed to compute indentation pressures. These include the reference stress method (Ponter et al., 1983) for low strain rate problems, fracture analysis method for high strain rate problems (Miller, 1980, and Palmer et al., 1983), and the probabilistic "Unit Cell" method proposed by Ashby et al. (1986).

A.5 Numerical Methods

Both finite element and discrete element methods have been used to solve ice boundary value problems. As an example, Murat (1976) performed axi-symmetric finite element analyses to calculate the deflection of a circular floating ice sheet under the effect of a uniform distributed load at the center. He considered the material to be isotropic, and its behaviour was represented by a secondary creep equation of a power form.

It is important to point out that most of the numrical work and the proposed analytical methods were based on the following simplifying assumptions:

1. A perfect contact exists between the ice and the indentor,
2. Ice is an elastic-perfectly plastic material, and
3. Ice is a homogeneous and isotropic material.

A.6 Criticism

The most common drawbacks of the existing methods for the calculation of ice forces on offshore structures, for all categories, are listed in Chapter 1 (Statement of the Problem). These drawbacks justify the need for a general 3-D mathematical model for ice that can be used in conjuction with a numerical method (such as finite element) to analyze ice-structures interaction problems, including the calculation of ice loads.

In the following, two selected examples of field measurements of ice force histories are presented. These are the records of ice forces on Hans Island and Gulf's Molikpaq structure. The purpose is to emphasize the following two statements:

1) The calculation of ice forces exerted on offshore structures is a task underlined by a high degree of complexity, and the use of empirical and analytical methods to compute ice loads on offshore structures could result in unrealistic design of the structure.

2) The development of accurate methods to predict ice forces on offshore structures is not an academic exercise. Experimental measurements have shown that ice could exert forces in excess of the design ice load, and generate vibrations of the structure that could lead to the liquefaction of the soils of the foundations, resulting in the collapse of the structure.

Example No. 1

Sanderson (1988) presented field data of ice force histories recorded during the impact of multi-year ice floes with Hans Island Ice Foot. Hans Island is a natural island located in the center of Kennedy Channel, and it has dimensions of about 1700m X 1300m. During the months of July and August, the ice becomes very mobile and the island is subjected to numerous impacts by large multi-year ice floes travelling south west. Generally, these impacts occur in the northeast side of the island. On that side, however, a permanent ice foot is

formed, Fig. A.5a. Therefore, ice impacts do not occur with the island itself, but they occur with the island ice foot.

On the 10th of August 1983, a 5.2 thick multiyear ice floe impacted with the island ice foot. The 3200m diameter ice floe was travelling southwest at a velocity of 0.88 m/sec. During the impact, ice forces were calculated by means of measuring the floe deceleration and estimating its mass. The global ice forces generated during this impact are given in Fig. A.5b. They fluctuate in an irregular manner as function of time with force peaks occurring at random intervals.

Example No. 2

Jefferies and Wright (1988) presented field measurements of ice forces exerted on Gulf's Molikpaq structure at Amauligak. The Molikpaq is a hybrid sand-steel structure, Fig. A.6. It consists of a steel caisson set down on a previously prepared sand berm. The interior of the caisson is filled with sand to form the island core. Ice forces are measured using Medof panels and strain gauges.

An impact of a multi-year ice floe with the Molikpaq occurred on the 7th of March 1986. The ice conditions at the start of the impact are shown in Fig. A.7. A portion of the global ice force history generated during the impact is given in Fig. A.8. This force history is characterized by a random fluctuation of the ice load as function of time. A gradual increase of the magnitude of the force peaks is observed for the first 30 minutes of the impact time. Afterwards, a sporadic trace of the ice force history has occurred.

Local ice force histories, however, are shown in Fig. A.9. These ice forces are monitored at three separate locations on the exposed face of the caisson, location A, B, and C in Fig. A.9. The trace of their history vary in a periodic manner with a period of about 3.5 sec.

The Molikpaq experienced moderate vibrations during the 7th of March 1986 impact. On the 12 of April 1986, however, the structure undergone severe vibrations when a 2000m X 1000m multi-year ice floe was continuously crushing against the caisson. During this impact, the magnitude of ice forces were in excess of the design ice loads, and the structural vibrations have led to the liquefaction of the sand in the island core.

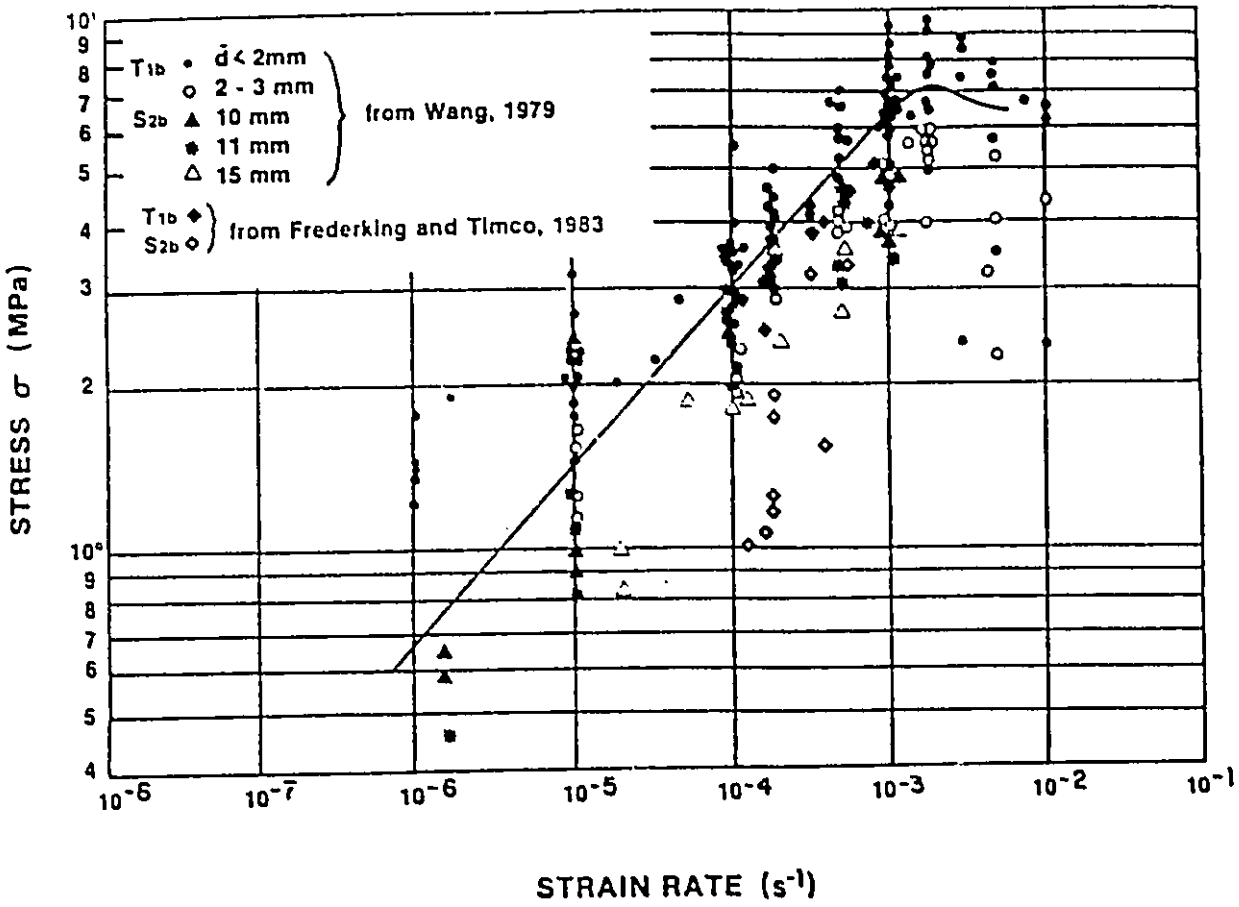

Figure A.1: Crushing strength of ice versus strain rate (Nadreau and Michel, 1984)

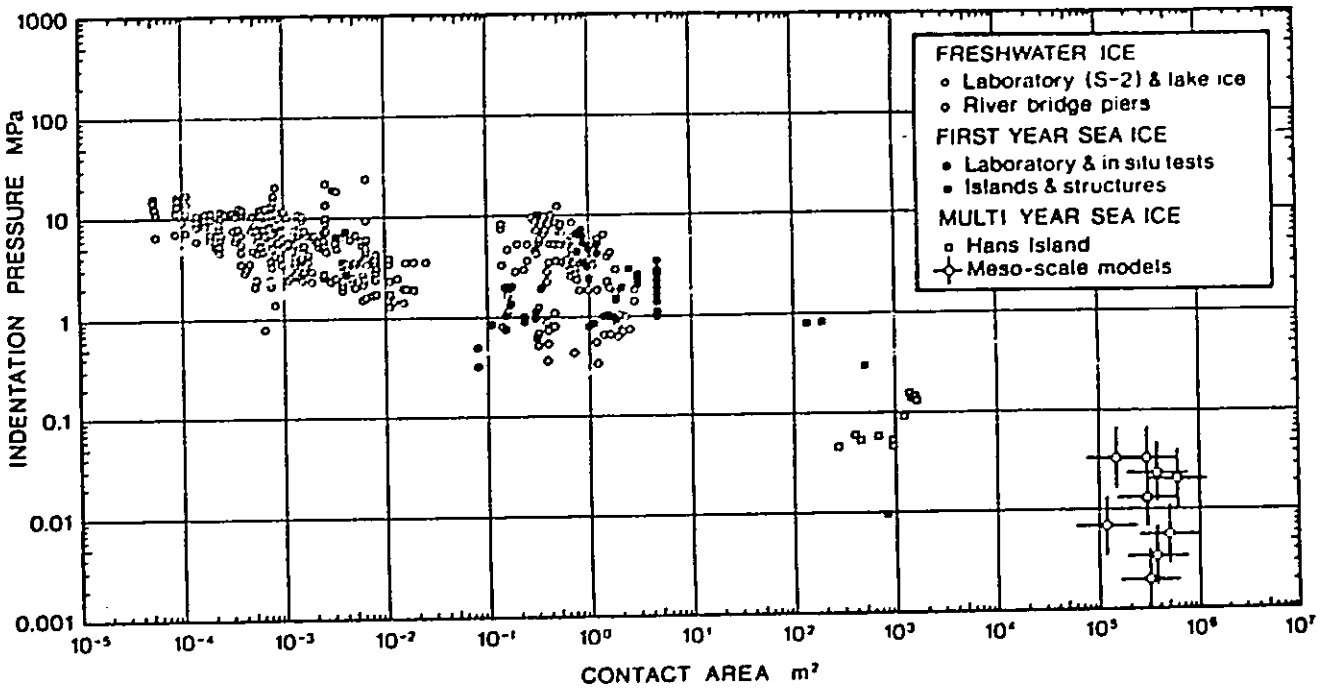

Figure A.2: Indentation pressure versus contact area (Sanderson, 1988).

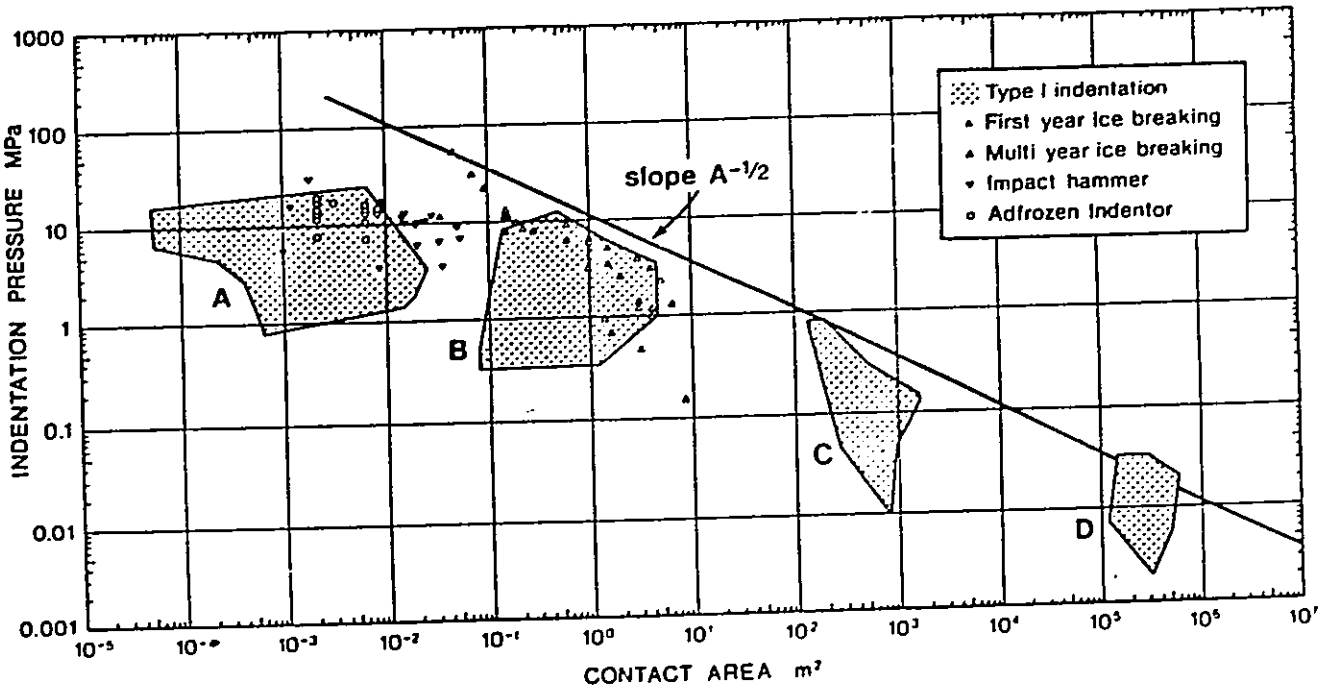

Figure A.3: Best fit curve for the data shown in Fig. A.2 (Sanderson, 1988).

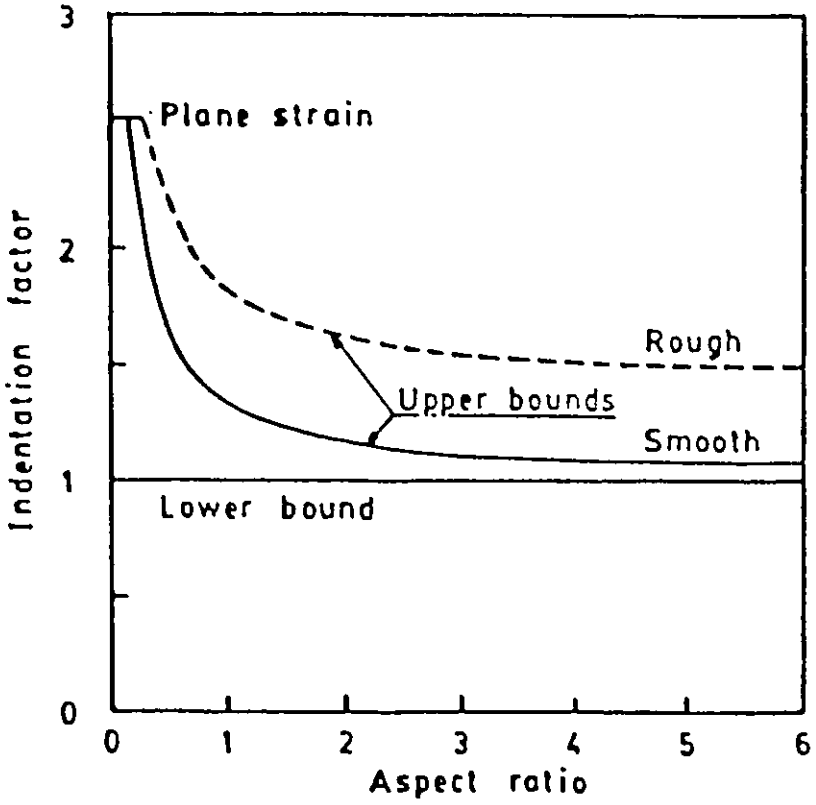

Figure A.4: Indentation factor versus aspect ratio (Croasdale et al., 1977).

a) Hans Island Ice Foot.

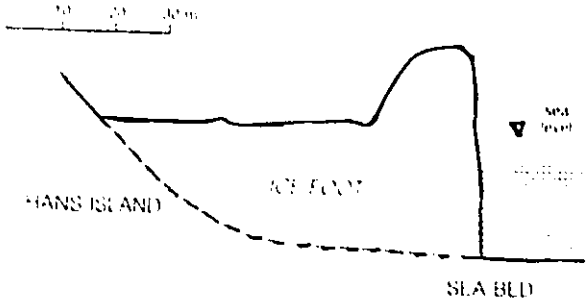

b) Ice force history generated during the impact of an ice floe with the island ice foot.

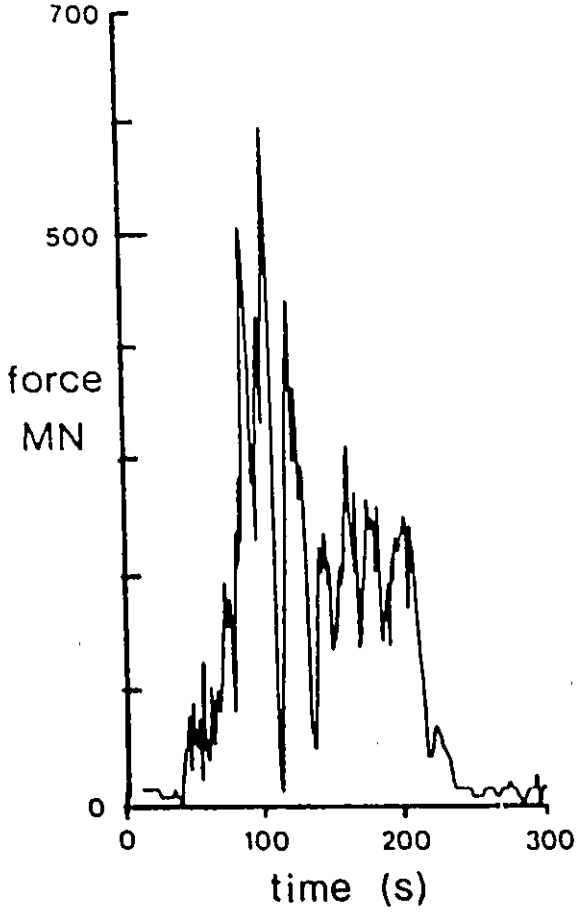

Figure A.5: Hans Island, field data from the impact of the 10th of August 1983 (Sanderson, 1988).

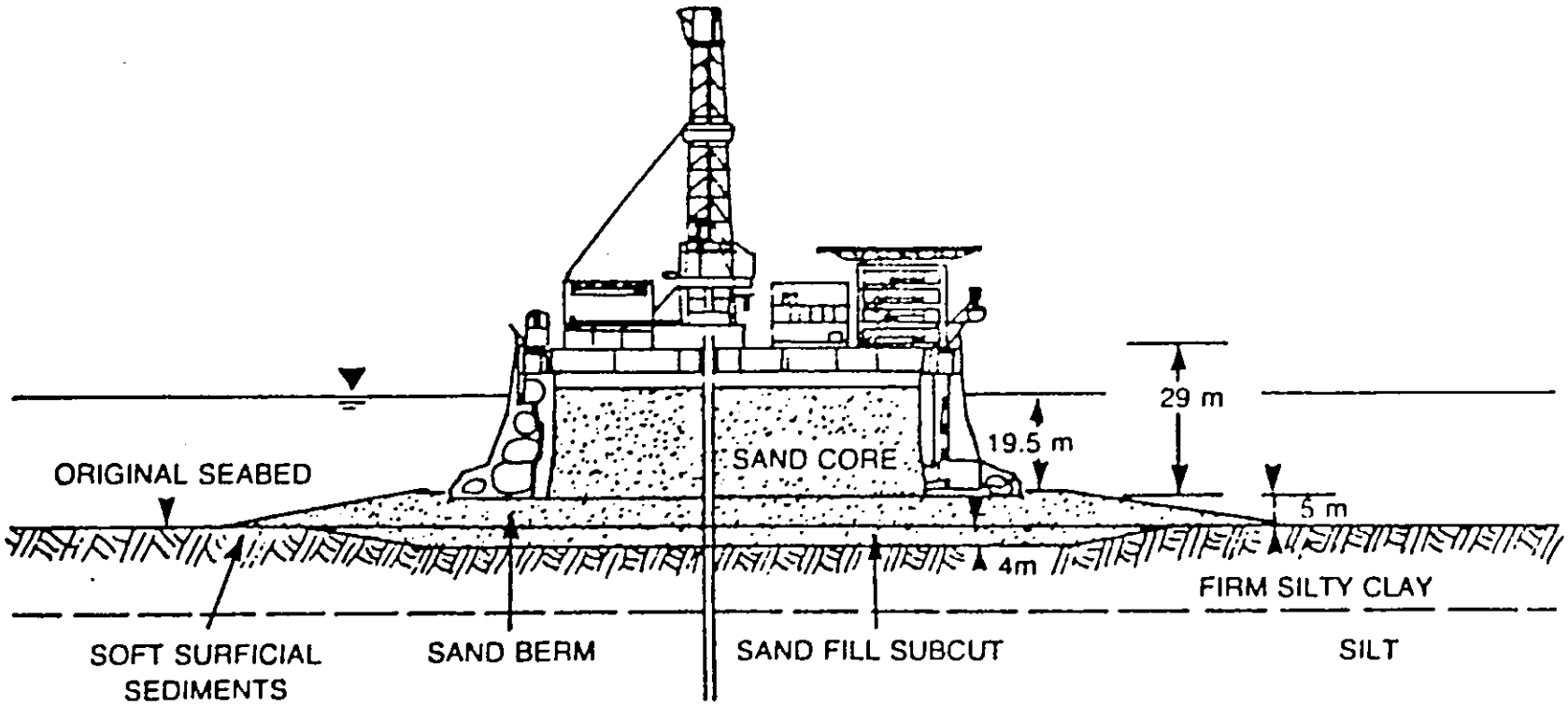

Figure A.6: The Molikpaq structure.

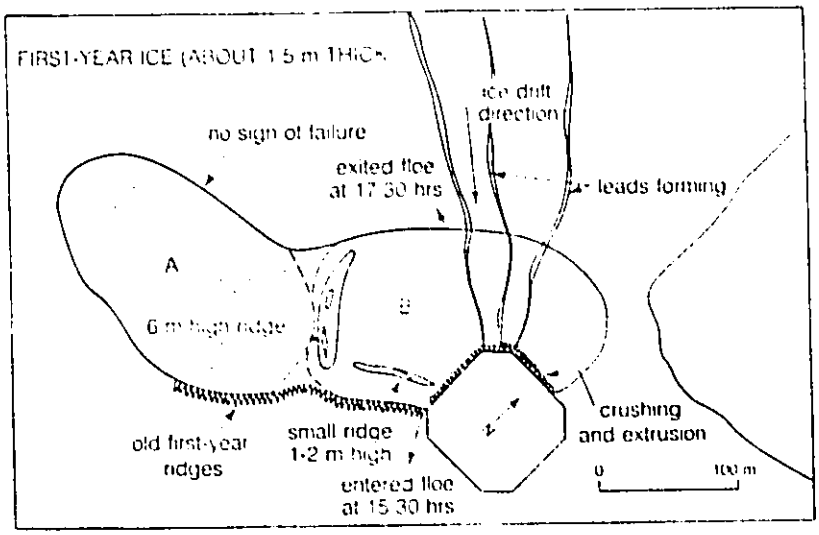

Figure A.7: Ice conditions just before the impact of the 7th of March 1986 (Jefferies and Wright, 1988)

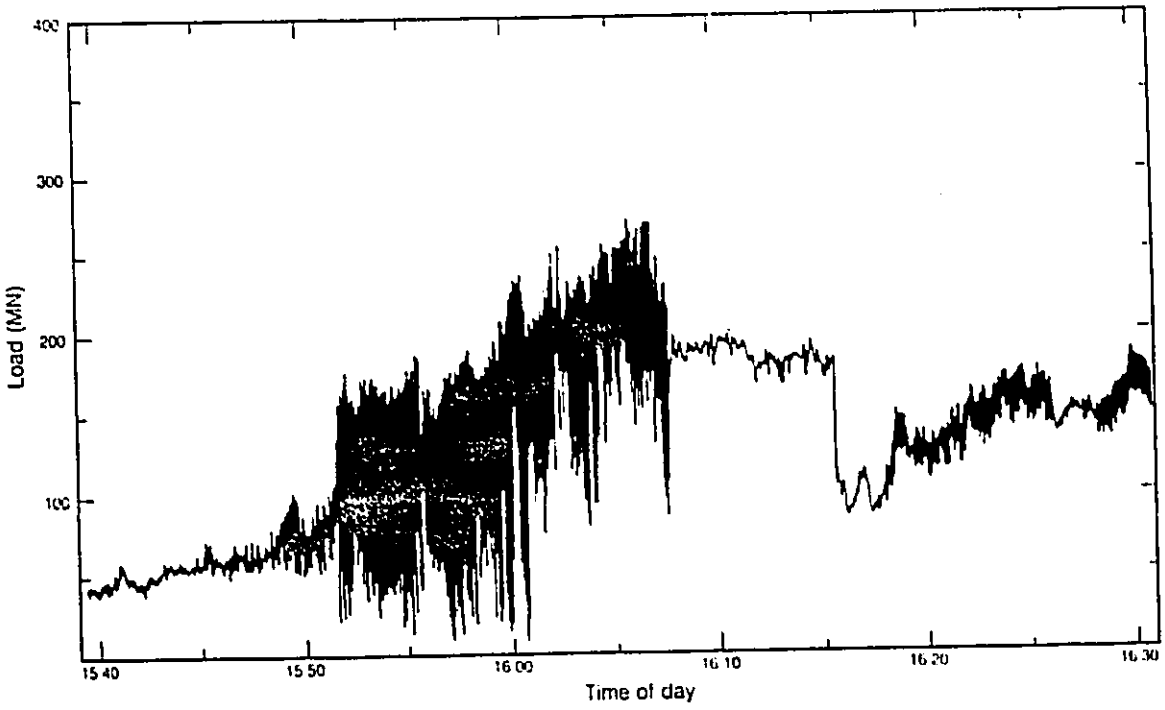

Figure A.8: Total ice force on the Molikpaq during the impact of the 7th of March 1986 (Jefferies and Wright, 1988)

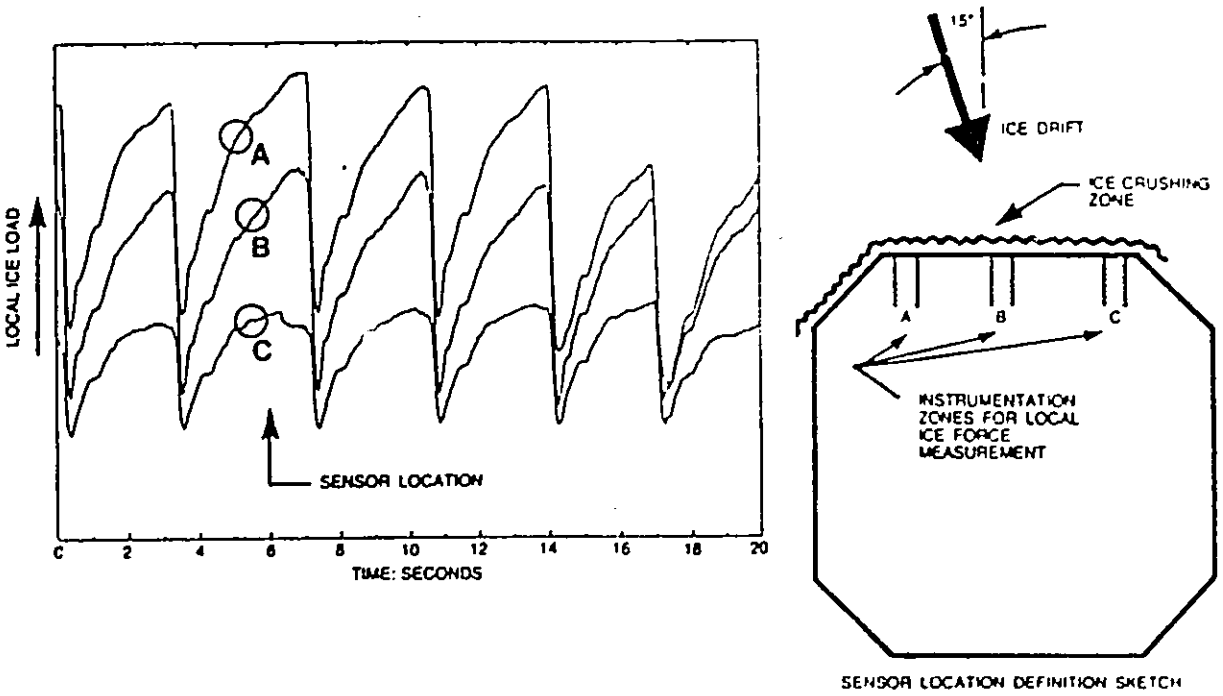

Figure A.9: Local ice forces on the Molikpaq during the impact of the 7th of March 1986 (Jefferies and Wright, 1988)

APPENDIX B

STRESS AND STRAIN INVARIANTS

APPENDIX B

STRESS AND STRAIN INVARIANTS

The stress and strain invariants used in this work are presented. The notation is similar to that of Desai and Siriwardane (1984).

B.1 Stress Invariants

1- The first invariant of the stress tensor, $I_{1\sigma}$:

$$I_{1\sigma} = (\sigma_x + \sigma_y + \sigma_z) \tag{B.1}$$

2- The octahedral shear stress, τ_{oct}:

$$\tau_{oct} = \frac{1}{3}\left[(\sigma_x-\sigma_y)^2+(\sigma_y-\sigma_z)^2+(\sigma_z-\sigma_x)^2+ 6(\tau_{xy}^2 + \tau_{yz}^2 + \tau_{zx}^2)\right]^{1/2} \tag{B.2}$$

3- The second invariant of deviatoric stress tensor, J_{2D}:

$$J_{2D} = \frac{3}{2}\tau_{oct}^2 = \frac{1}{2}\,tr(S)^2 \tag{B.3}$$

where S is the deviatoric stress tensor.

In Chapters 5 and 6, the shear stress, q, was used:

$$q = \sqrt{3\, J_{2D}} = (3/\sqrt{2})\, \tau_{oct} = \left[\frac{3}{2}\, S_{ij}\, S_{ij} \right]^{1/2} \qquad (B.4)$$

In terms of principal stresses, the hydrostatic pressure, p, and the shear stress, q, are given as follows:

$$p = \frac{1}{3} (\sigma_1 + \sigma_2 + \sigma_3) \qquad (B.5)$$

$$q = (1/\sqrt{2}) \left[(\sigma_1 - \sigma_2)^2 + (\sigma_2 - \sigma_3)^2 + (\sigma_3 - \sigma_i)^2 \right]^{1/2} \qquad (B.6)$$

B.2 Strain Invariants

The strain invariants corresponding to $I_{1\sigma}$ (Eq. B.1) and τ_{oct} (Eq. B.2) are the first invariant of the strain tensor, $I_{1\varepsilon}$, and the octahedral shear strain, γ_{oct}, respectively:

$$I_{1\varepsilon} = (\varepsilon_x + \varepsilon_y + \varepsilon_z) \qquad (B.7)$$

$$\gamma_{oct} = \frac{2}{3} \left[(\varepsilon_x - \varepsilon_y)^2 + (\varepsilon_y - \varepsilon_z)^2 + (\varepsilon_z - \varepsilon_x)^2 + \frac{3}{2} (\varepsilon_{xy}^2 + \varepsilon_{yz}^2 + \varepsilon_{zx}^2) \right]^{1/2} \qquad (B.8)$$

Corresponding to the shear stress, q, is the generalized (or equivalent) shear strain, $\bar{\varepsilon}$,

$$\bar{\varepsilon} = \frac{1}{\sqrt{2}}\, \gamma_{oct} \qquad (B.9)$$

In terms of principal stresses, the volumetric strain, ε_v, and the generalized shear strain, $\bar{\varepsilon}$, are given as follows:

$$\varepsilon_v = (\varepsilon_1 + \varepsilon_2 + \varepsilon_3) \tag{B.10}$$

$$\bar{\varepsilon} = \frac{\sqrt{2}}{3} \left[(\varepsilon_1 - \varepsilon_2)^2 + (\varepsilon_2 - \varepsilon_3)^2 + (\varepsilon_3 - \varepsilon_1)^2 \right]^{1/2} \tag{B.11}$$

B.3 Stress Invariants for Anisotropic Plastic Materials

Since the hydrostatic pressure does not influence the plastic behaviour of ice (see Section 5.4.1), its anisotropy must be associated with the shear stress, q. A second invariant of deviatoric stress tensor for an anisotropic material is proposed as:

$$\bar{J}_{2D} = \frac{1}{2} \bar{S}_{ij} \bar{S}_{ij} \tag{B.12}$$

where the deviatoric stress tensor, $\bar{S}_{ij}$, is expressed as follows:

$$\bar{S}_{ij} = \begin{vmatrix} a_1(\sigma_{11} - p) & a_4\sigma_{12} & a_5\sigma_{13} \\ a_7\sigma_{21} & a_2(\sigma_{22} - p) & a_6\sigma_{23} \\ a_8\sigma_{31} & a_9\sigma_{32} & a_3(\sigma_{33} - p) \end{vmatrix} \tag{B.13}$$

where p is the hydrostatic pressure, and a_i (i =1, 9) are parameters characteristic of the current state of the material anisotropy.

Since columnar grained (S-1 and S-2) is considered to undergo plastic deformations only in the directions perpendicular to the long axis of the grains (see Section 5.4.3), the anisotropic parameters a_i (i = 3, 9) should be zeros.

The condition of zero plastic volumetric strains ($\varepsilon_v^p = 0.$, see Section 5.4.1) requires that:

$$\sum_1^3 \bar{S}_{ii} = a_1(\sigma_{11} - p) + a_2(\sigma_{22} - p) + a_3(\sigma_{33} - p) = 0. \qquad (B.14)$$

Since the parameter $a_3 = 0$, only two unknowns (a_1 and a_2) have to be determined. Without loss of the generality, the value of the parameter a_1 can be fixed to 1, and the parameter a_2 is calculated with respect to a_1.

The value of a_2 is determined from Eq. B.14 (for $a_1 = 1$).

$$a_2 = \frac{\sigma_{11} - p}{p - \sigma_{22}} \qquad (B.15)$$

The shear stress, $\bar{q}$, for an anisotropic material is calculated as follows:

$$\bar{q} = \left[\frac{2}{3} \bar{S}_{ij} \bar{S}_{ij} \right]^{1/2} \qquad (B.16)$$

In terms of principal stresses, the shear stress, $\bar{q}$ is given as follows:

$$\bar{q} = (1/\sqrt{2})\left[A_1(\sigma_1 - \sigma_2)^2 + A_2(\sigma_2 - \sigma_3)^2 + A_3(\sigma_3 - \sigma_1)^2\right]^{1/2} \quad \text{(B.17)}$$

where:

$$A_1 = \frac{2}{3}(1 + a_2^2),$$

$$A_2 = \frac{1}{3}(2a_2^2 - 1), \text{ and}$$

$$A_3 = \frac{1}{3}(2 - a_2^2)$$

In order to ensure that the axes of the material anisotropy coincide with the axes of the principal stresses. The expression of $\bar{q}$ (in Eq. B.17) is modified as follows:

$$\bar{q} = \frac{\sqrt{3}}{\sqrt{2}}\left[\frac{A_1(\sigma_x - \sigma_y)^2 + A_2(\sigma_y - \sigma_z)^2 + A_3(\sigma_z - \sigma_x)^2}{1/2(1 + a^2) + 1/2|a^2 - 1|}\right] \quad \text{(B.18)}$$

Equation B. 18 ensures that for uniaxial loading situations $\bar{q}$ is equal to σ. For example, for uniaxial compression loading, $\bar{q} = \sigma_{11}$.

APPENDIX C

REVIEW OF THE
CLASSICAL THEORY OF PLASTICITY

APPENDIX C

CLASSICAL THEORY OF PLASTICITY

The visco-plastic strain component of the non-cracking sub-model, Eq. 5.21, was formulated on the basis of the classical theory of plasticity. In view of this, a brief review of the classical theory of plasticity is given this Appendix. The conceptional differences between the formulation developed in this thesis and those of the classical theory of plasticity are pointed out. The main references used in this review are those of Hill (1950) and Prager (1949).

C.1 Introduction

The objective of the classical theory of plasticity is to offer a mathematical description for the mechanical behaviour of metals undergoing plastic deformations. Originally, the theory was based on certain simplifying assumptions:

1- The stress-strain relations are independent of time and temperature.

2- The material is assumed to be isotropic and Bauschinger effect is neglected (the negligence of Bauschinger effect means that the yield stress in compression equals to that in tension).

In general, constitutive equations based on the classical theory of plasticity contain the following items:

1- A yield criterion specifying the state of stress at which the material undergoes plastic deformations.

2- A hardening rule specifying the change of the plastic material properties in the course of plastic deformations.

3- A flow rule specifying the direction of the plastic strain vectors.

Brief descriptions of these items are given in the following Sections.

C.2 Yield Surface and Concept of Yield Criterion

For many materials, an elastic region exists around the origin of the stress space. This elastic region is bounded by a plastic domain where a change in the stresses produces a change in the permanent strains. The surface bounding the elastic region, in the stress space, is called the yield surface while the mathematical law defining the limit of elasticity, under any combination of stresses, is known as the yield criterion.

Isotropic plastic yielding depends only on the magnitude of the principal stresses, and any yield criterion can be expressed as function of all three invariants of the stress tensor. However, experimental evidence indicated that yielding of metals is unaffected by the hydrostatic stresses either

applied alone or superposed on some combined state of stress. Therefore, The yield criterion can be expressed as function of only the second and third invariants of the stress tensor.

The material isotropy, the absence of Bauschinger effect, and the fact that yielding is independent on the hydrostatic stresses dictate that the yield surface can be, geometrically, represented by a cylinder of infinite length whose axis is the space diagonal (for example, von Mises yield surface).

C.3 Hardening Concept and Hardening Rules

Two hypotheses have been proposed to define the degree of hardening. The first indicates that hardening depends only on the plastic work, W^p. The second, however, employs the equivalent plastic strain ($\bar{\varepsilon}^p$, Appendix A) as the measure for hardening. In the theory of plasticity, if the hardening is formulated in terms of the plastic work, the material is said to be work harden, otherwise the material is said to be strain harden.

As hardening occurs, the yield surface changes size and location in the stress space. However, its shape and orientation do not change. The change of the geometric configuration of the yield surface expresses the changes of the plastic properties of the material. It can be formulated as function of either the plastic work or plastic strains according to the two hypotheses of hardening.

C.4 Flow Rule

The flow rule defines the direction of the plastic strain vectors. The theory of plasticity assumes the existence of a plastic potential function, g, to which the incremental plastic strain vectors are orthogonal:

$$d\varepsilon^{p}_{ij} = \Lambda \frac{\partial g}{\partial \sigma_{ij}} \qquad (C.1)$$

where Λ is a positive scalar factor of proportionality.

Equation C.1 is known, also, as the normality rule of plasticity. Two types of flow rules can be used to formulate the plastic constitutive relations. These are the associative and non-associative flow rules. Associative flow rule referees to the case where the same formulation is adopted for both yield surface, f, and plastic potential, g, functions. However, the non-associative flow rule reefers to the case where the formulation of the functions f and g are different.

C.5 Requirements for the Formulation of Plastic Stress-Strain Relations

The development of a plastic stress-strain relationship should satisfy certain requirements: Among these are: the irreversibility, continuity, and consistency conditions.

Condition of Irreversibility: This condition dictates that the plastic work done on a material cannot be reclaimed. In other words, the plastic work done on a material is always positive.

Continuity Condition: In the classical theory of plasticity, the plastic strains are generated only during loading. However, loading and unloading are defined according to whether the stress vector is directed toward the exterior or the interior of the yield surface, respectively.

If the stress vector is tangential to the yield surface, the loading is said to be neutral. The neutral loading, however, is considered to be the dividing case between the loading and unloading situations. In order to avoid any discontinuities in the plastic stress-strain relations, the condition of continuity requires that the neutral loading does not cause any plastic deformations.

Consistency Condition: This condition requires that loading from one plastic state leads to an-other plastic state. In other words, during loading, the stress point should be always on the yield surface.

During loading, the yield surface changes its geometric configuration, size and location. This is due to the consistency condition which requires that both the stress point and the yield surface move together, in the stress space. The change of the geometric configuration of the yield surface (required by the consistency condition) expresses the hardening of the material. Three various hardening rules can be used to formulate plastic constitutive relations:

1- Isotropic hardening rule: The yield surface undergoes a uniform expansion without any change in the location. For example, in the case of von Mises yield surface, the

circle changes size (radius) and does not change its co-ordinates of the center.

2- Kinematic hardening: The yield surface undergoes movement (change in location) without any change of its size.

3- A combined isotropic and kinematic hardening rules: The yield surface undergoes changes in both size and location.

C.6 Present Model Versus Classical Theory of Plasticity

The following is a list of the main differences between the formulation of the present model and those of the classical theory of plasticity:

1-The visco-plastic constitutive equation developed in this thesis (Eq. 5.21, Chapter 5) has neither a yield criterion nor a yield surface. The absence of the yield surface from the present model formulation results in two advantages.

a-There is no elastic zone around the origin of the stress space where the behaviour of ice is completely elastic. Creep experiments (Chapter 3) have indicated that the time dependent permanent (visco-plastic) strains are generated in the ice samples event if the applied stress is small (for example, 0.5 MPa in creep test No. 2).

b-The absence of a yield surface function dictates the elimination of the continuity condition. Under any loading combination, the model predicts plastic (permanent) strains (regardless whether the stress vector is directed towards the exterior, the interior, or tangential to the yield

surface). Hence, the model predicts permanent strains during unloading-reloading situations. In the classical theory of plasticity, however, no permanent strains take place during: 1) unloading and 2) while the stress point is in side the yield surface

2-The structural change function ($\Delta\lambda$, in Eq. 5.34) is equivalent to the hardening rule in the classical theory of plasticity. Both define the degree of the structural modification of the material induced by the plastic strains.

3-Similarly to the classical theory of plasticity, the model satisfies the irreversibility condition: The plastic work is always positive.

4-During loading, the condition required by the equilibrium plastic state function (F, in Eq 5.6) has to be satisfied as long as the material is in plastic state. This condition is similar to the consistency condition outlined above.

APPENDIX D

LABORATORY EXPERIMENTS
(figures)

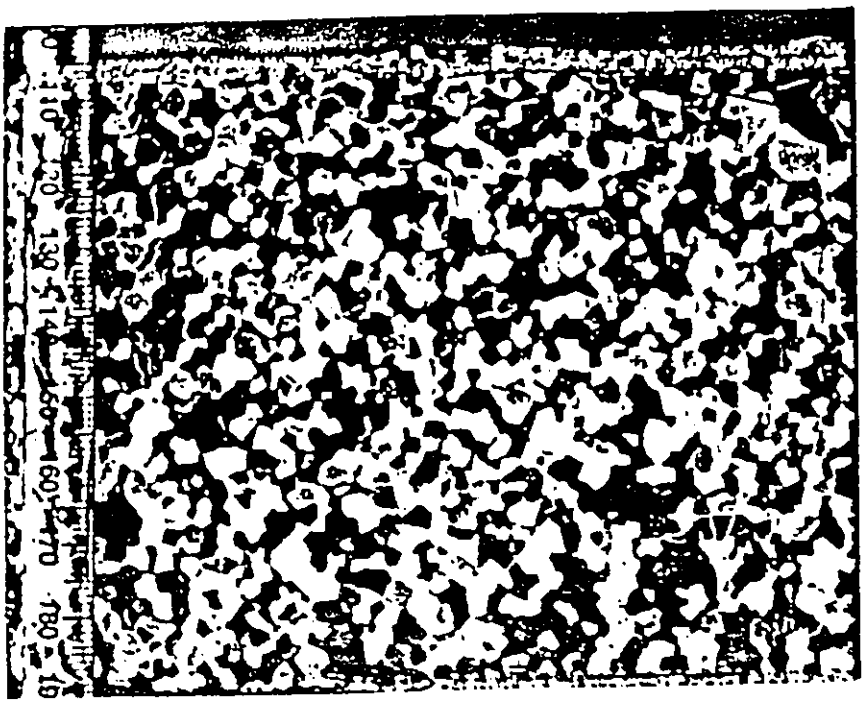

(A)

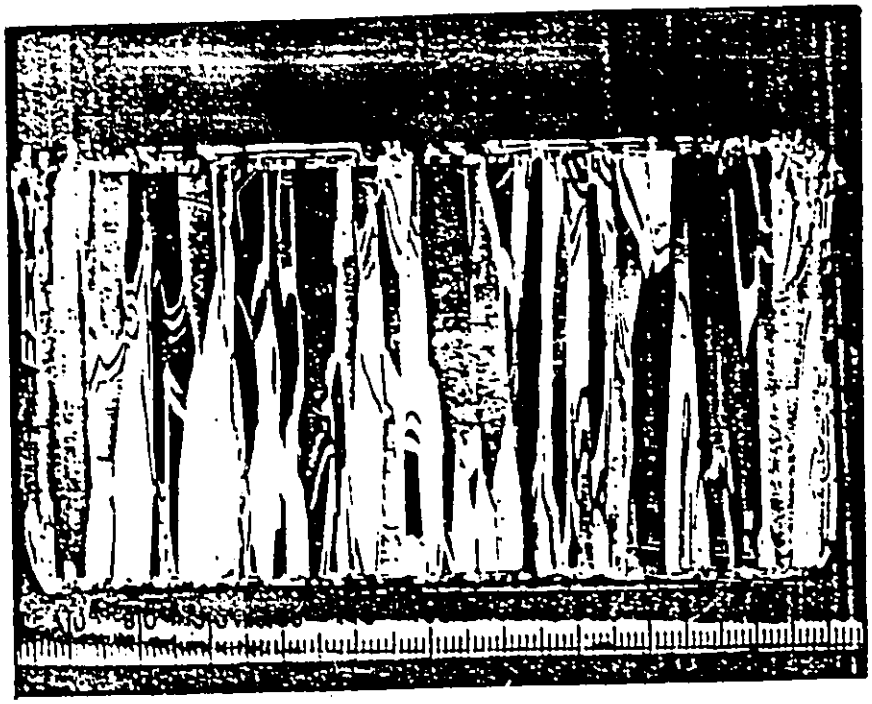

(B)

Figure D.1: Microtomed thin sections under cross polarized light a) horizontal section b) vertical section.

(A)

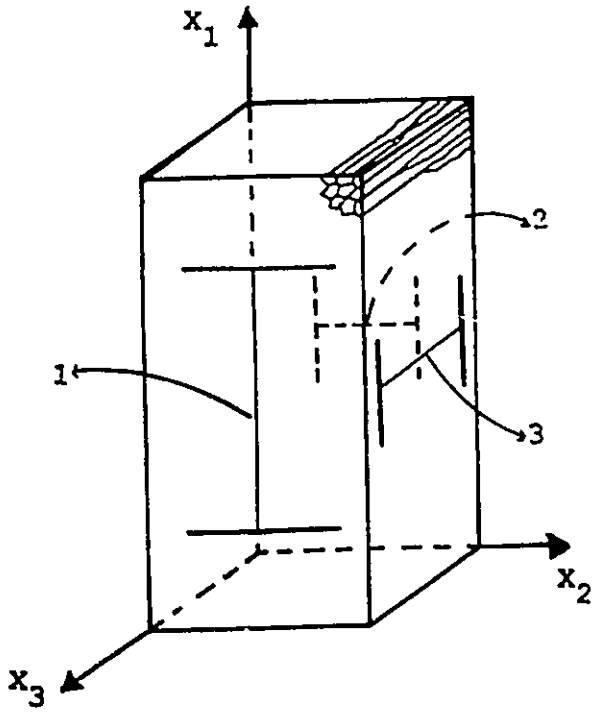

Extensometers:

1 Axial

2 normal to the columns

3 along the columns

(B)

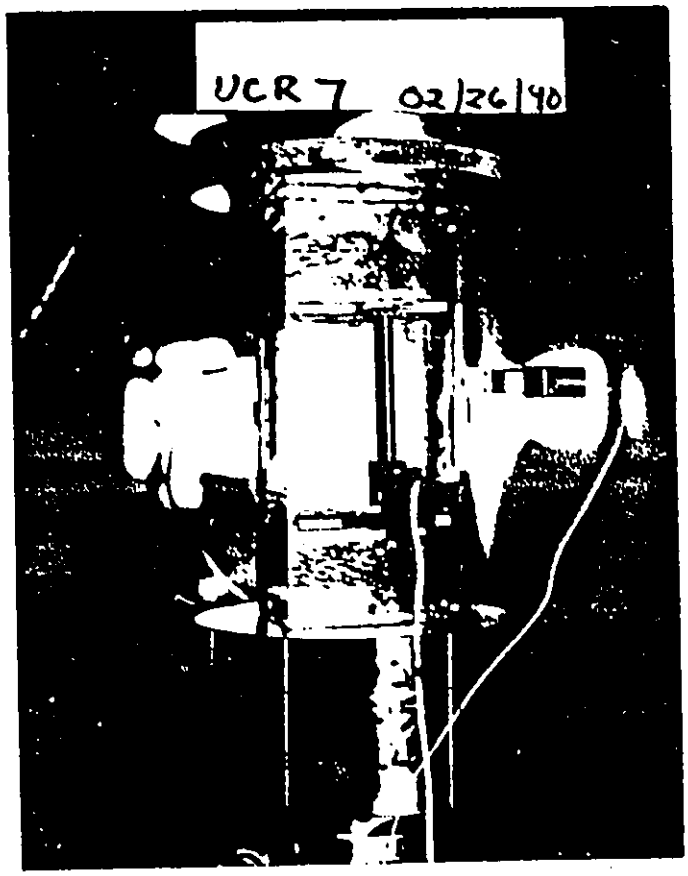

Figure D.2: Experimental setup: a) schematic representation for the extensometers on the sample b) test machine photographed during an experiment.

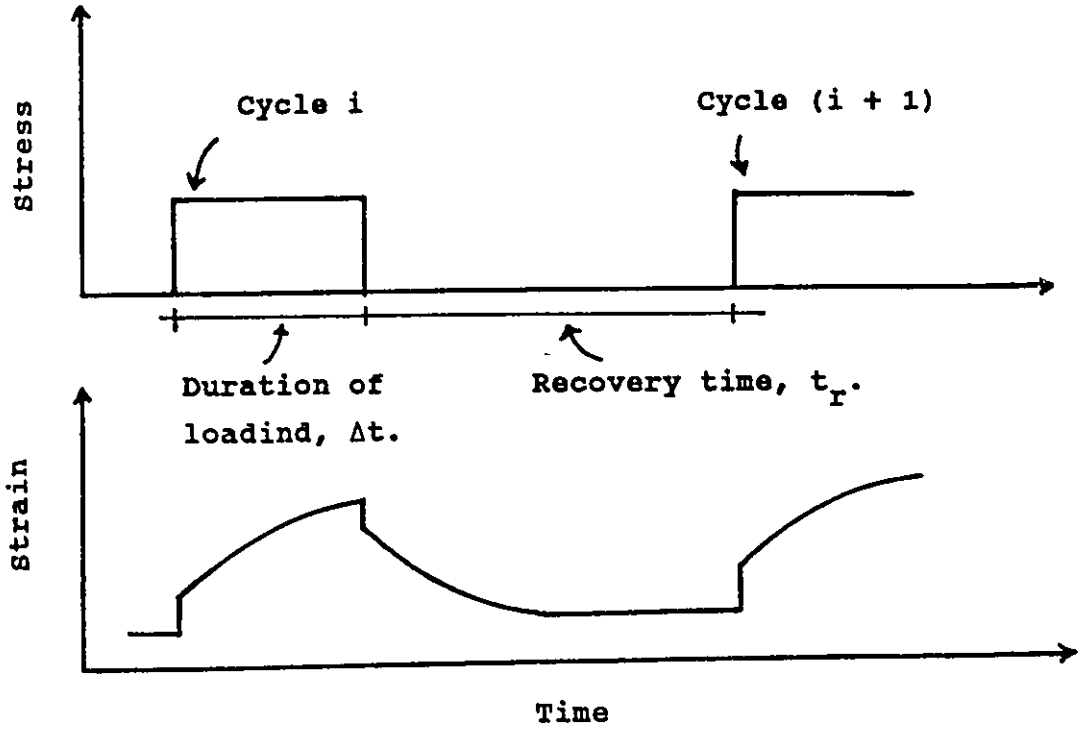

Figure D.3a: Schematic of stress and strain histories.

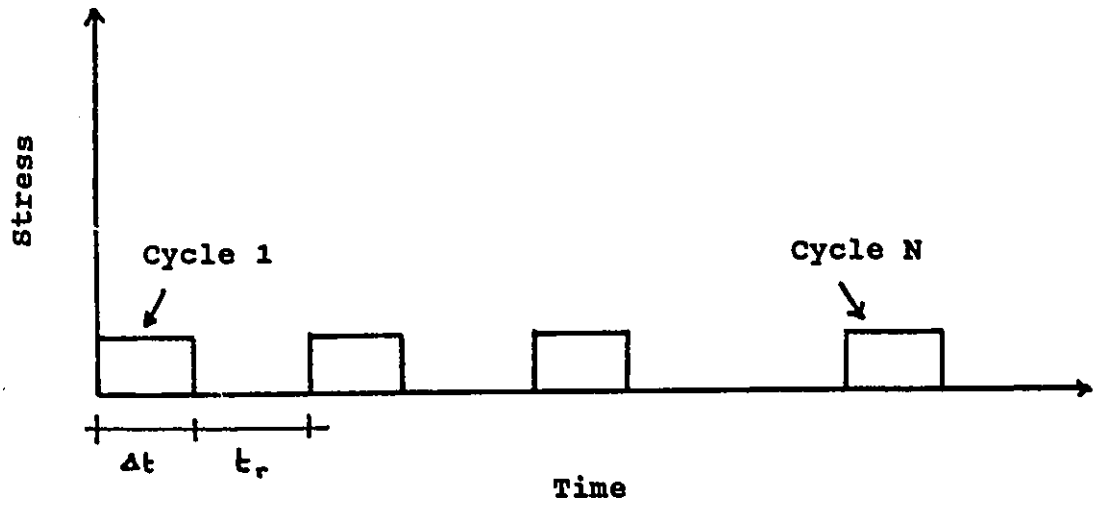

Figure D.3b: Schematic representation of the stress history followed during testing.

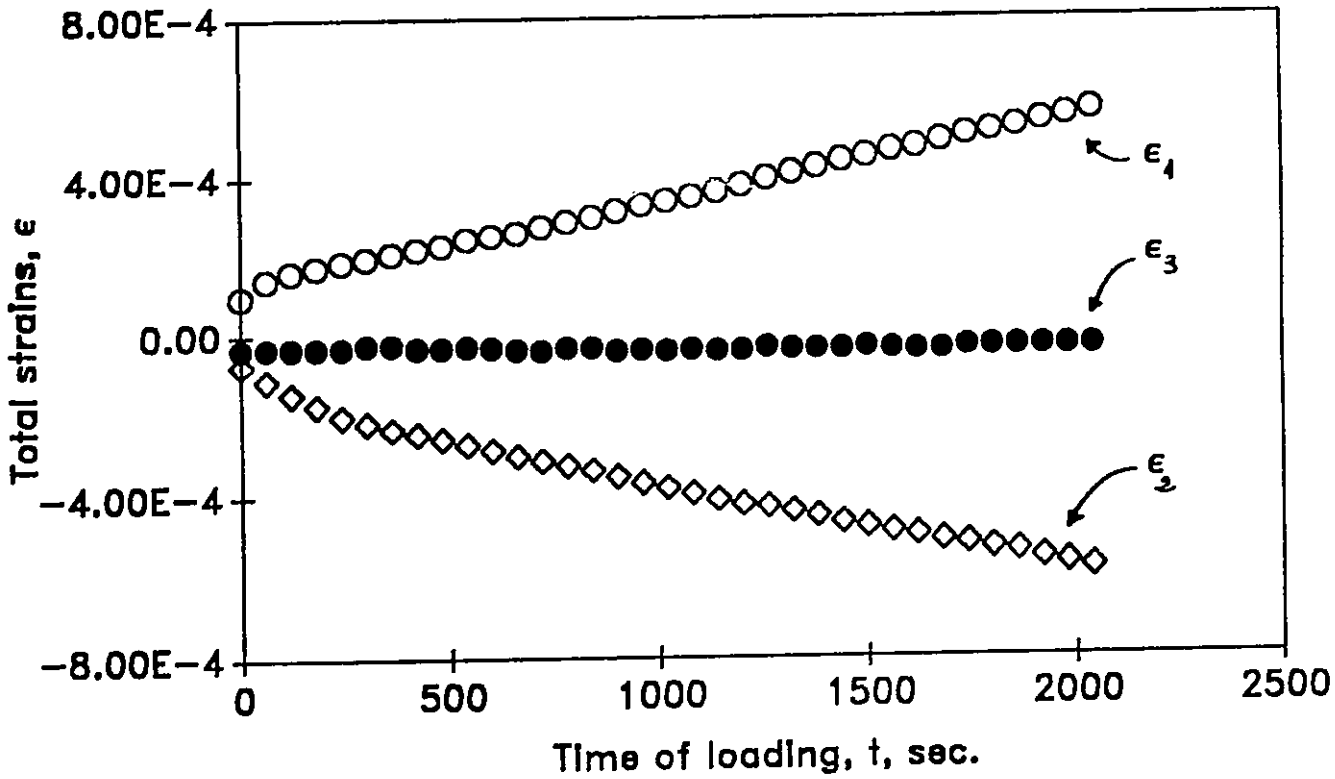

Figure D.4: Creep test No. 1, measured axial and lateral total strain histories. The measured strains correspond to those at the end of the loading cycles. Stress of 1.0 MPa was applied for 60 sec, then the load was removed, for a total of 34 cycles.

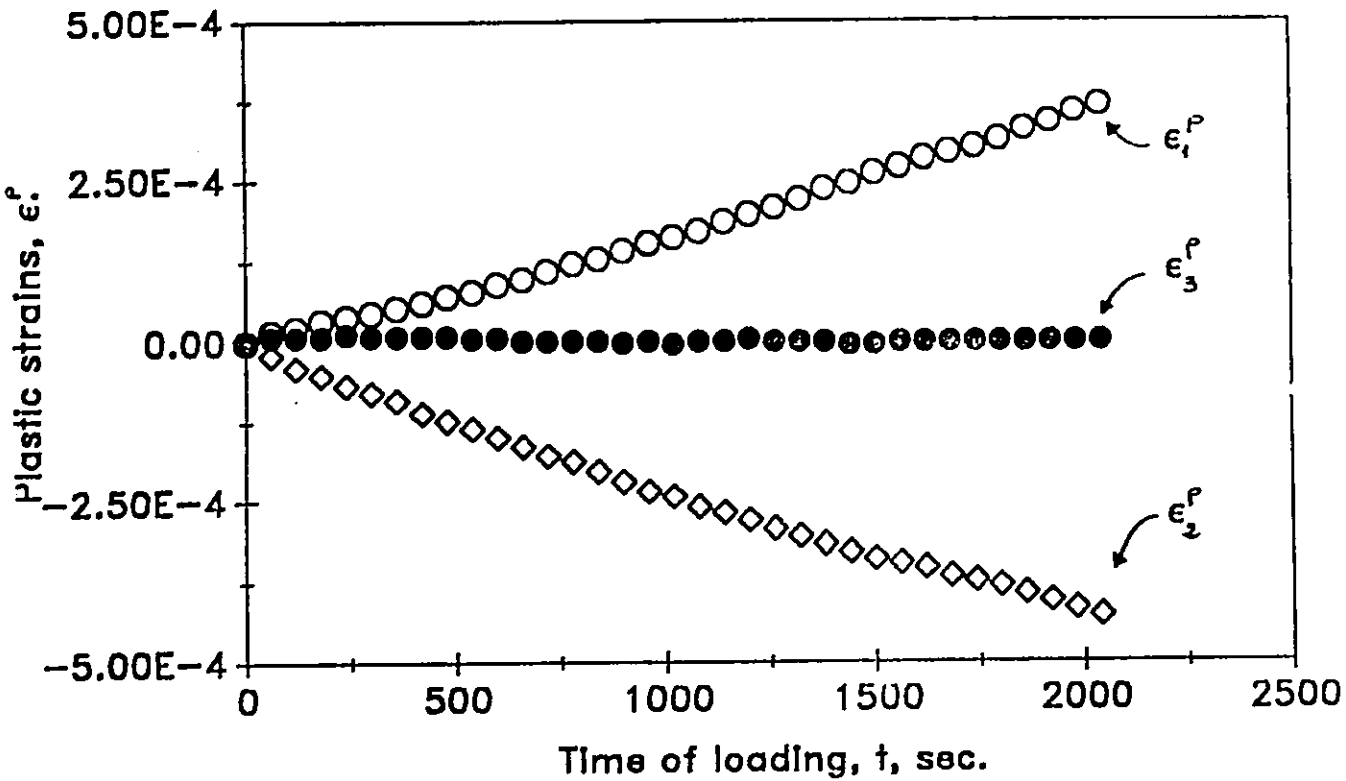

Figure D.5: Creep test No. 1, measured axial and lateral plastic strain histories.

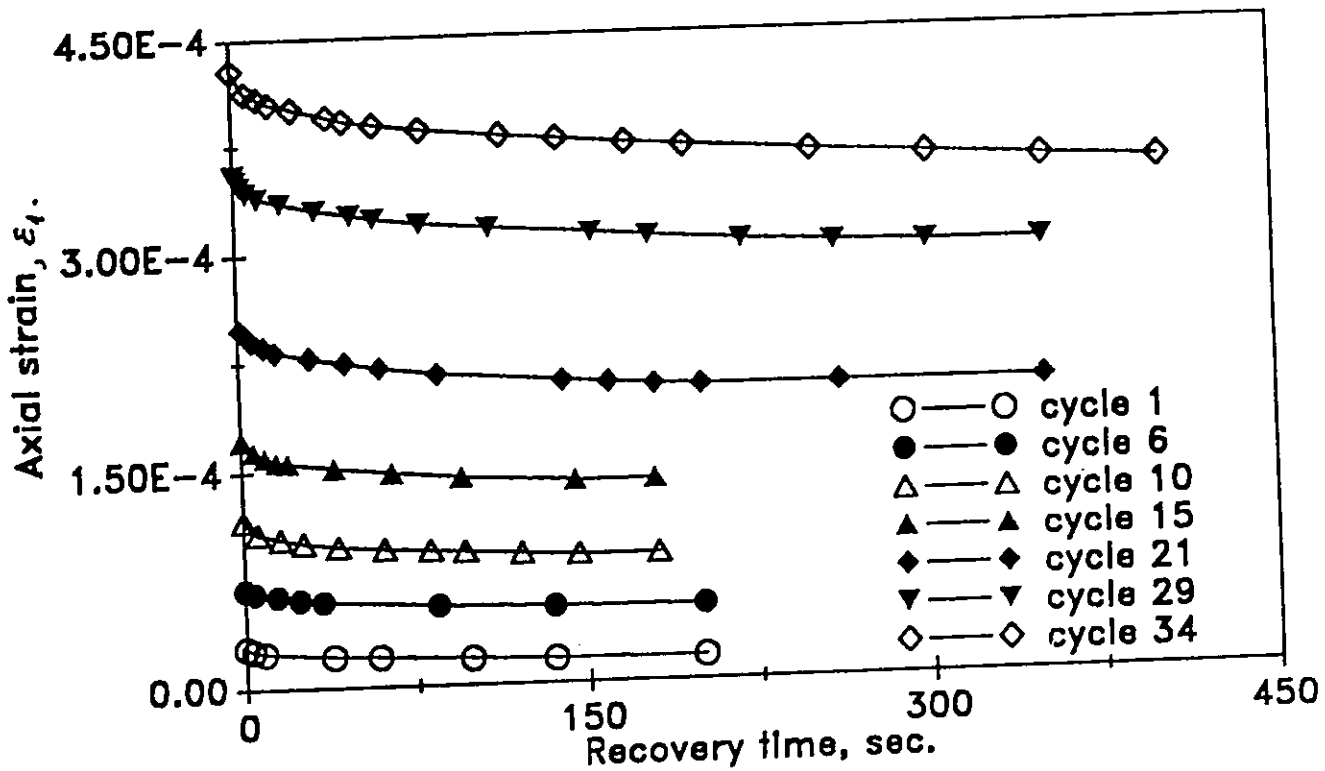

Figure D.6: Creep test No. 1, measured recoverable axial strain histories for various cycles of loading.

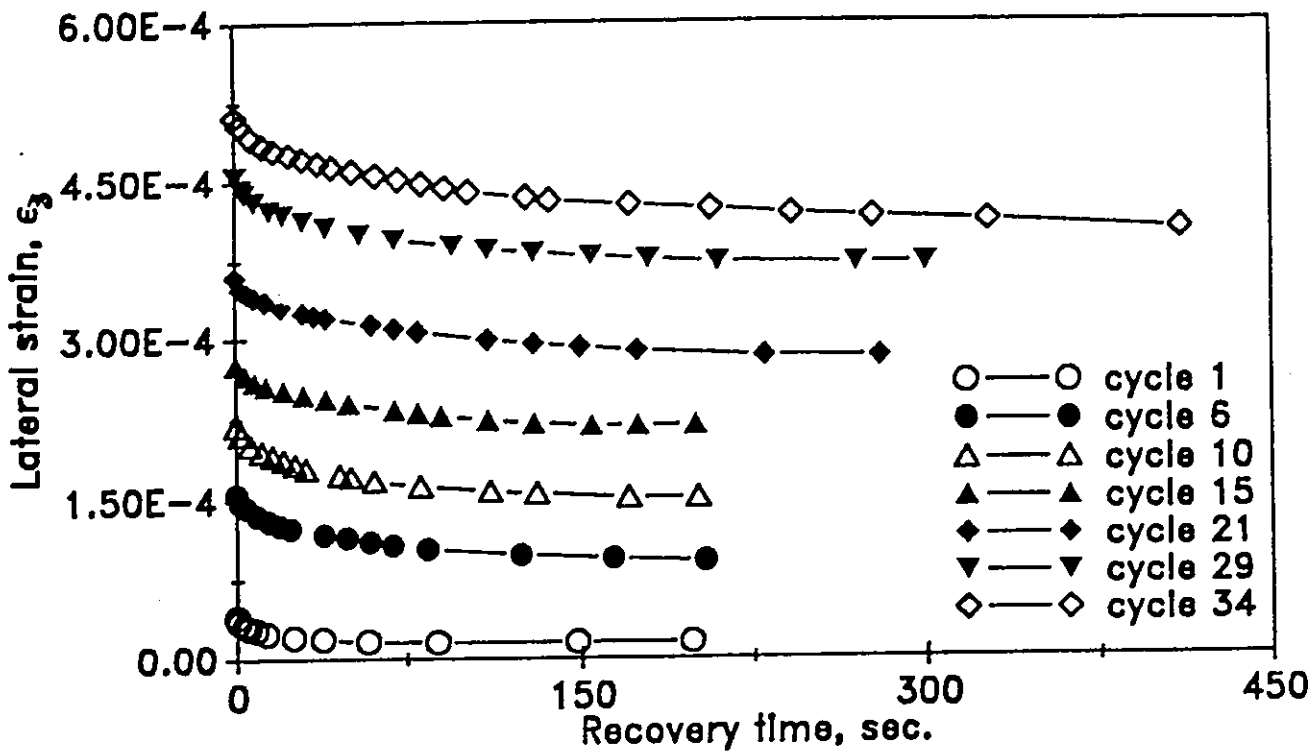

Figure D.7: Creep test No. 1, measured recoverable lateral strain histories for various cycles of loading.

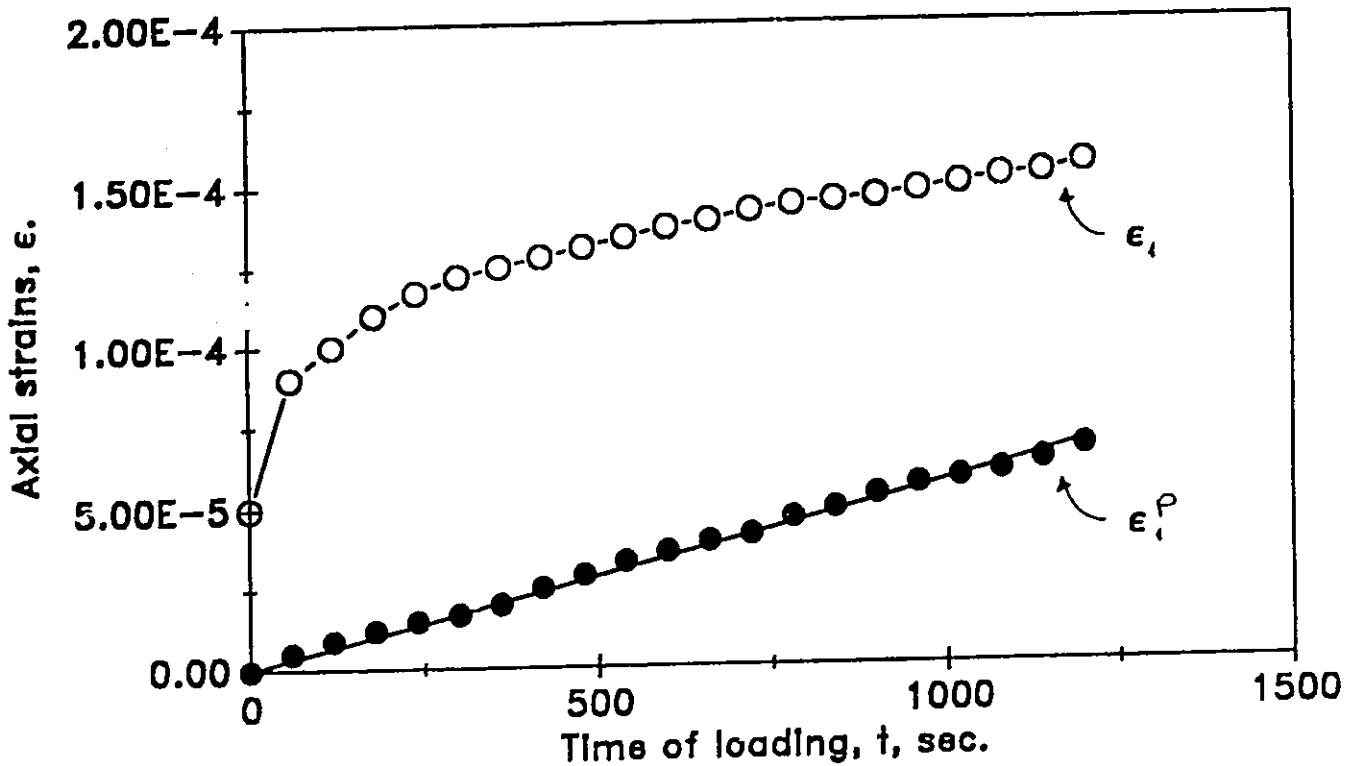

Figure D.8: Creep test No. 2, measured total and plastic axial strain histories. Stress of 0.5 MPa was applied for 60 sec, then the load was removed, for a total of 20 cycles.

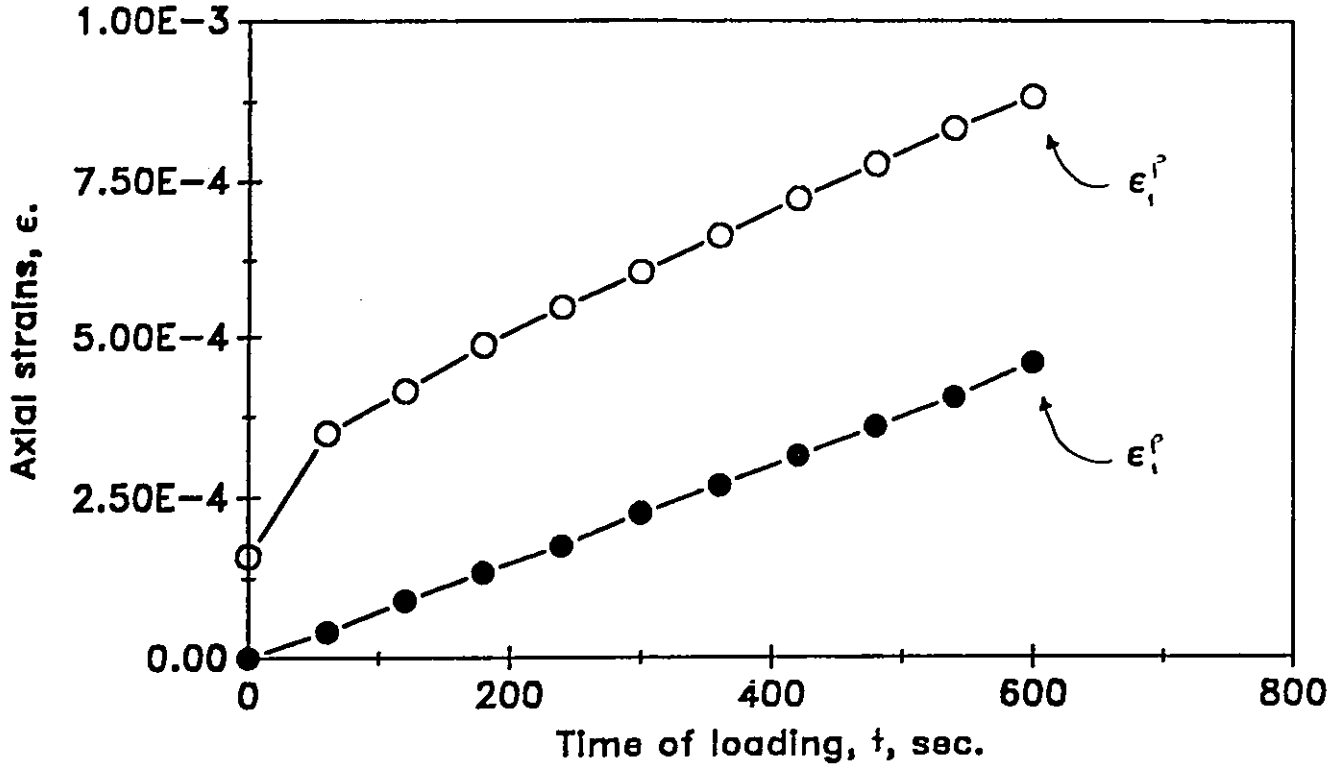

Figure D.9: Creep test No. 3, measured total and plastic axial strain histories. Stress of 1.5 MPa was applied for 60 sec, then the load was removed, for a total of 10 cycles.

APPENDIX E

PRACTICAL ELASTIC MODULI FOR ICE
(figures)

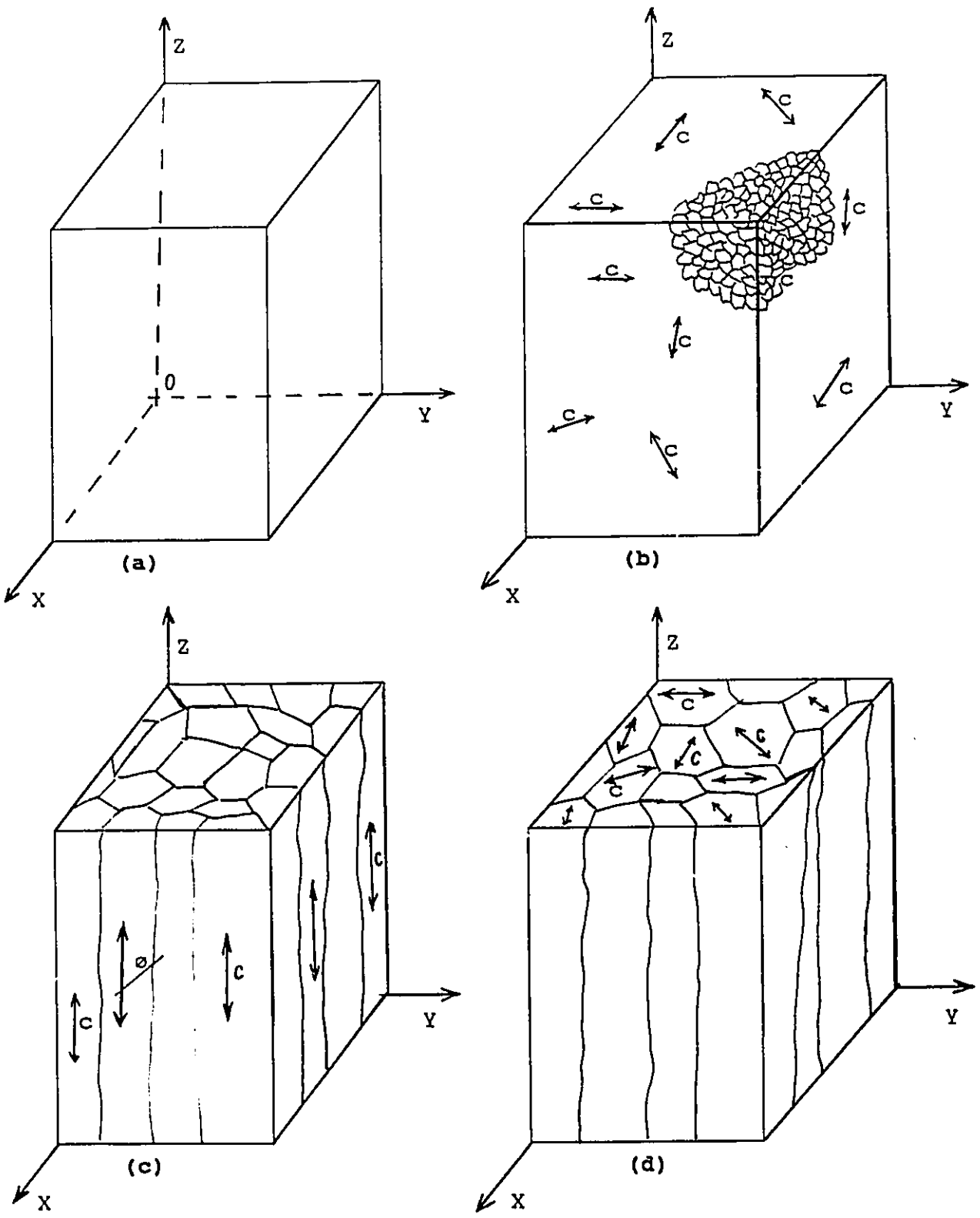

Figure E.1: Schematic of ice types a) Co-ordinates system <xyz> b) granular ice c) columnar grained S-1 ice d) columnar grained S-2 ice.

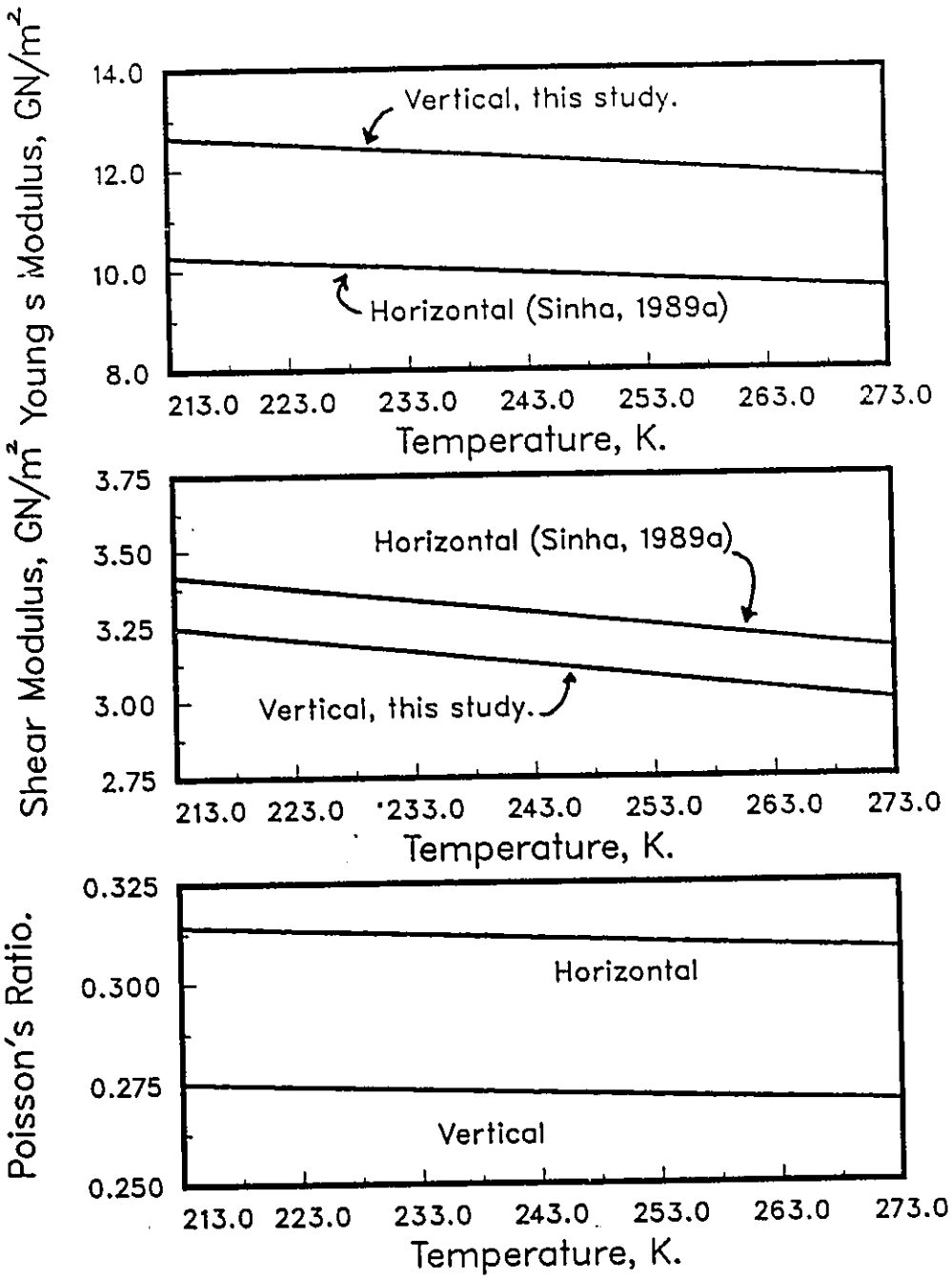

Figure E.2: Practical elastic moduli for columnar grained S-1 ice: a) Young's modulus b) shear modulus c) Poisson's ratio.

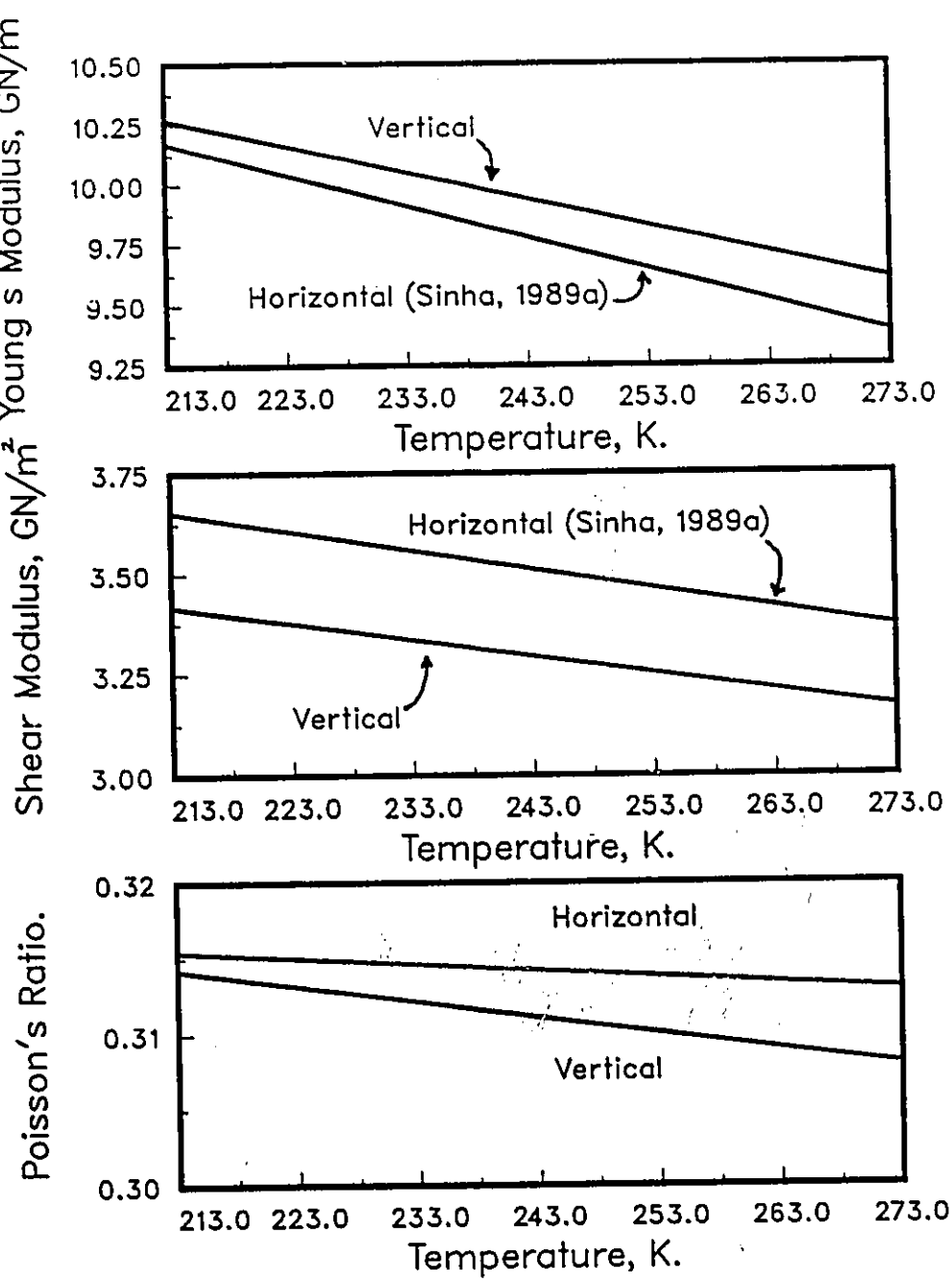

Figure E.3: Practical elastic moduli for columnar grained S-2 ice: a) Young's modulus b) shear modulus c) Poisson's ratio.

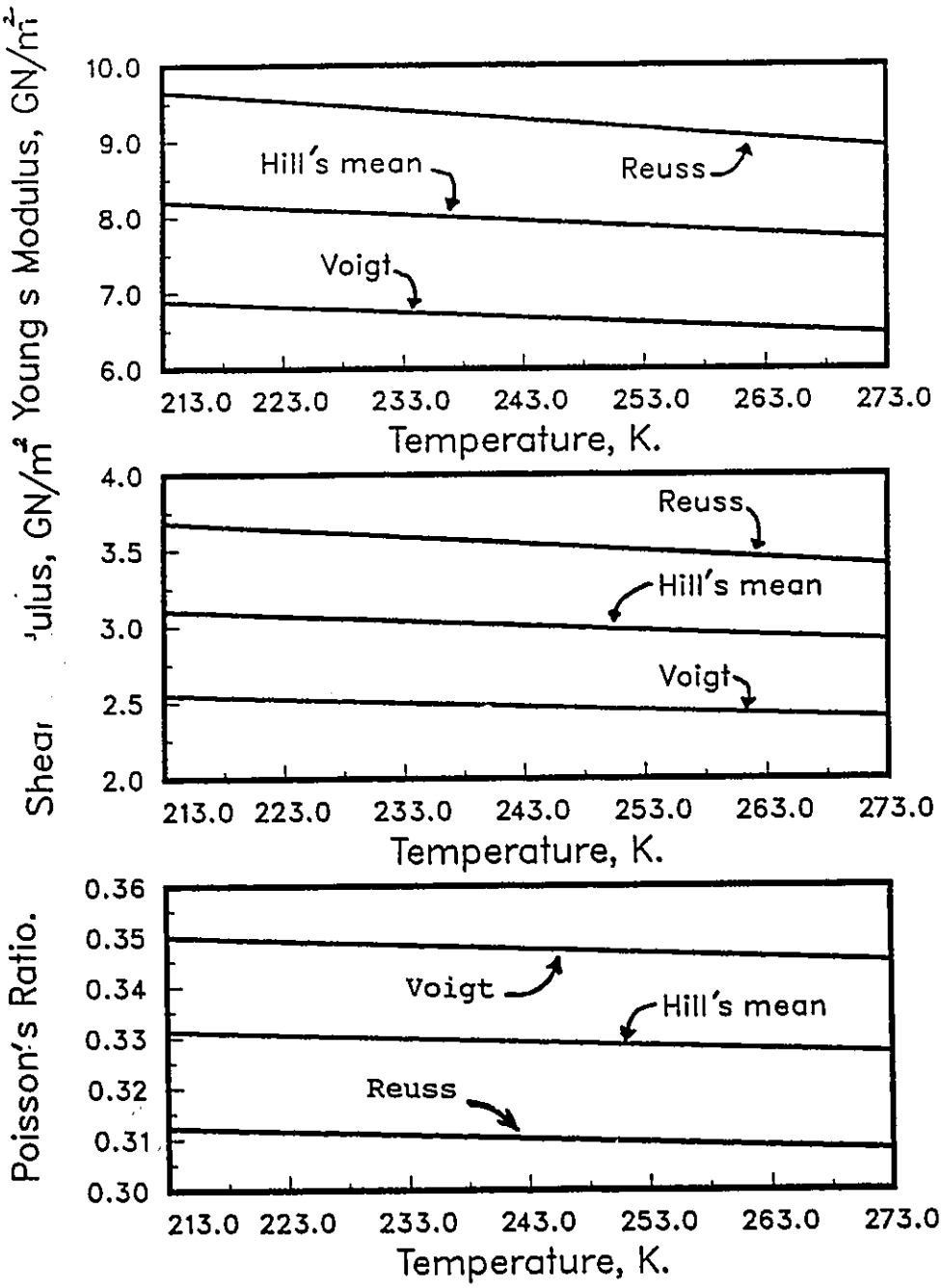

Figure E.4: Practical elastic moduli for granular (isotropic) ice: Comparison among the Reuss, Voigt, and Hill's methods

APPENDIX F

FORMULATION OF THE NON-CRACKING MODEL
(figures)

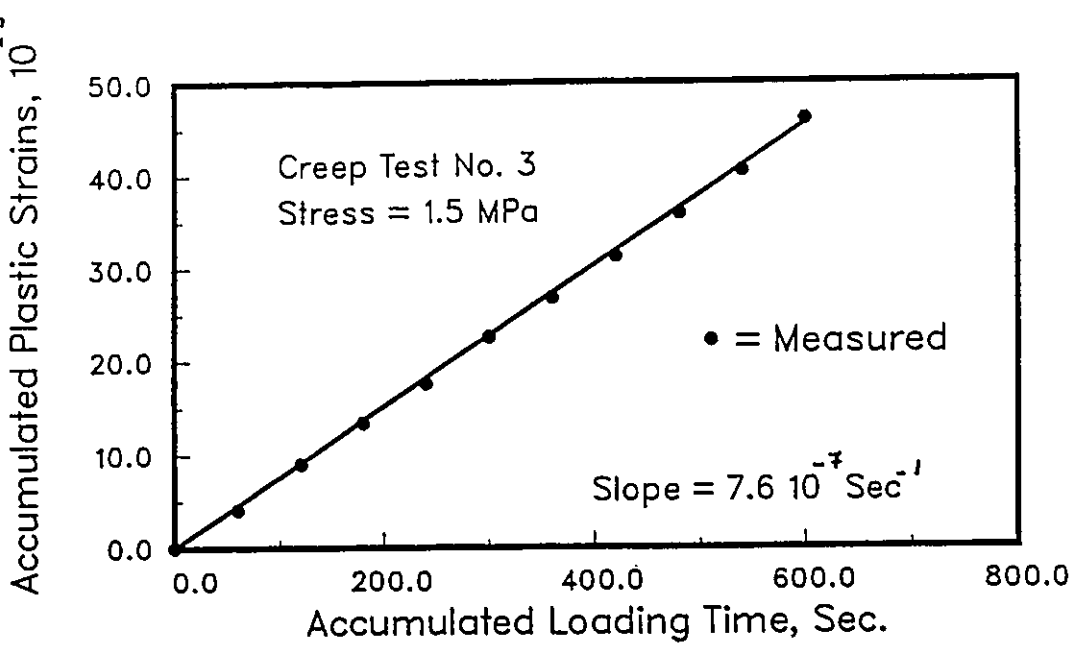

Figure F.1: Creep test No. 3: Measured plastic strain rate.

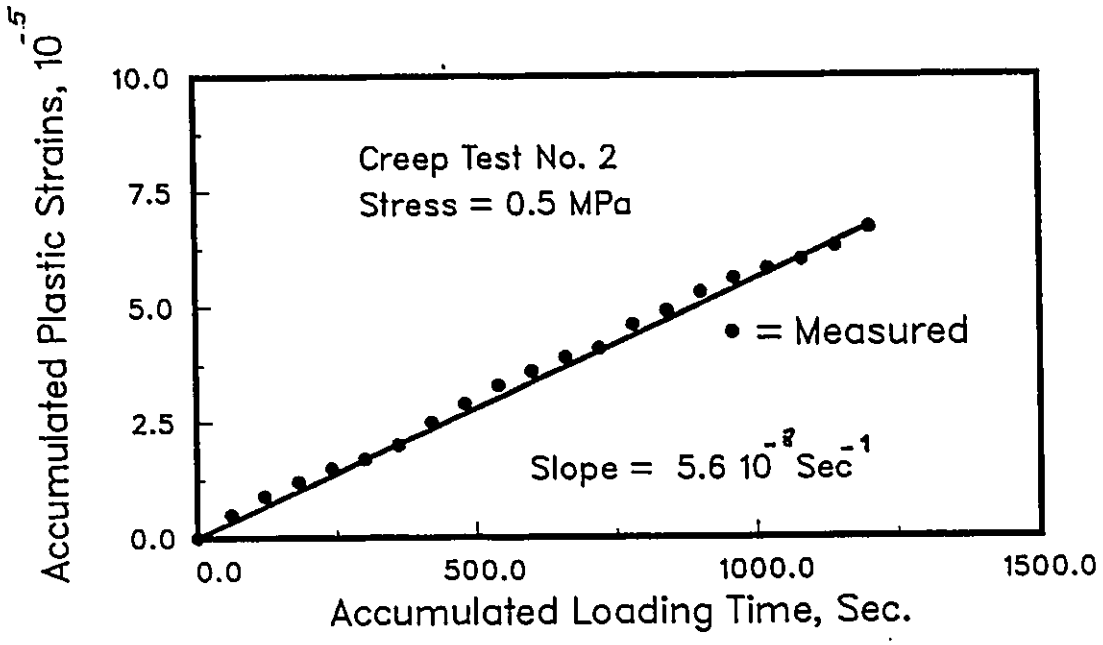

Figure F.2: Creep test No. 2: Measured plastic strain rate.

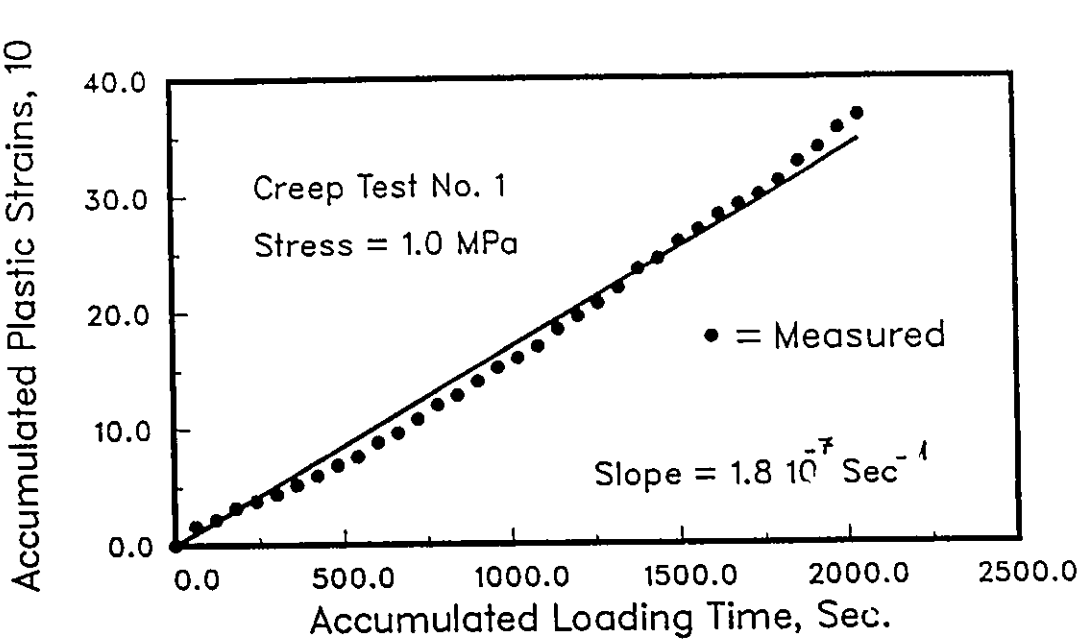

Figure F.3: Creep test No. 1: Measured plastic strain rate.

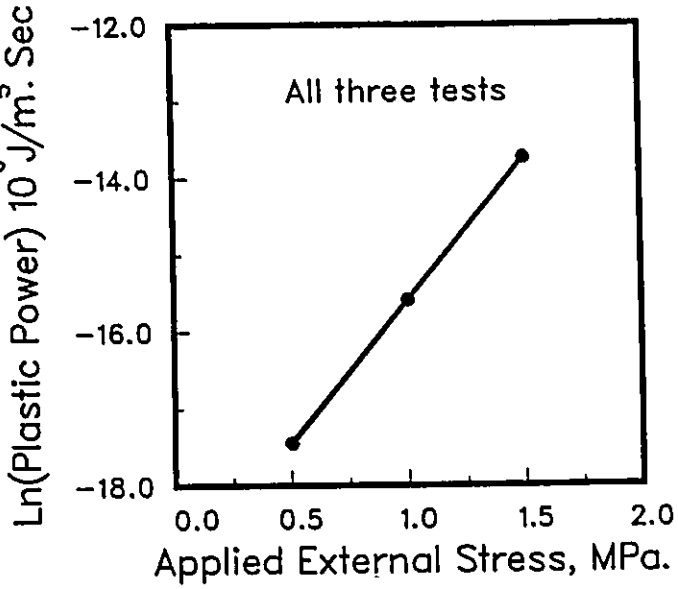

Figure F.4: All three tests: A semi-log plot of applied stresses versus plastic power.

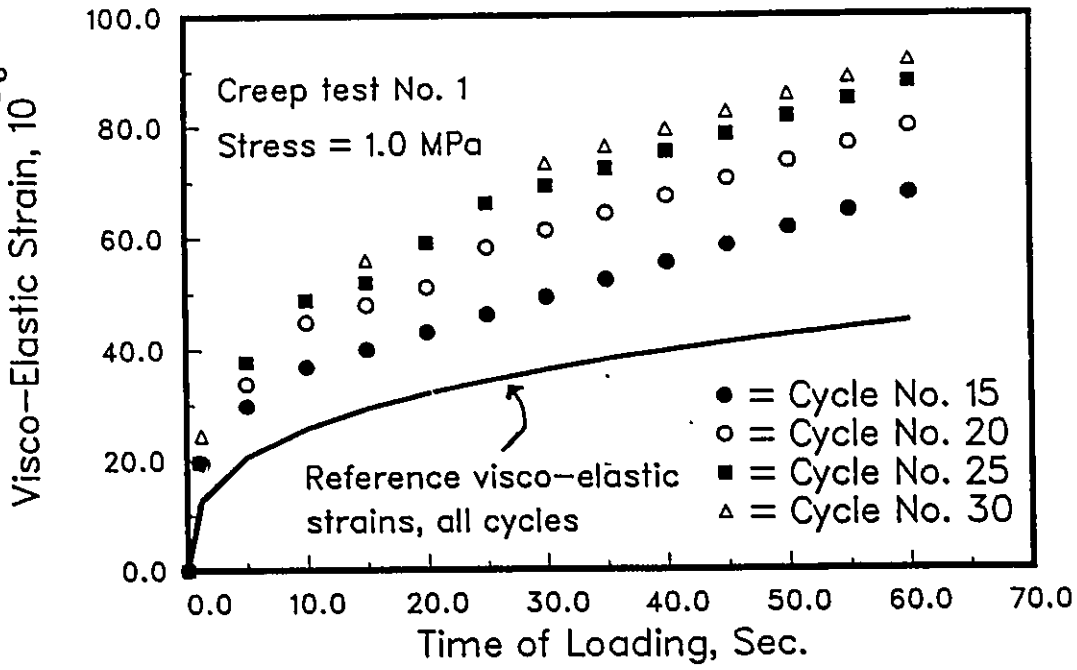

Figure F.5a: Creep test No. 1: Measured visco-elastic and reference visco-elastic strain histories for 4 loading cycles.

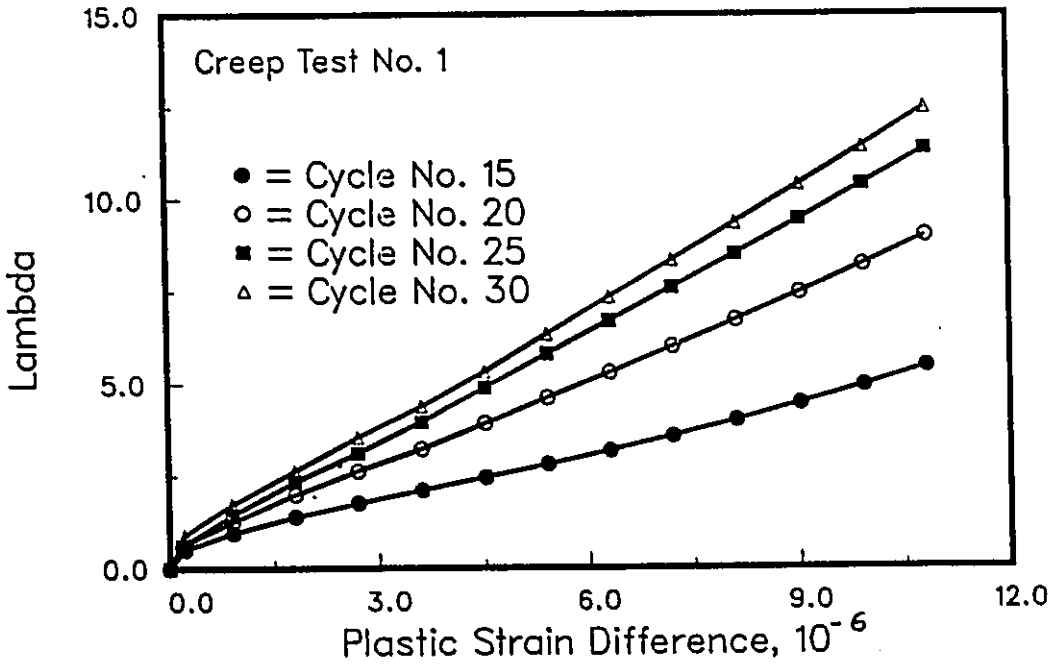

Figure F.5b: Creep test No. 1: Computed values of λ versus the plastic strains $(\varepsilon^p - \varepsilon^p_o)$ for the same cycles as in Fig. F.5a.

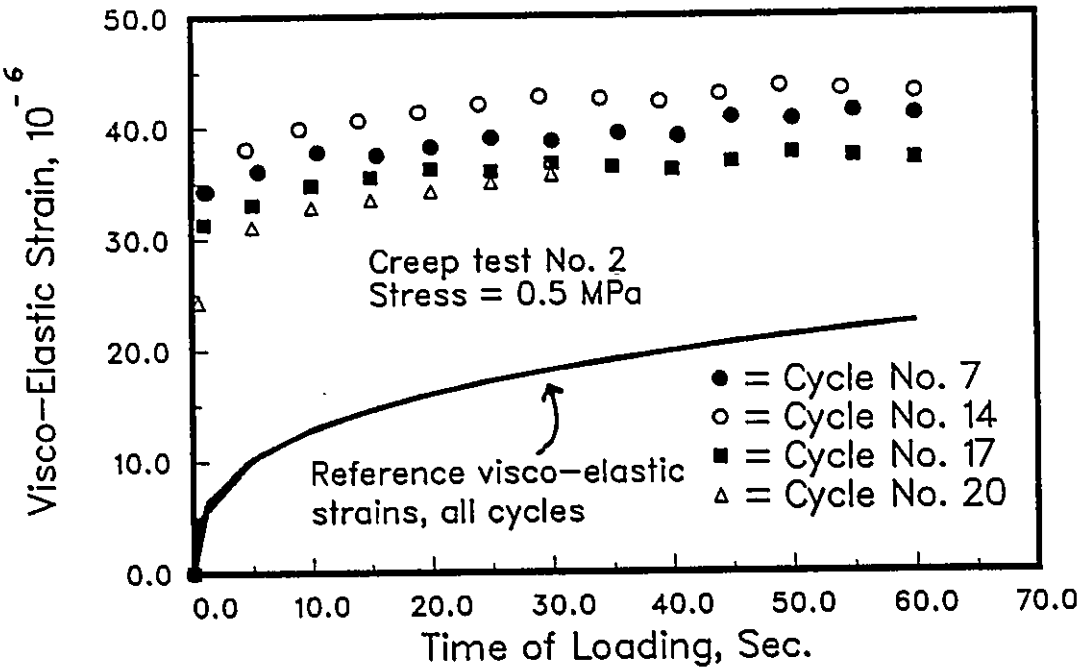

Figure F.6a: Creep test No. 2: Measured visco-elastic and reference visco-elastic strain histories for 4 loading cycles.

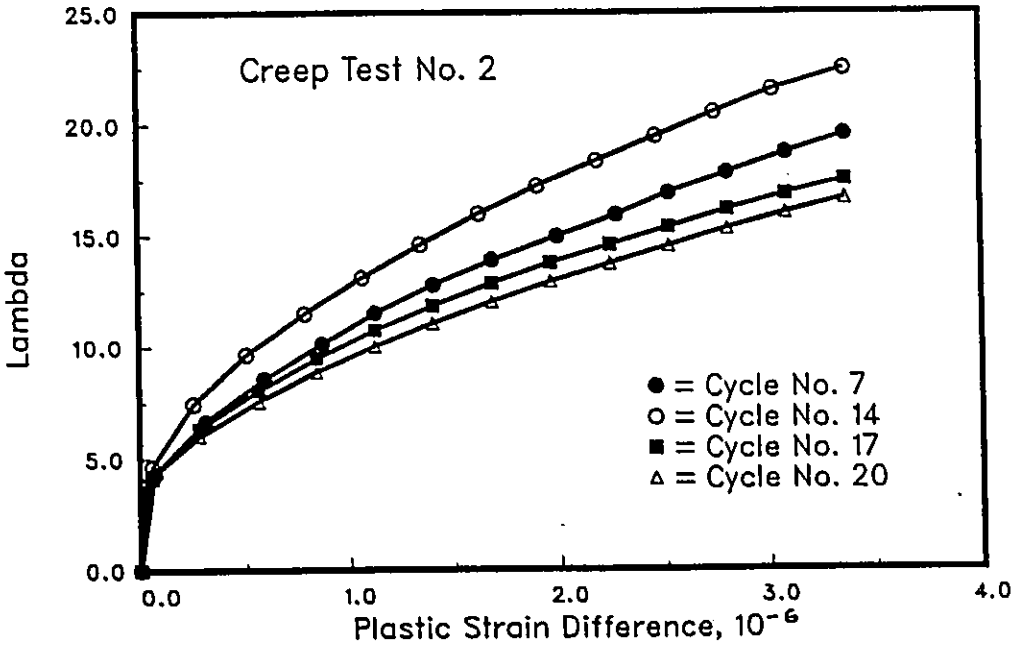

Figure F.6b: Creep test No. 2: Computed values of λ versus the plastic strains $(\varepsilon^p - \varepsilon^p_o)$ for the same cycles as in Fig. F.6a.

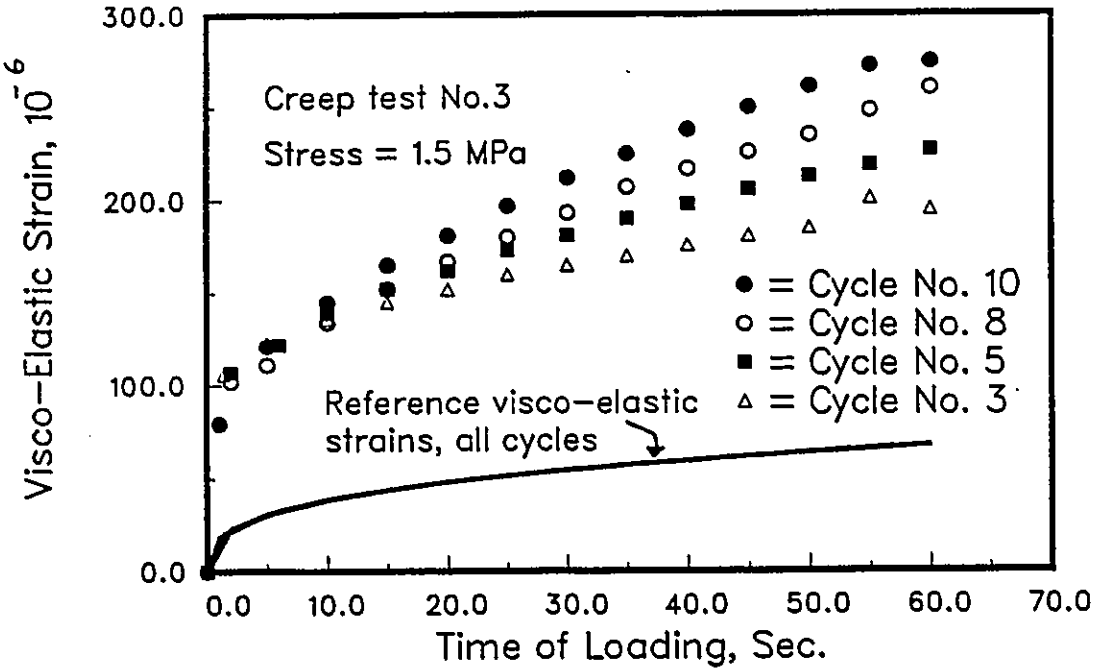

Figure F.7a: Creep test No. 3: Measured visco-elastic and reference visco-elastic strain histories for 4 loading cycles.

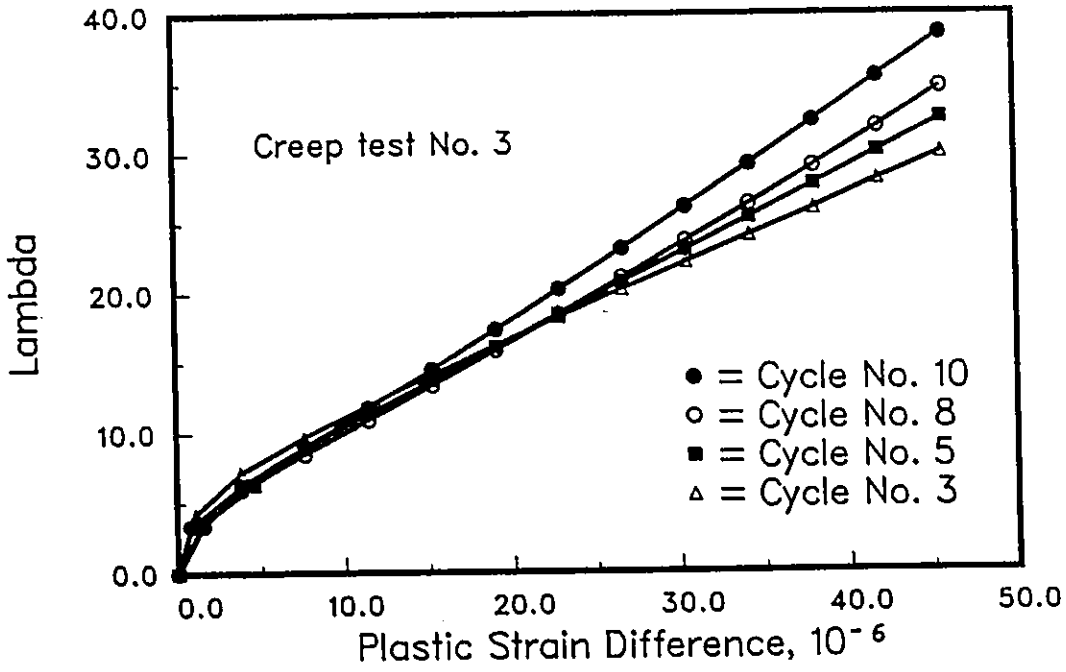

Figure F.7b: Creep test No. 3: Computed values of λ versus the plastic strains $(\varepsilon^p - \varepsilon^p_o)$ for the same cycles as in Fig. F.7a.

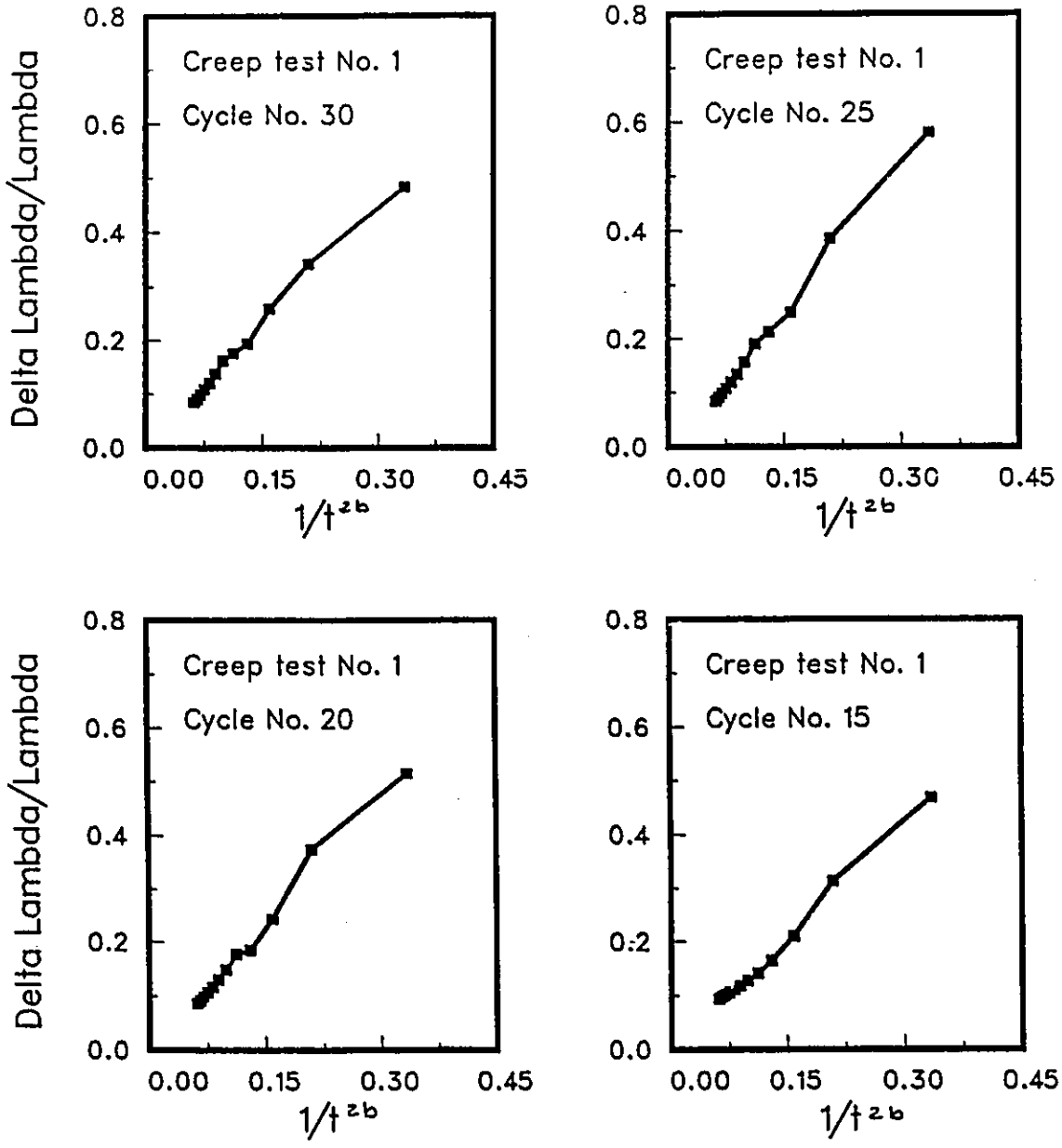

Figure F.8: Creep test No. 1: Ratio $\Delta\lambda/\lambda$ versus duration of loading, t^{2b}, for the same loading cycles shown in Fig. F.5.

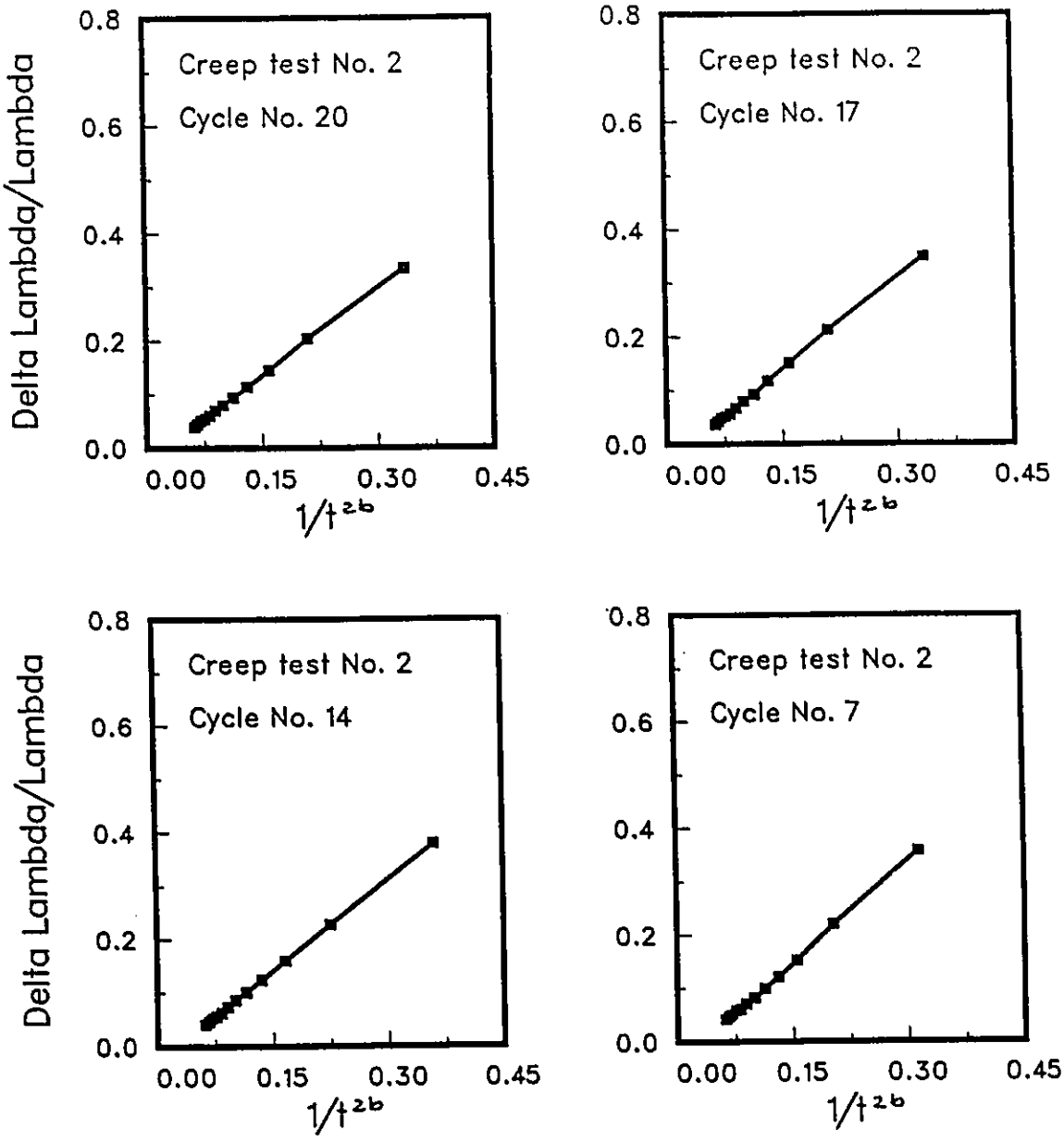

Figure F.9: Creep test No. 2: Ratio $\Delta\lambda/\lambda$ versus duration of loading, t^{2b}, for the same loading cycles shown in Fig. F.6.

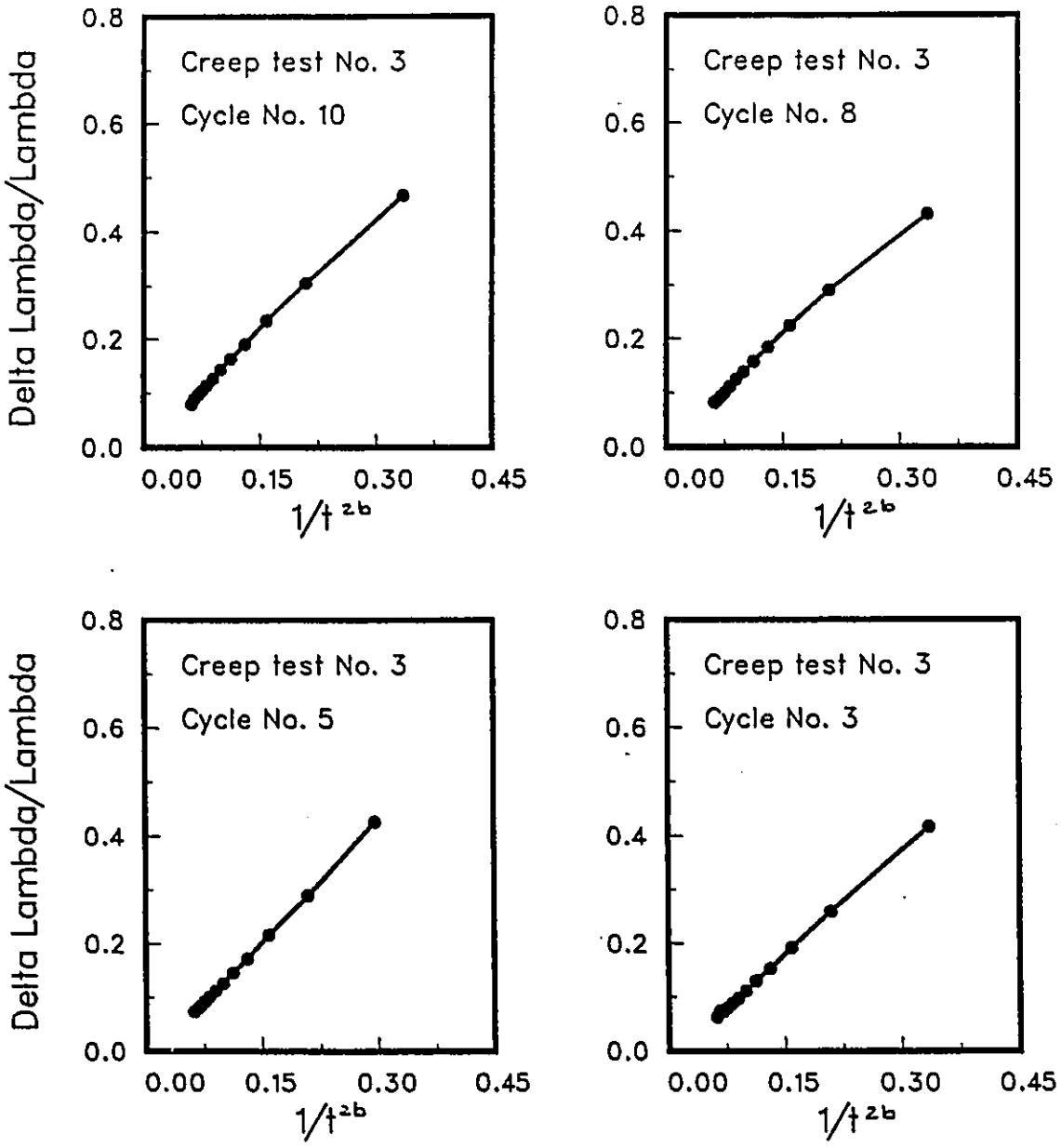

Figure F.10: Creep test No. 3: Ratio $\Delta\lambda/\lambda$ versus duration of loading, t^{2b}, for the same loading cycles shown in Fig. F.7.

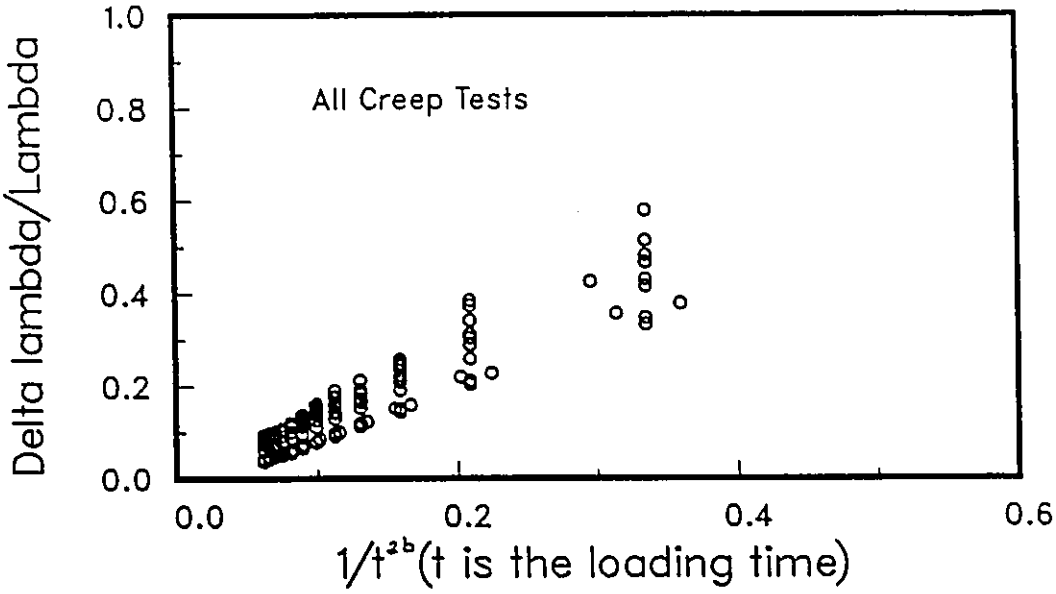

Figure F.11a: Three creep tests: Ratio $\Delta\lambda/\lambda$ versus duration of loading, t^{2b}, for a total of 12 loading cycles.

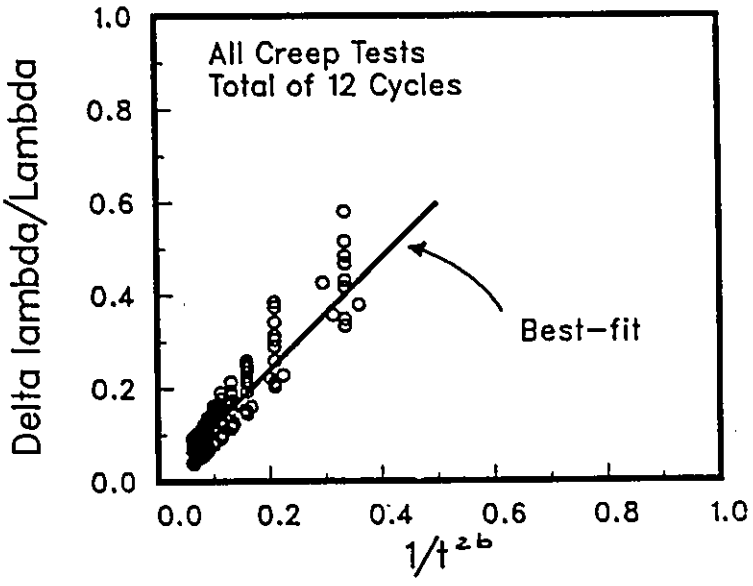

Figure F.11b: Best fit curve for the data shown in Fig. F.11a.

APPENDIX G

EVALUATION OF THE MODEL
(figures)

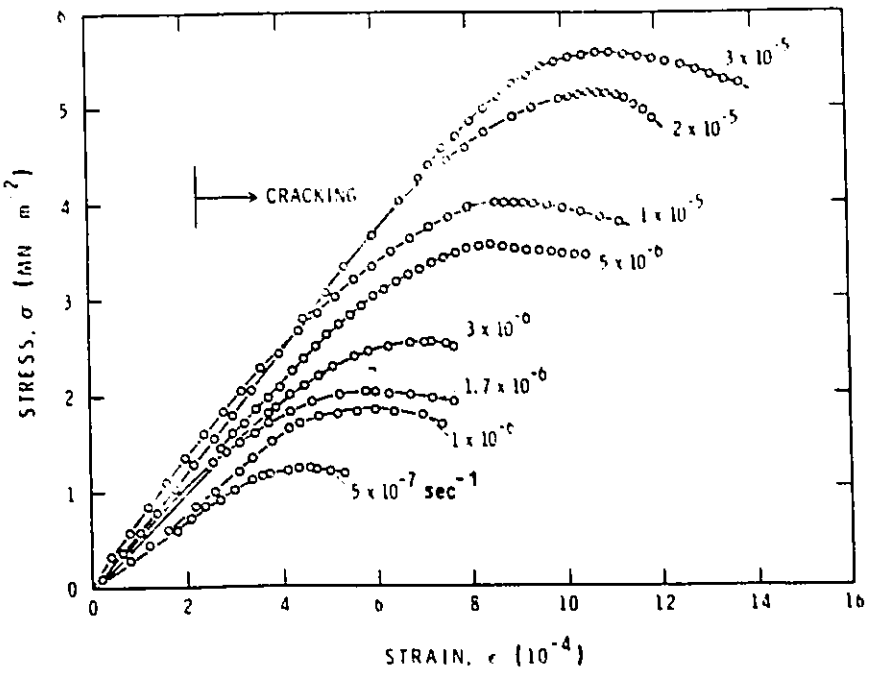

Figure G.1a: Sinha's (1982) stress-strain experimental results.

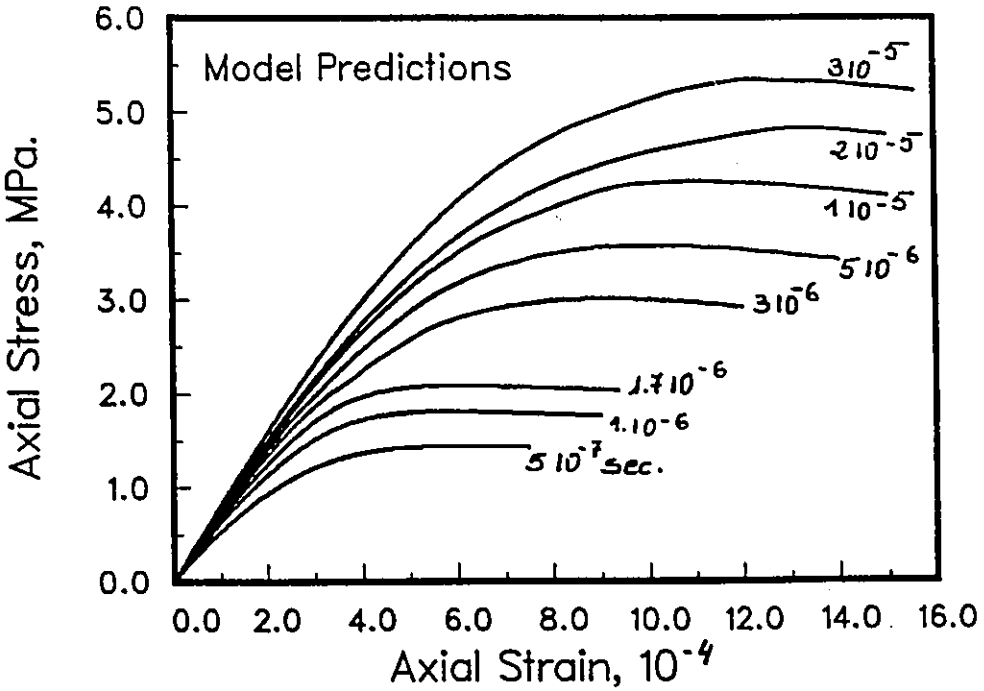

Figure G.1b: Model predictions of Sinha's (1982) test results, columnar grained S-2 ice of average grain size of 5 mm at -10°C subjected to constant strain rates as indicated by each curve.

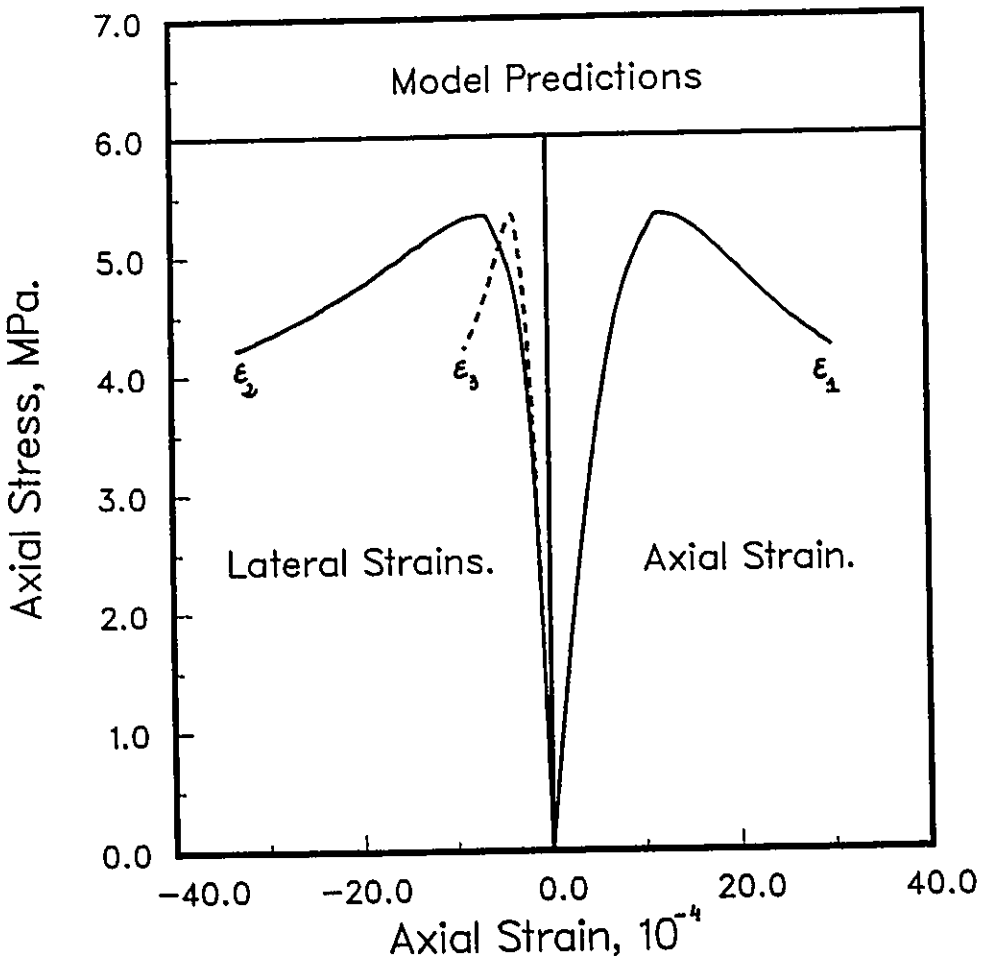

Figure G.2: Predicted stress-strain curves for a columnar grained S-2 ice (anisotropic) sample with an average grain size of 5 mm at temperature of -10°C: Uniaxial test, strain rate $3.10^{-5}sec^{-1}$.

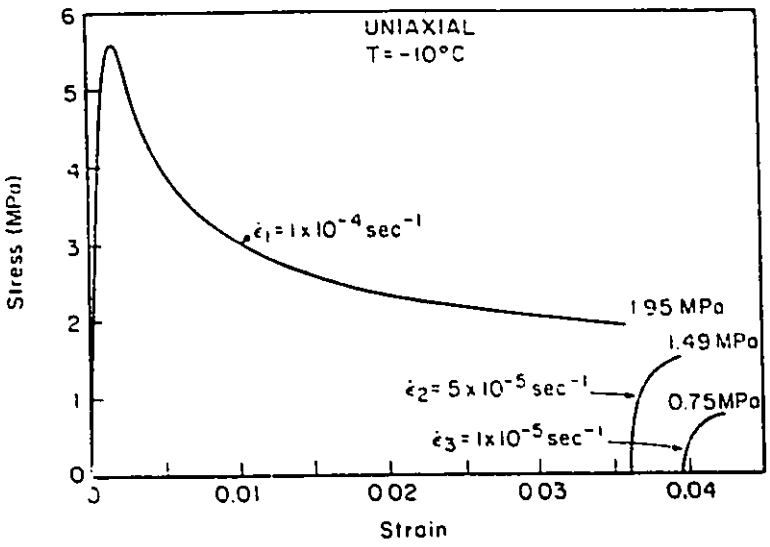

Figure G.3a: Experimental stress-strain curve (Stone et al. 1989)

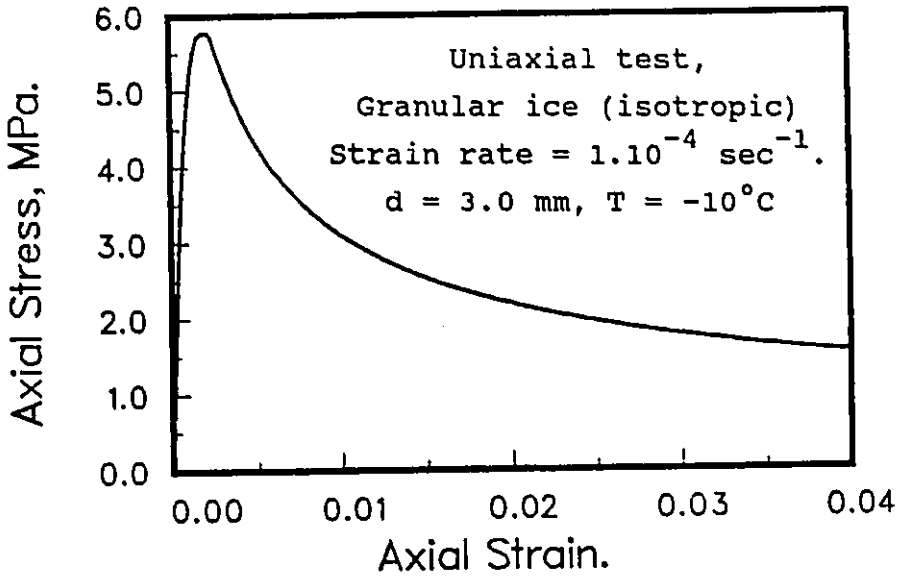

Figure G.3b: Model prediction of Stone's et al. (1989) test results (Fig. G.3a).

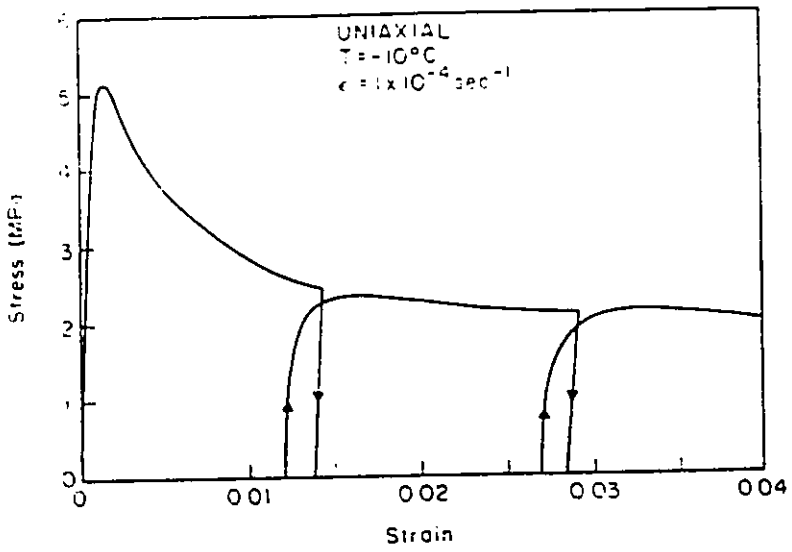

Figure G.4a: Experimental stress-strain curve (Stone et al. 1989)

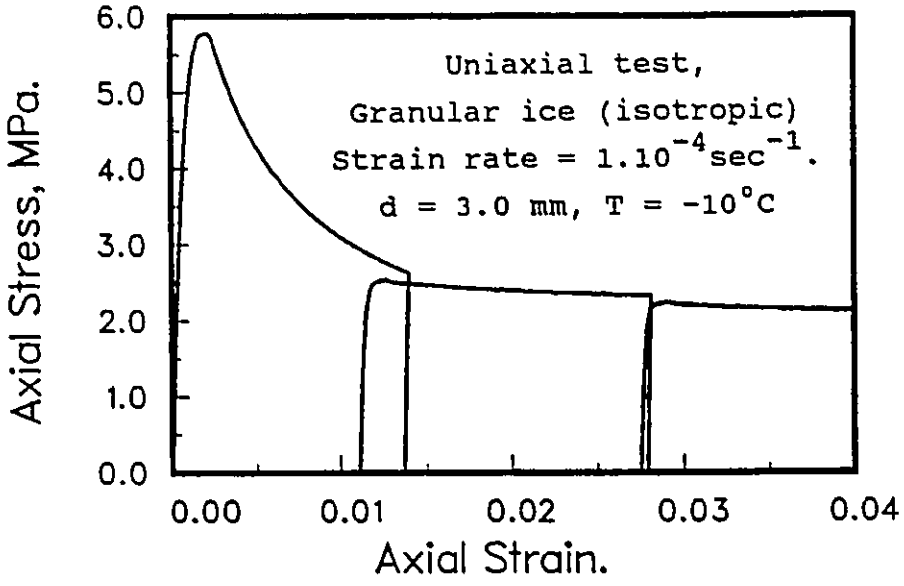

Figure G.4b: Model prediction of Stone's et al. (1989) test results (Fig. G.4a).

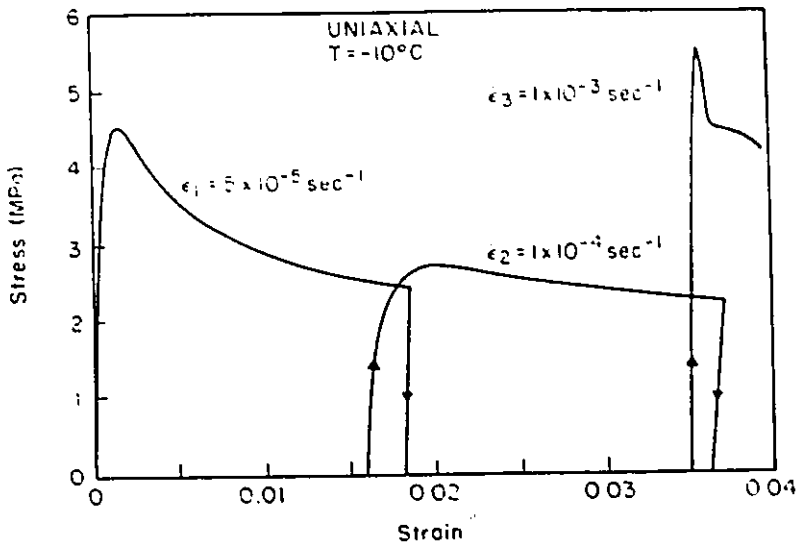

Figure G.5a: Experimental stress-strain curve (Stone et al. 1989)

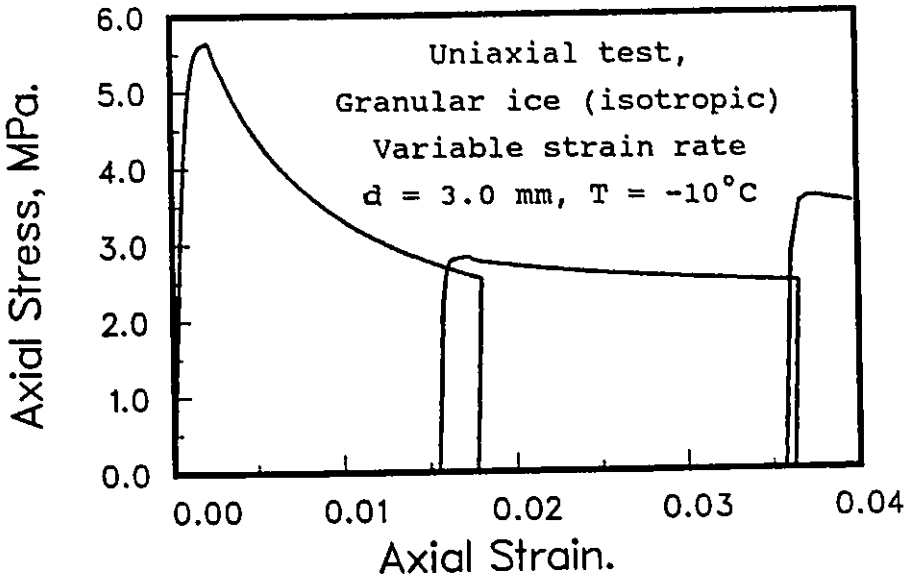

Figure G.5b: Model prediction of Stone's et al. (1989) test results (Fig. G.5a).

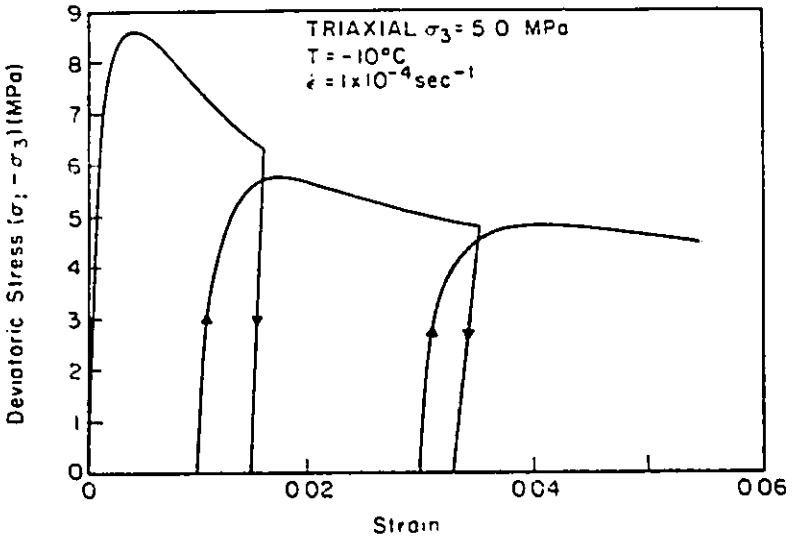

Figure G.6a: Experimental stress-strain curve (Stone et al. 1989)

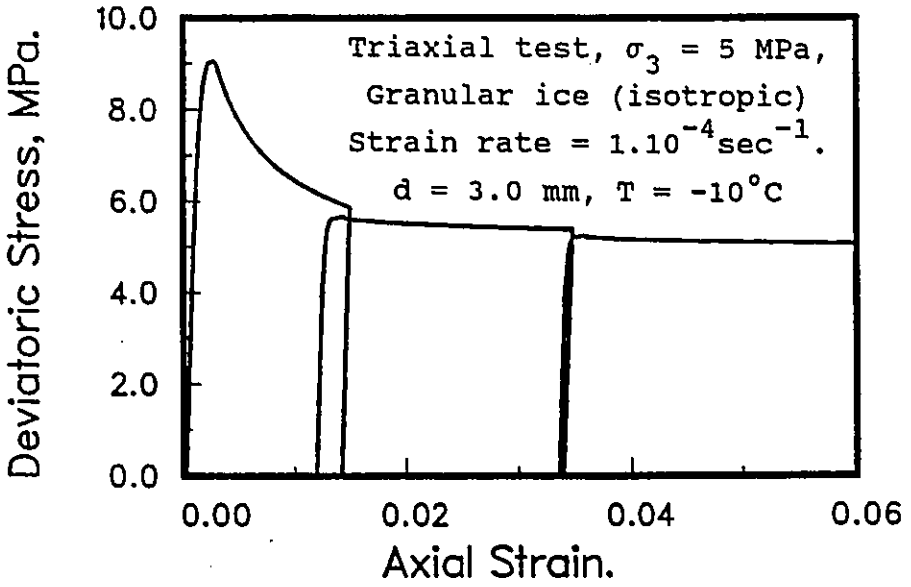

Figure G.6b: Model prediction of Stone's et al. (1989) test results (Fig. G.6a).

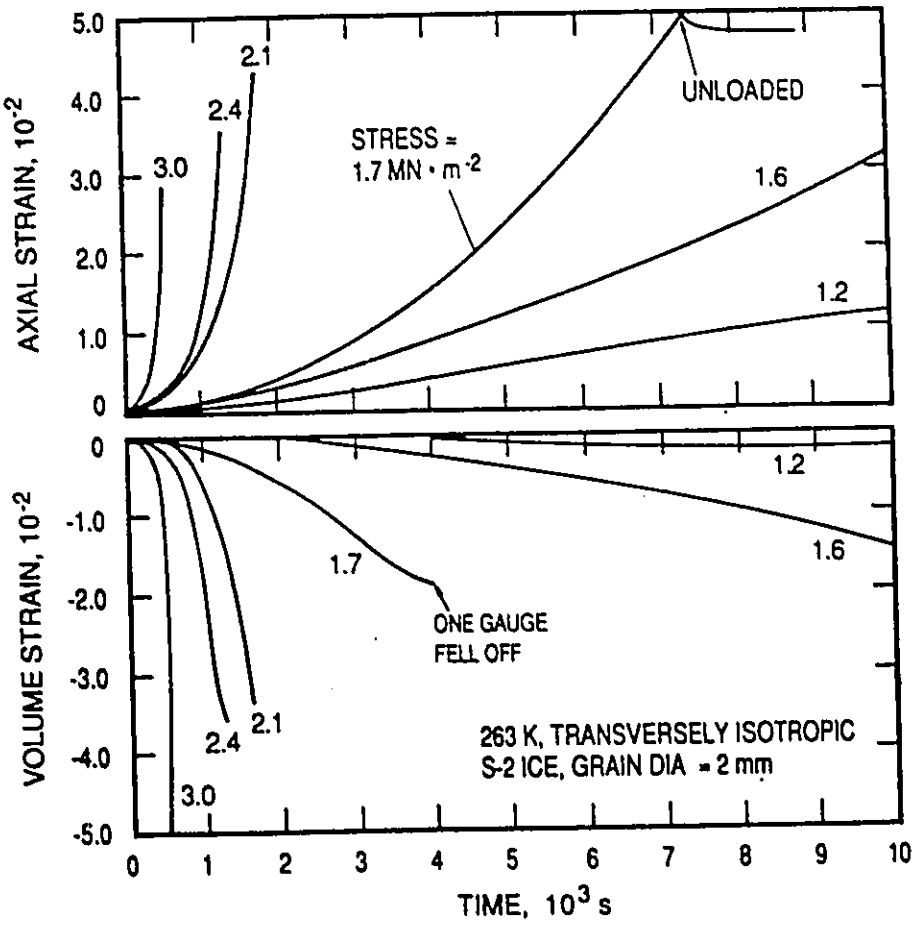

Figure G.7: Sinha's (1989c) creep experimental results.

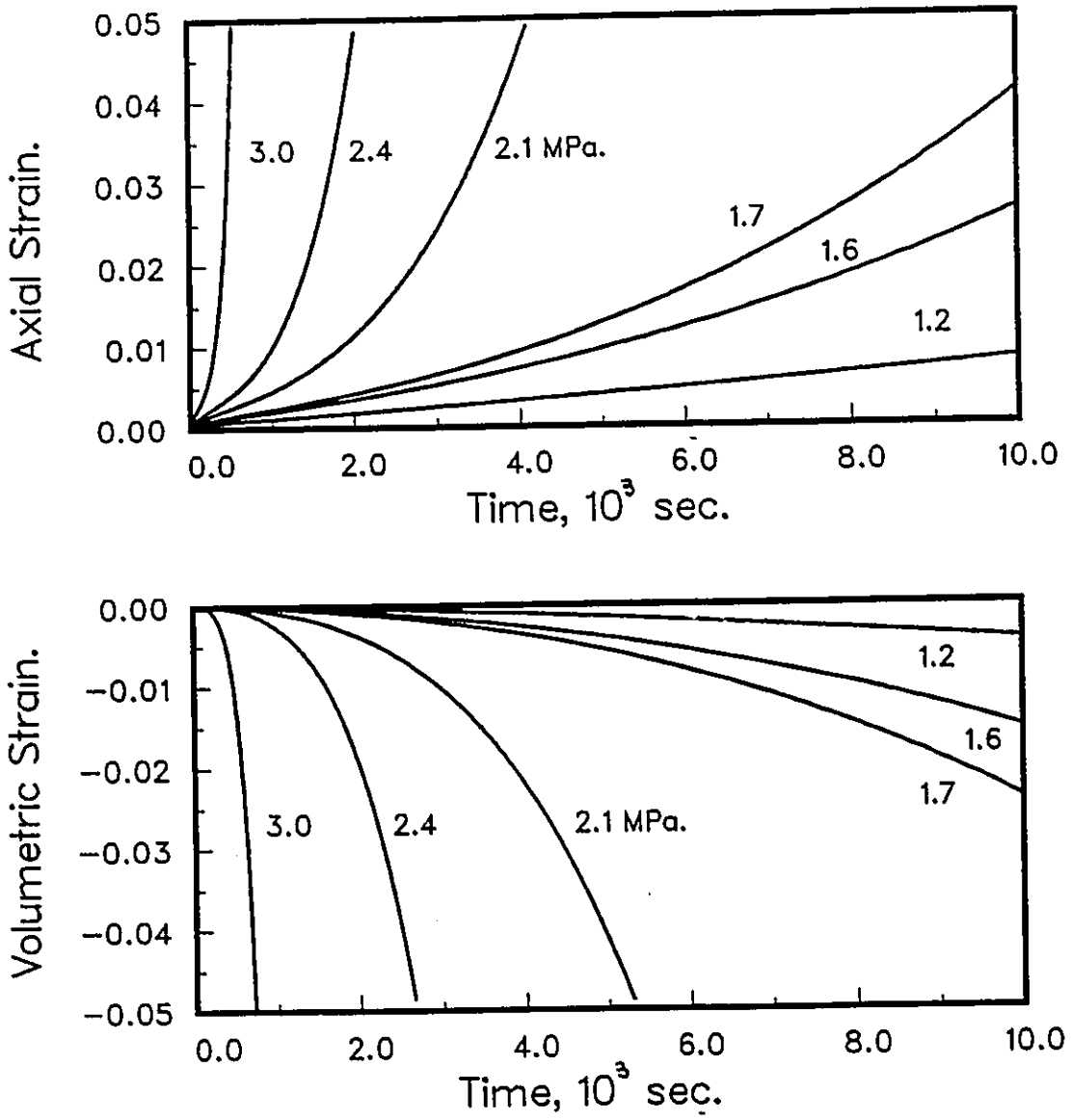

Figure G.8: Model predictions of Sinha's (1988c) creep test results (Fig. G.7).

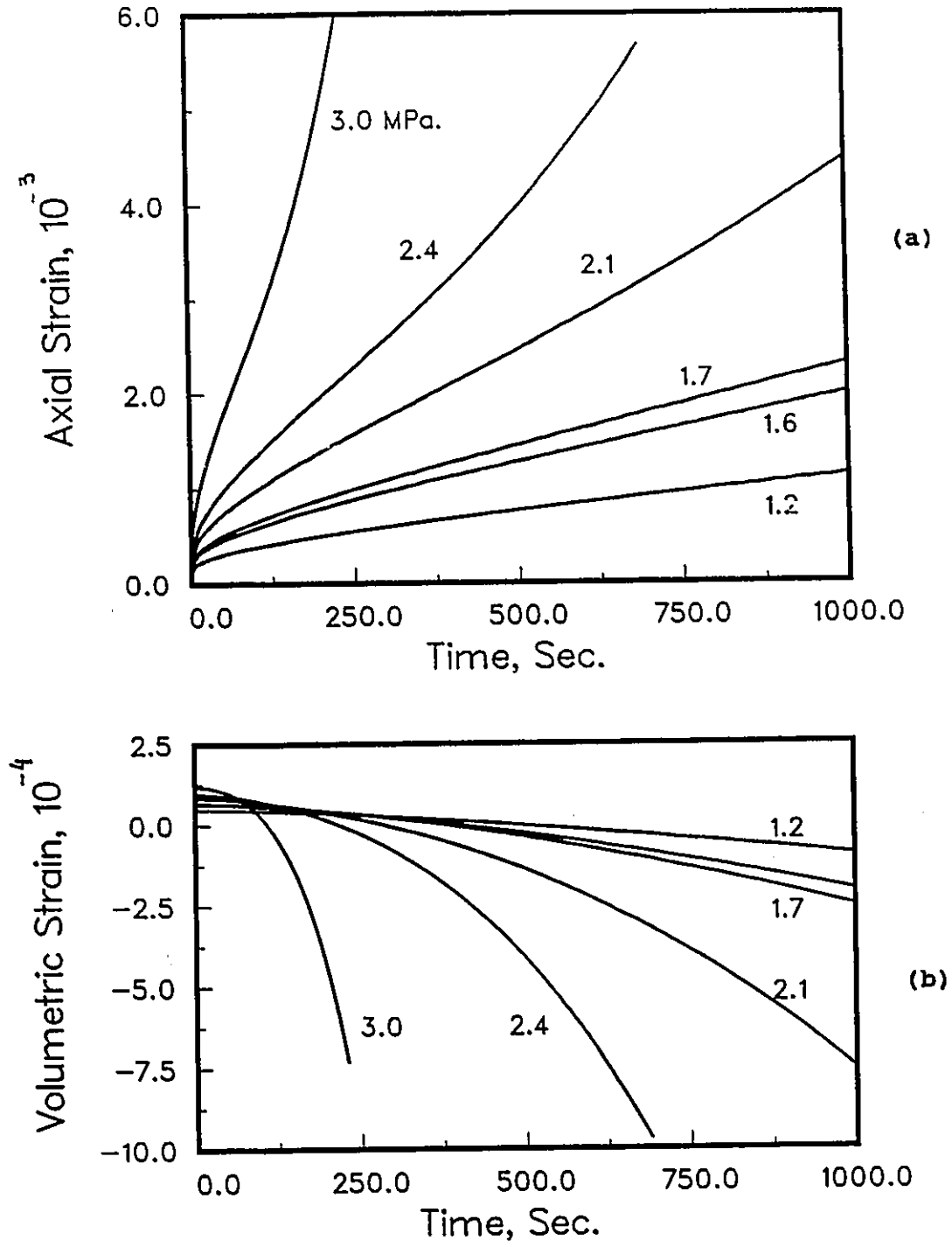

Figure G.9: Short term model predictions of the creep test results shown in Fig. G.7.

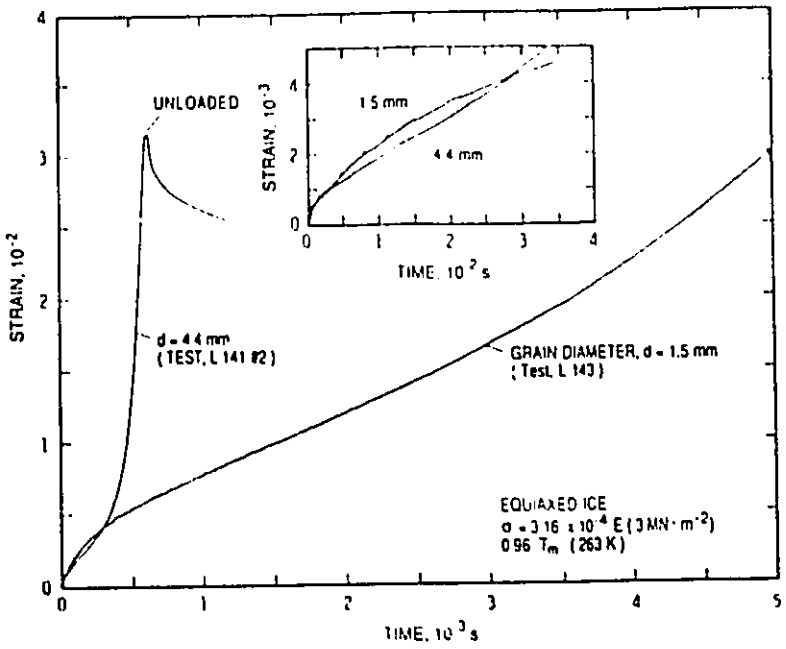

Figure G.10a: Observed creep curves of granular (isotropic) ice for two different grain sizes (Sinha, 1989b).

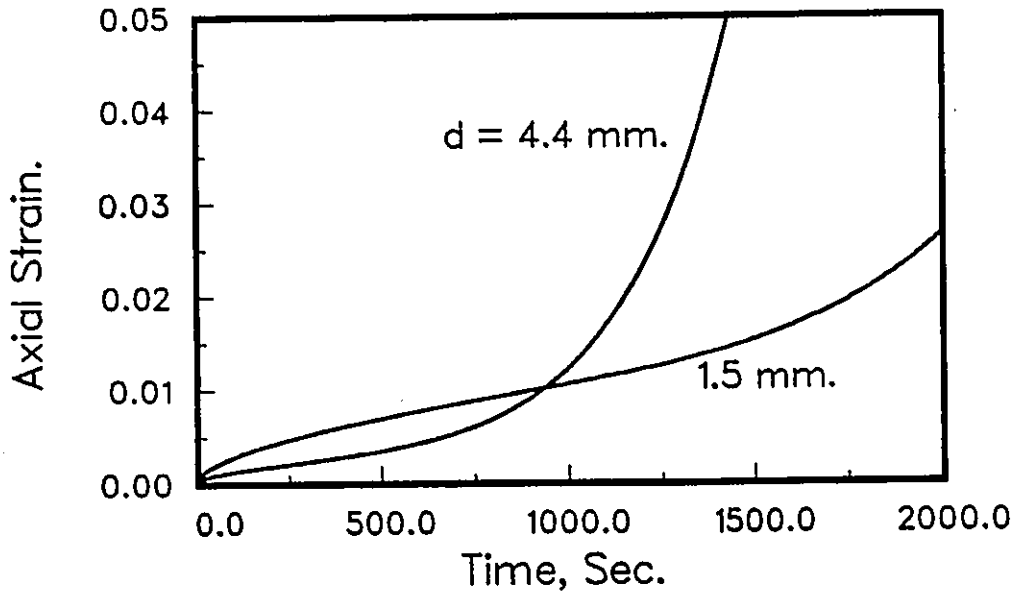

Figure G.10b: Predicted creep curves of granular (isotropic) ice for two different grain sizes.

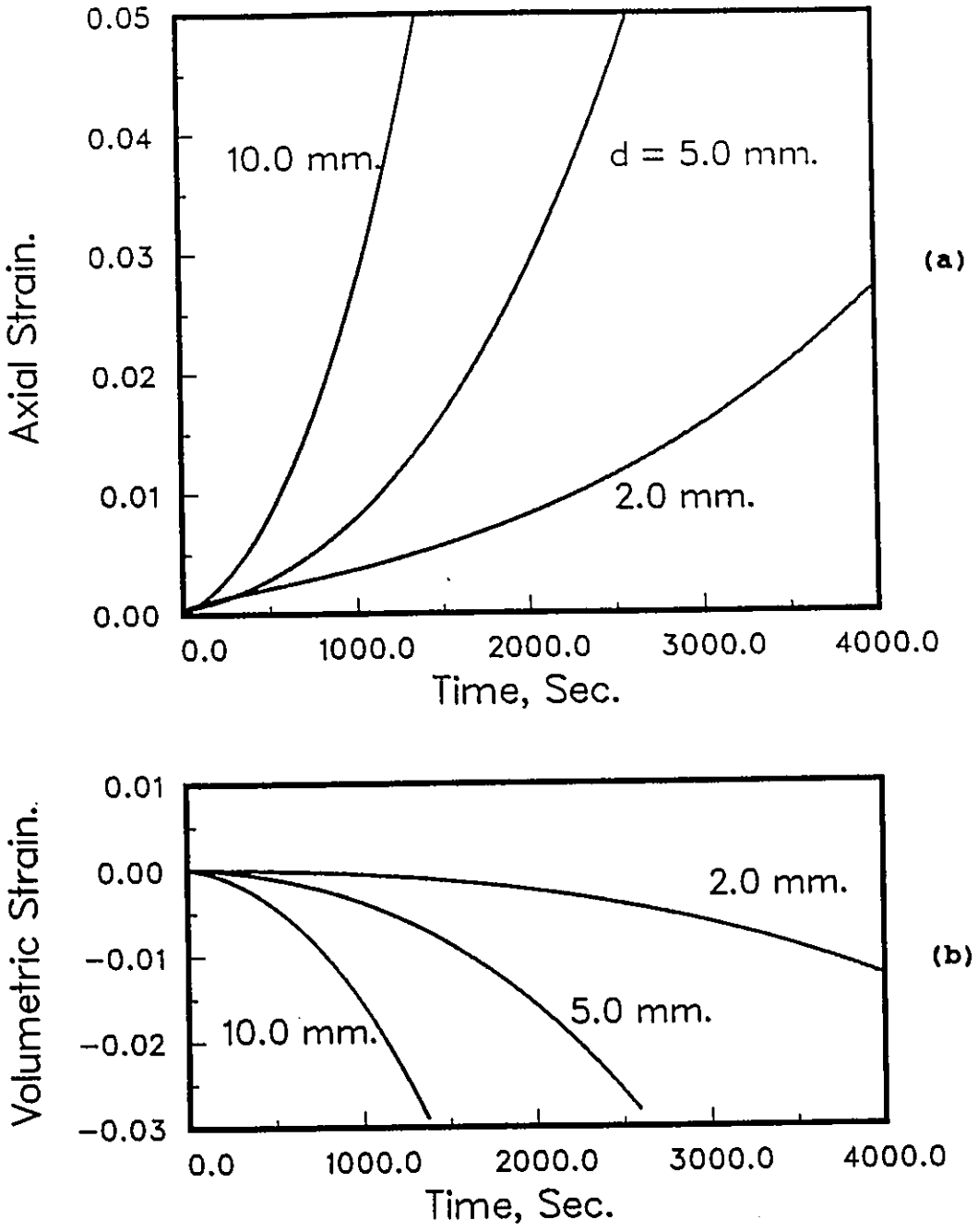

Figure G.11: Predictions of the effect of the grain size on the creep behaviour of columnar grained (anisotropic) S-2 ice for an applied stress of 3 MPa and temperature of -10°C.

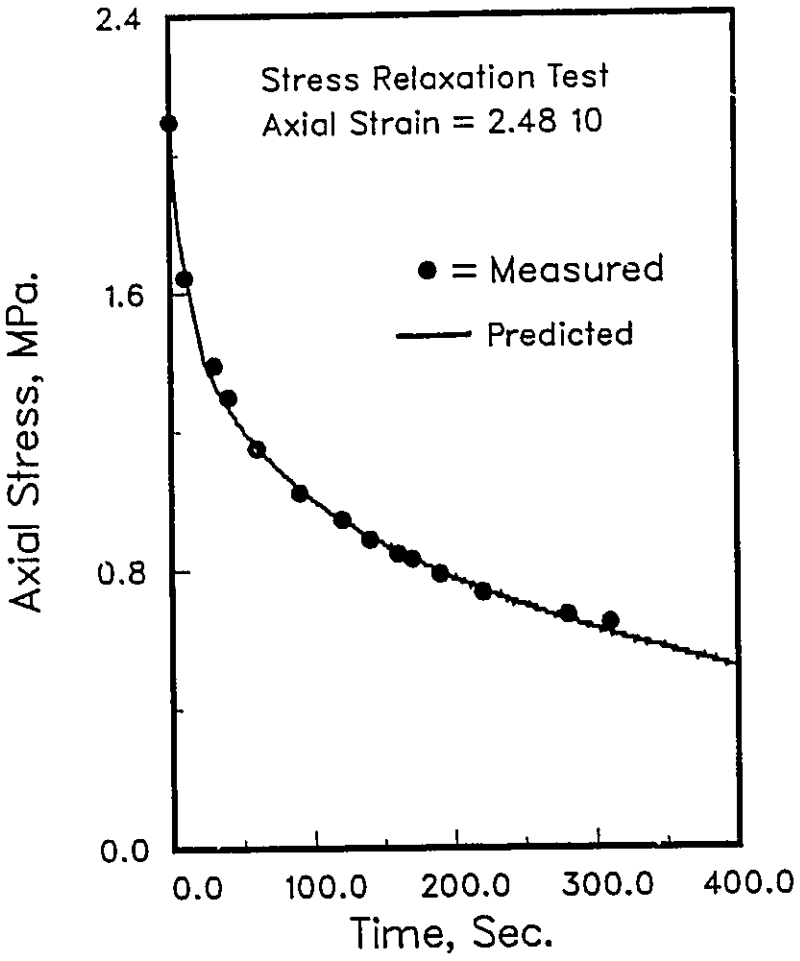

Figure G.12: Stress relaxation test: Predicted versus measured axial stress history. Test was carried out on columnar grained S-2 ice sample with an average grain size of 4.5 mm at -10°C.

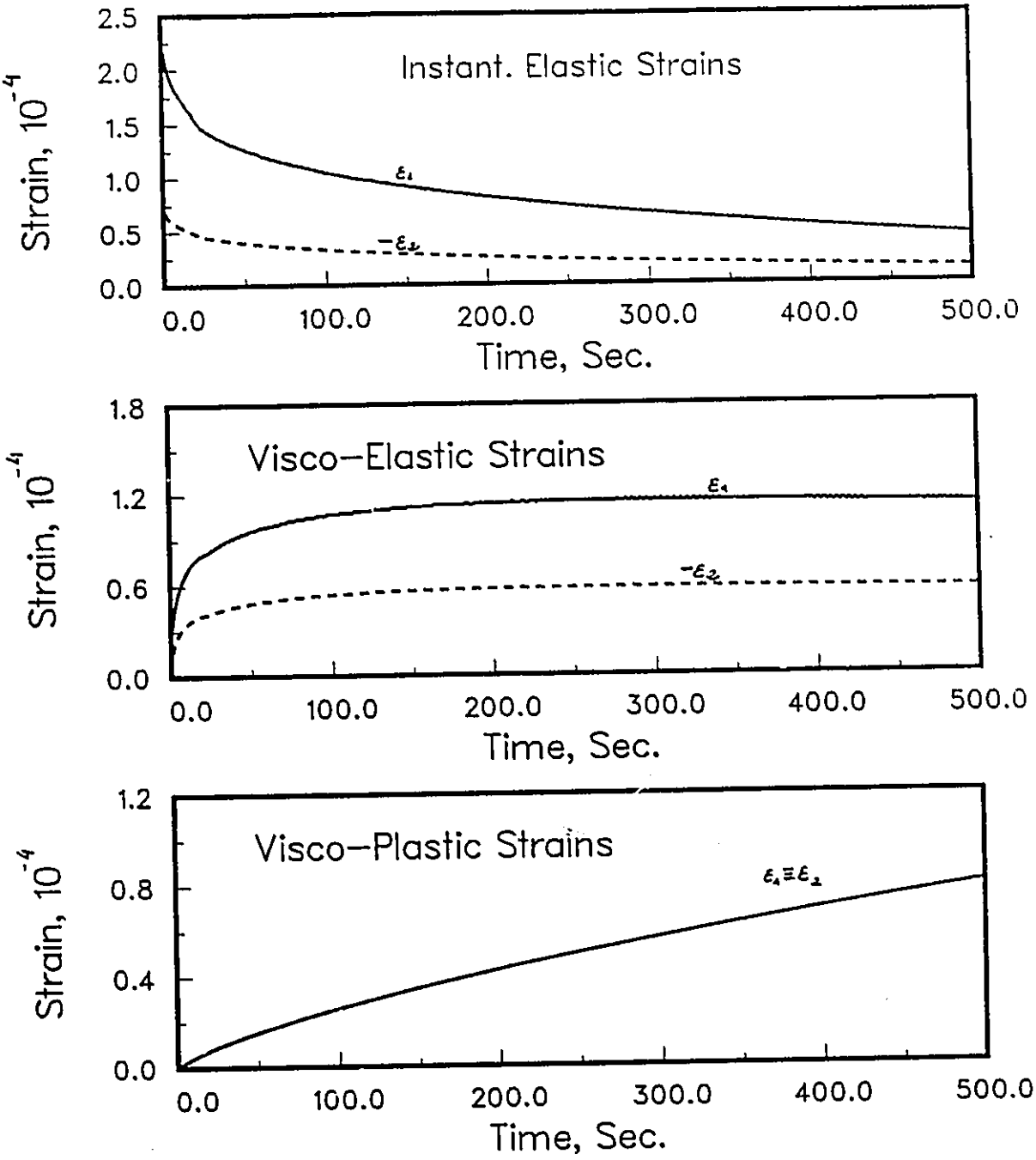

Figure G.13: Stress relaxation test: Predicted axial and lateral strain (components) histories. These strain components correspond to the test given in Fig. G.12.

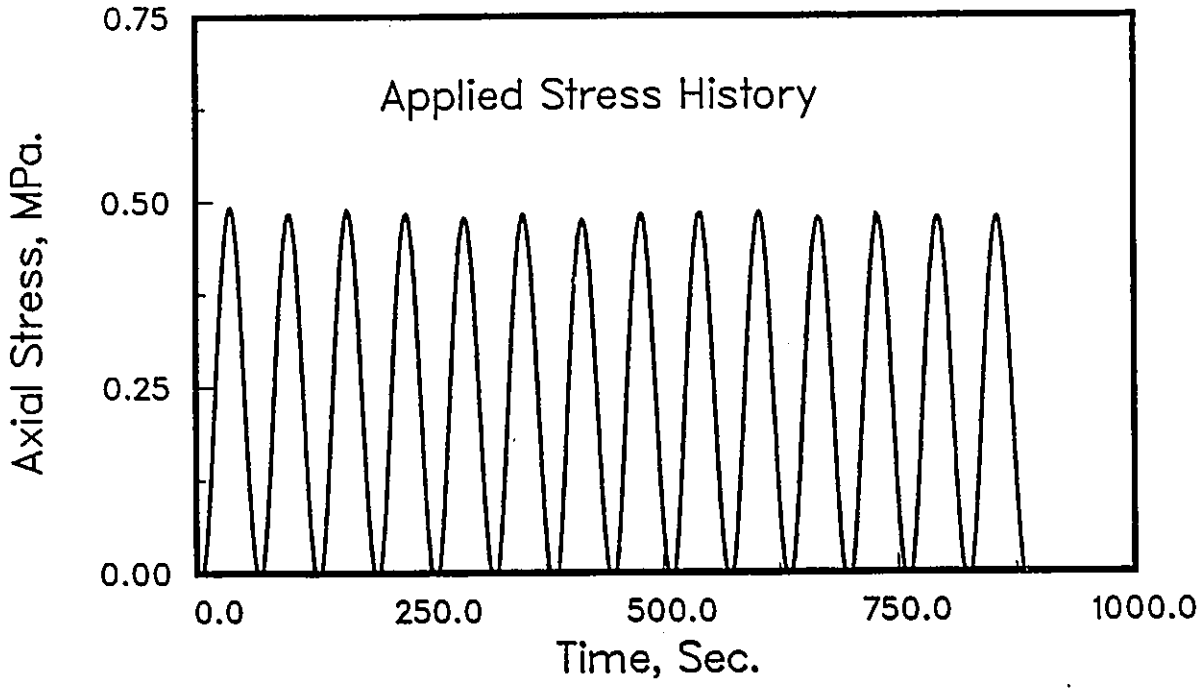

Figure G.14: Cyclic test: Applied stress history. The test was carried out on columnar grained S-2 ice sample with an average grain size of 4.5 mm at temperature of -10°C

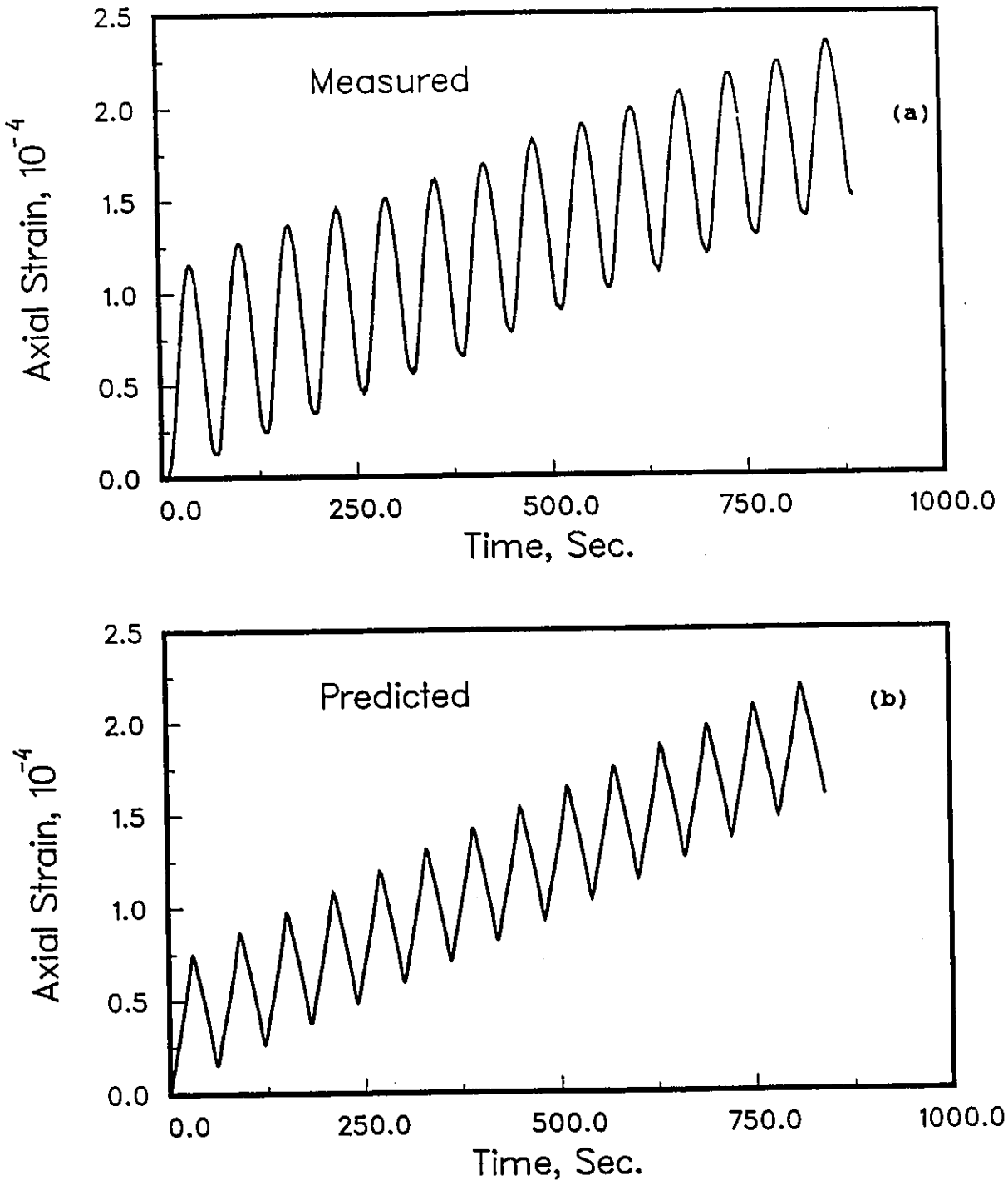

Figure G.15: Cyclic test: Predicted versus measured axial strain history (for the stress history shown in Fig. G. 14).

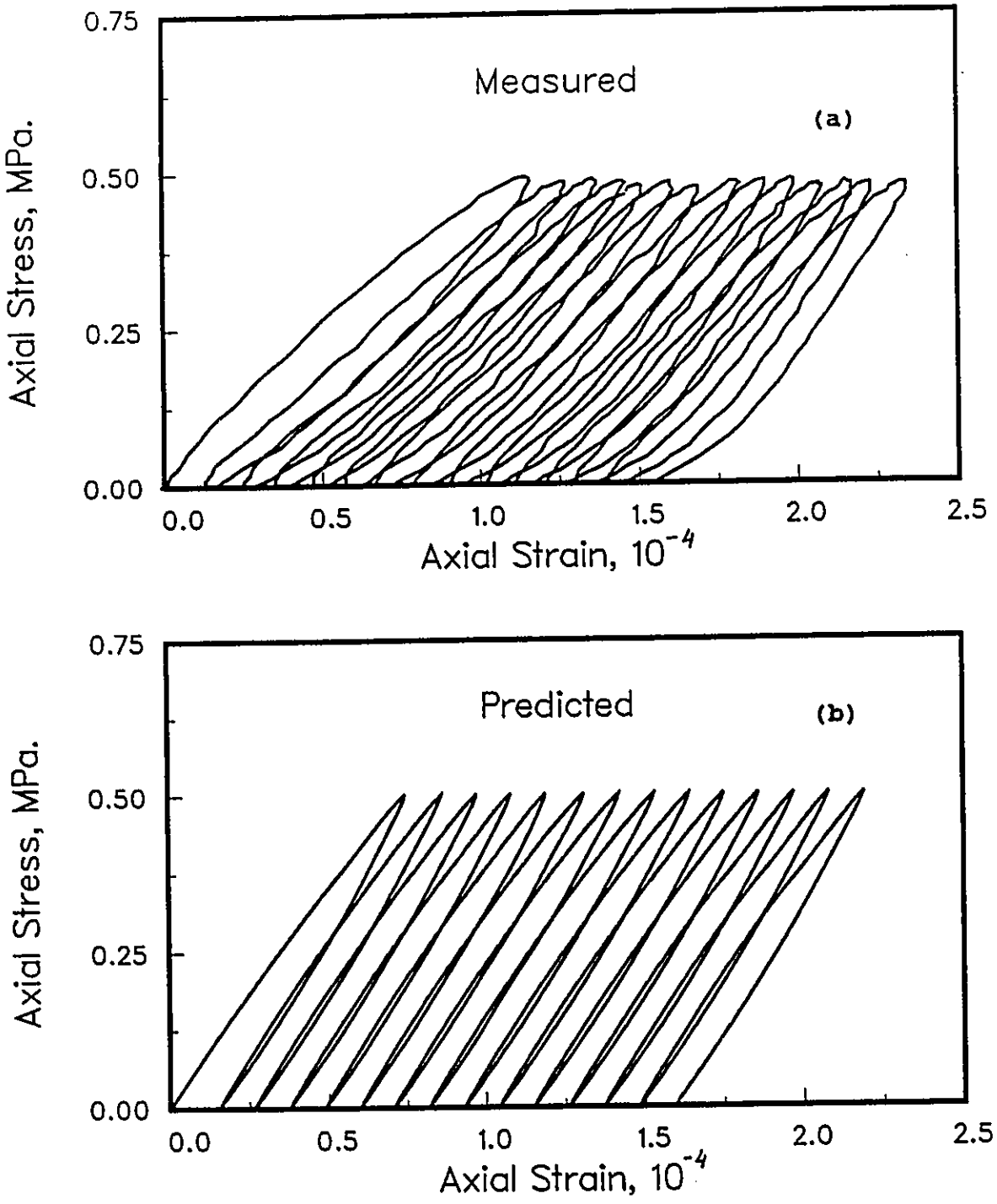

Figure G.16: Cyclic test: Predicted versus measured stress-strain curve (for the stress history shown in Fig. G. 14).

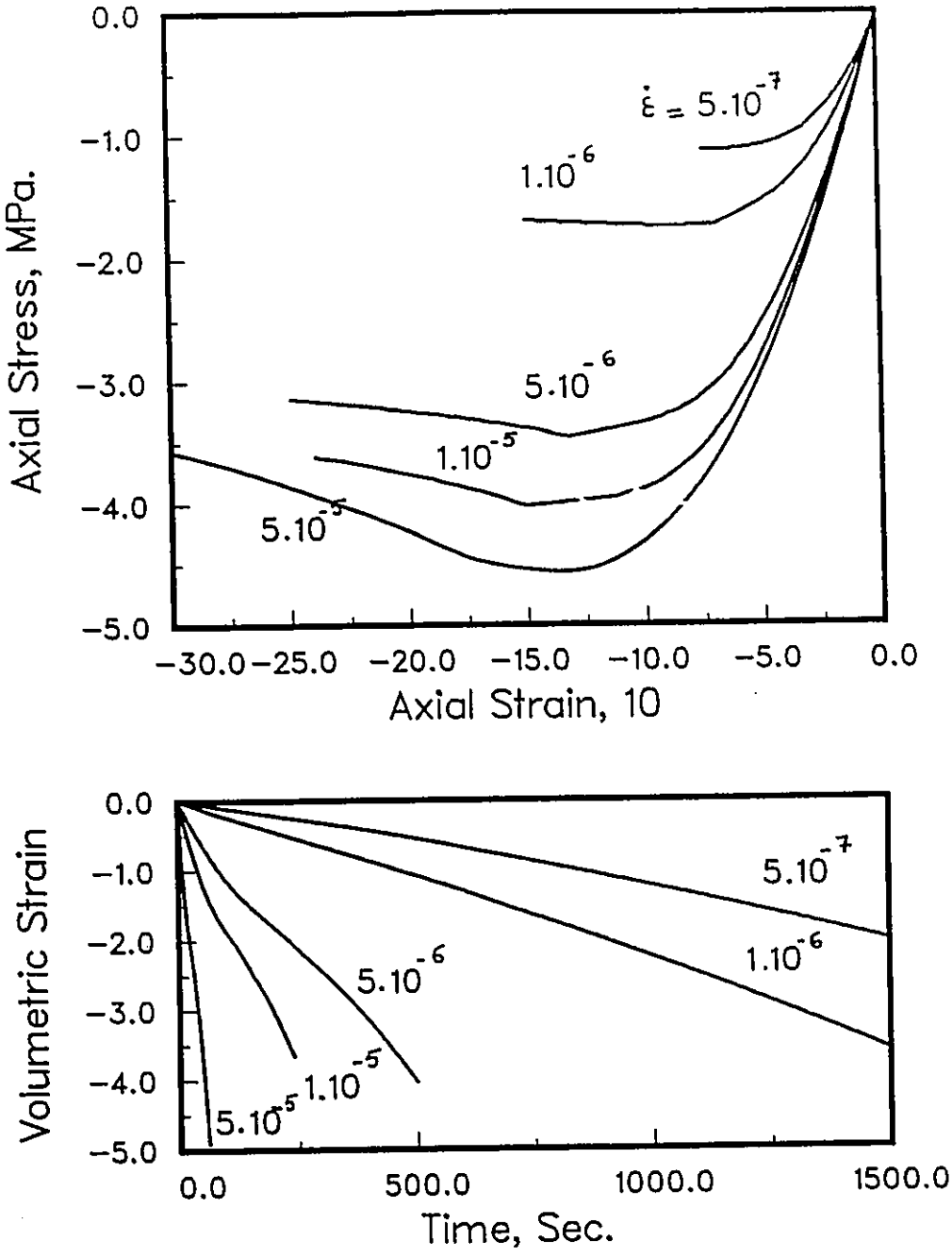

Figure G.17: Model simulations of the tensile behaviour of granular (isotropic) ice under constant strain rate conditions, average grain size of 3 mm and temperature of -10°C.

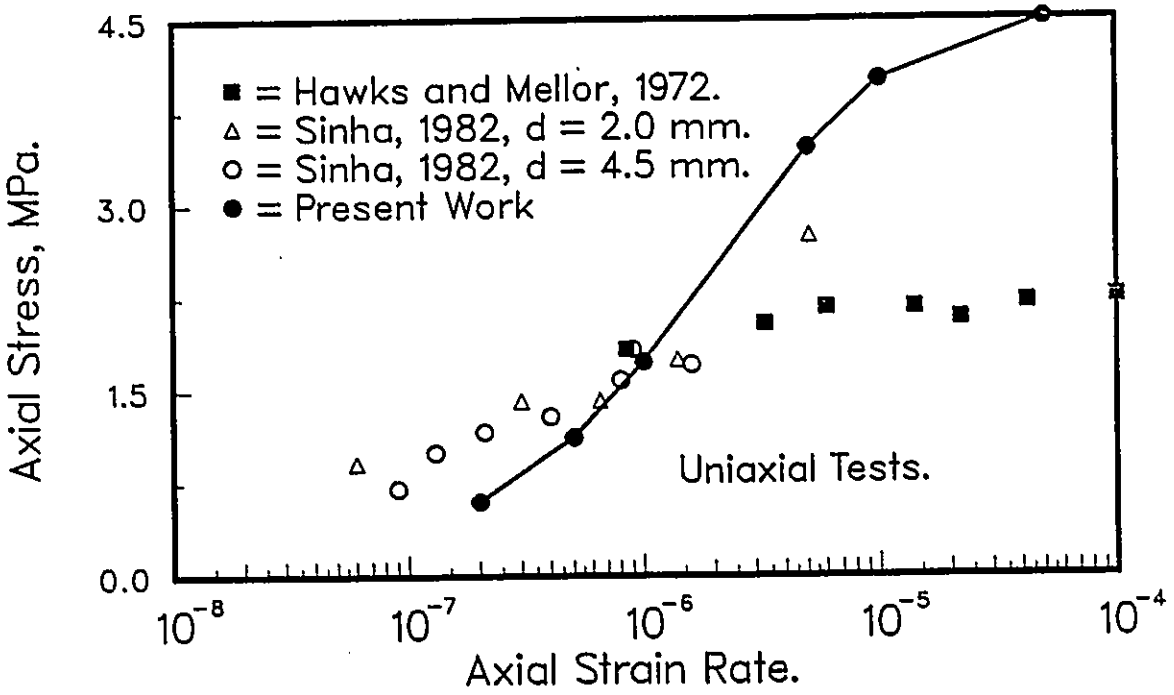

Figure G.18: Simulated and measured maximum tensile stress of granular (isotropic) ice. The maximum tensile stress values are those corresponding to the tests predicted in Fig. G.17.

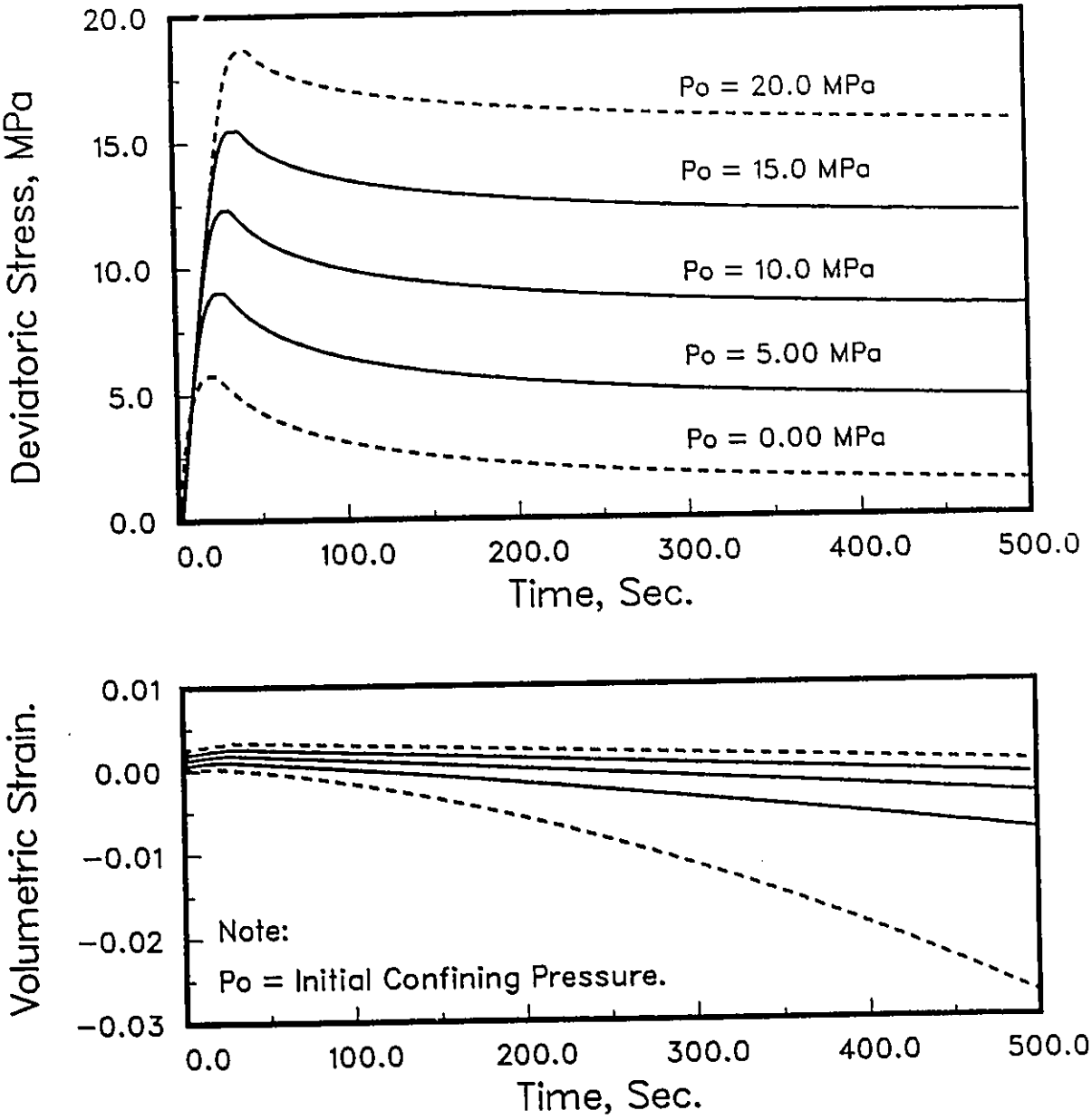

Figure G.19: Model predictions of the effect of initial confining pressure on the behaviour of granular ice subjected to constant strain rate of $1.10^{-4}sec^{-1}$, average grain size of 3 mm at $-10^{\circ}C$.

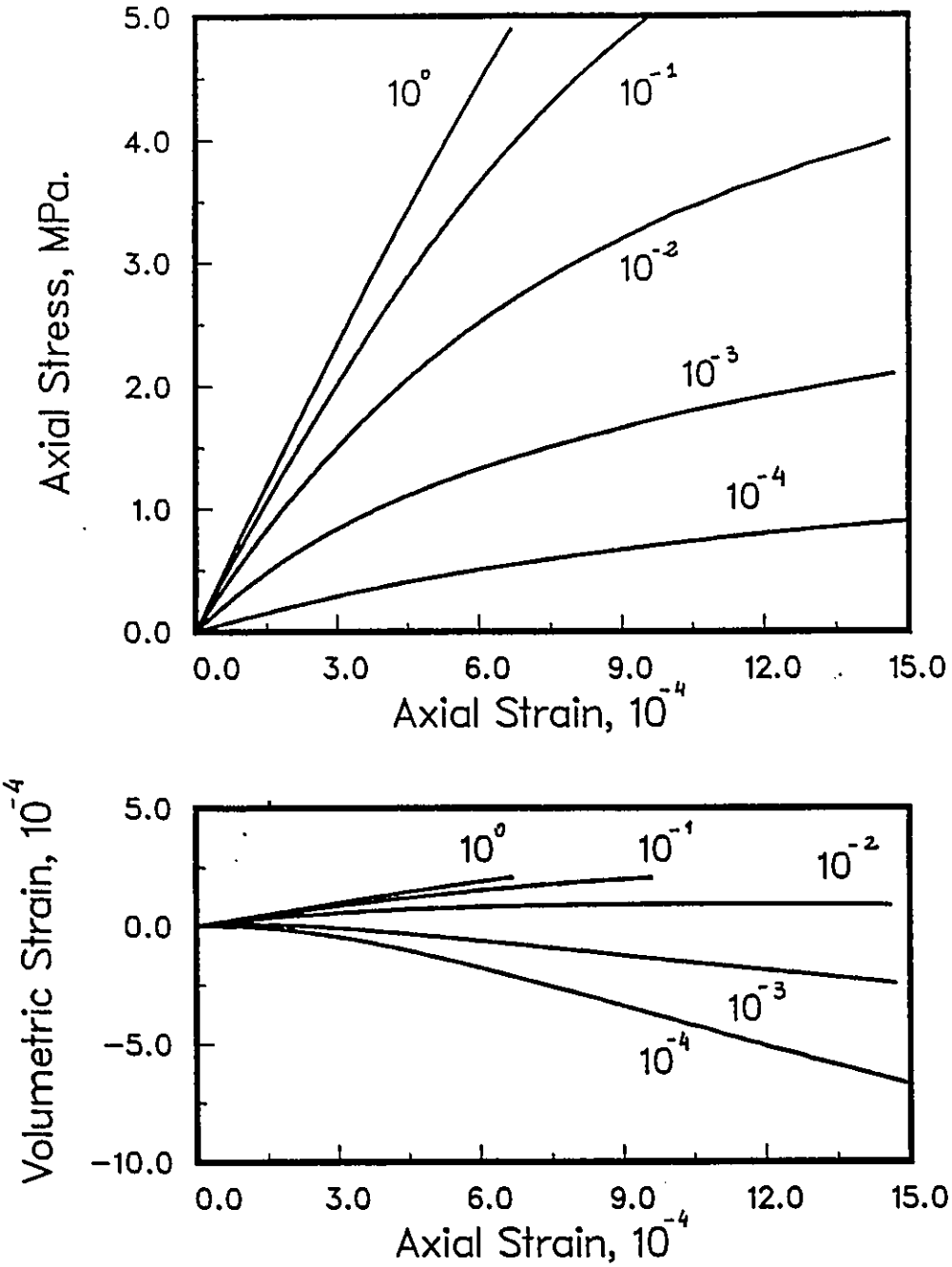

Figure G.20: Model predictions of the effect of stress rate on the behaviour of ice, the stress rates are indicated by each curve. The predictions are made for granular (isotropic) ice with an average grain size of 3 mm and temperature of -10°C.